Memoirs of the Faculty of Science, Kyoto University, Series of Physics, Astrophysics, Geophysics and Chemistry, Vol. XXXVII, No. 2, Article 5, 1988

Systematics of the Hexadecapole (Y_{42}) Strength of the γ-vibration in Deformed Nuclei ($152 \leqq A \leqq 192$) from Inelastic Scattering of Polarized Protons at 65 MeV

By

Takashi ICHIHARA*

Department of physics, Kyoto 606, Japan

(Received January 7, 1987)

Abstract

Inelastic scattering exciting the 2^+ and 4^+ members of the $K^\pi=2^+$ γ-vibrational band in ^{152,154}Sm, ^{160}Gd, ^{164}Dy, ^{166,168}Er, ^{176}Yb, ^{182,184}W and ^{192}Os has been measured with 65-MeV polarized protons. Coupled-channel analyses have been performed assuming the γ-vibrational model or the asymmetric rotor model. A large hexadecapole (Y_{42}) term in the γ-motion is necessary in both models in order to reproduce the experimental data. The quadrupole (Y_{22}) and hexadecapole (Y_{42}) transition strengths to the γ-vibrational band have been extracted systematically from the optical potential parameters and the deformation parameters for the first time. These show a strong mass number dependence, and can be understood qualitatively by a simple geometrical picture together with the quadrupole (Y_{20}) and hexadecapole (Y_{40}) moments. The experimental Y_{22} and Y_{42} strengths have been compared with an RPA calculation. This suggests the importance of the haxadecapole degree of freedom in the γ-vibration. A density-dependent Hartree-Fock calculation explains the quadrupole (Y_{20}) moments and the trend of the hexadecapole (Y_{40}) moments of the deformed optical potentials very well. The effect of the density dependence of the effective interaction is also discussed througth the Y_{20} moments and Y_{22} strengths. Coupled-channel analyses of the octupole-vibrational band are also discussed.

CONTENTS

I. INTRODUCTION 192
II. EXPERIMENTAL METHOD 193
III. FORM FACTORS FOR SURFACE VIBRATION OF DEFORMED NUCLEI 197
IV. ANALYSIS AND RESULT 202
A. Analysis assuming the γ-vibrational model 202
B. Analysis assuming the asymmetric rotor model 204
V. DISCUSSION 208
A. Quadrupole (Y_{22}) and hexadecapole (Y_{42}) transition strengths to the γ-vibrational band 208
B. Qualitative interpretation of the Y_{22} and Y_{42} transition strengths 212
C. Comparison of the Y_{22} and Y_{42} strengths with RPA calculations 214
D. Asymmetric rotor model 216
E. Multipole moments of deformed optical potential and DDHF calculations 217

* Present address: The Institute of Physical and Chemical Research (RIKEN), Hirosawa, Wako, 351-01, Japan

F. Comparison with other measurements and density-dependence of the effective interaction 219
VI. SUMMARY AND CONCLUSIONS 223
VII. ACKNOWLEDGMENTS 224
VIII. APPENDIX A: Octupole-vibrational states 224
IX. APPENDIX B: Numerical values of the measured differential cross section and the analyzing powers 227
X. REFERENCES 248

I. Introduction

For the study of nuclear collective motion, it is of considerable interest to investigate the γ-vibrational band in the $152 \leqq A \leqq 192$ region[1-4], where the nuclei are well-deformed and the non-collective components are suppressed up to the gap energy (2Δ) owing to the superconductivity of the ground state. Experimentally, recent progress in high quality beams and high resolution spectrographs has made it possible to measure the low-lying inelastic sattering for deformed nuclei in the $152 \leqq A \leqq 192$ region.[1-24] Therefore, we have recently performed a precise measurement on the cross sections and analyzing powers in ^{168}Er (p,p') at 65 MeV, and studied the excitaion to γ-vibrational states.[1] The results have clearly shown the importance of the haxadecapole (Y_{42}) component in the γ-vibration.

The possible existence of the hexadecapole (Y_{42}) component in the γ-vibration was reported in early work on inelastic scattering.[25-28] Tjϕm and Elbek first suggested the possibility of the direct excitation of the 4^+ states of the γ-vibrational band (4^+_γ states) of ^{162,164,166,468,170}Er by (d,d') scattering at 12.1 MeV, because these 4^+_γ states were strongly excited.[25] Mackintosh pointed out the necessity of the hexadecapole (Y_{42}) term in fitting the ^{166}Er (α,α') scattering at 50 MeV.[26] Recently, the importance of the Y_{42} term in describing the γ-vibrational states of ^{24}Mg has been pointed out by Ray *et al.*[27] in ^{24}Mg (p,p') scattering and Van der Borg *et al.*[28] in ^{24}Mg (α,α') scattering. Govil *et al.*[2] has also shown the importance of the Y_{42} term by ^{168}Er (α,α') scattering at 35 MeV.

Theoretically, it has been recognized recently that the hexadecapole degree of freedom in collective motion is very important in explaining collective motions in the quasiparticle phonon model.[29-31] Nesterenko *et al.*[31] have asserted that a hexadecapole-hexadecapole force is necessary in order to explain the experimental $B(E4)$ values of low-lying $K^\pi=3^+$ and 4^+ non-rotational states of rare earth nuclei and to explain our experimental result for the Y_{42} strength to the $K^\pi=2^+$ γ-vibrational band of ^{168}Er.[1] On the other hand, in the interacting boson model, the nucleon pair coupled to $L=4^+$ (G-pair) is considered to be important to reproduce the $B(E2)$ and the moment of inertia together with the 0^+ (S) and 2^+ (D) pairs.

The work presented here is aimed at investigating the hexadecapole (Y_{42}) component in the γ-vibrational band in deformed nuclei, the nature of which is a long-standing open problem. We have performed systematic measurements and analyses of the inelastic scattering of polarized protons at 65 MeV exciting the γ-vibrational states for ^{152,154}Sm, ^{160}Gd, ^{164}Dy, ^{166,168}Er, ^{176}Yb, ^{182,184}W and ^{192}Os. A part of this work has been described in our recent paper with a qualitative interpretation.[9]

Inelastic proton scattering in the 65-MeV region has many advantages in investigating nuclear structure. First, the measurements of inelastic hadron scattering bring us direct information about the transition strength for high-multipolarities ($\Delta\lambda \geqq 3$) which cannot be easily obtained by in-beam γ-ray measurements. Second, in this energy region, the reaction mechanism is considered to be relatively simple in contrast with the lower energy region. Therefore we can apply the direct reaction theory with little ambiguity. Third, the uncertainties in fitting the optical potential parameters and deformation parameters can be considerably reduced using analysing power data together with the cross sections, and therefore the transition strengths and multipole moments can be determined more precisely. Furthermore, in this energy region the real central part of the optical potential is deep, in contrast to the intermediate and high energy region, where the imaginary part of the optical potential is dominant.

In previous papers, we have studied the excitation to the 0^+-6^+ members of the ground state rotational band assuming the axially symmetric rigid rotor model.[5-7] The quadrupole moments of the deformed optical potentials of ^{166,168}Er, ^{174,176}Yb (Ref. 5), ^{178,180}Hf, ^{182,184}W (Ref. 6), ^{232}Th, and ^{238}U (Ref. 7) for (p,p') scattering at 65 MeV have been found to be 4-6% larger than those of the charge distributions. These differences can be explained by the density dependence of the effective interaction.[5-7,36-41]

In this paper, we extend the investigation to the collective vibrational states over the whole range of deformed nuclei. We describe the experimental method in Sec. II. The form factors for surface vibrations of deformed nuclei are presented in Sec. III and the coupled-channel analyses for the γ-vibrational band are described in Sec. IV. In Sec. V, the deduced quadrupole (Y_{22}) and hexadecapole (Y_{42}) transition strengths to the γ-vibratioanl band are presented and compared with various models. The systematic behavior of the quadrupole (Y_{20}) and hexadecapole (Y_{40}) moments of the deformed optical potentials is also discussed from various points of view. A summary and some conclusions are given in Sec. VI. Coupled-channel analyses of the octupole-vibrational band are also discussed in Appendix A. Numerical values of the measured cross sections and analyzing powers are presented in Appendix B.

II. Experimental Method

The experiment has been performed with 65-MeV polarized protons from the cyclotron at the Research Center for Nuclear Physics (RCNP), Osaka University, and the data have been obtained using the high resolution spectrograph RAIDEN.[42] Details of the experimental method are described in previous papers.[5-8] For the deformed nuclei, we have already measured the inelastic scattering of polarized protons at 65 MeV from ^{152,154}Sm, ^{164}Dy (Ref. 8), ^{166,168}Er, ^{174,176}Yb (Ref. 5), ^{178,180}Hf, ^{182,184}W (Ref. 6), ^{232}Th, and ^{238}U (Ref.7). The new measurements have been carried out for ^{160}Gd and ^{192}Os, and the supplementary measurements for inelastic scattering have been performed for ^{152,154}Sm and ^{176}Yb.

During the experiment, the beam polarization was periodically monitored by a sampling-type beam polarimeter with an interval of 10–30 sec.[43] The direction of the beam polarization was reversed every 0.5 sec by switching the rf transitions at the

atomic-type polarized ion source.[44] At the focal plane of the spectrograph, scattered particles were detected by a counter array consisting of a two-dimensional position-sensitive proportional counter (1.5 m length), a dual single-wire proportional counter ΔE counter) and a plastic scintillation counter (E counter).[45]

All the targets used were self-supporting enriched metal foils and their thicknesses and isotopec enrichments are summarized in table I. They were fabricated at the Oak Ridge National Laboratory (ONL) except for ^{192}Os. The ^{192}Os target was prepared by means of heavy ion sputtering using 10-KeV Ar ions at the Institute of Nuclear Study (INS), University of Tokyo. The beam intensity on target was 20–60 nA and beam polarization was 80-85%. The overall energy resolution was 20–26 KeV (FWHM).

Table I. Thicknesses and isotopic enrichmehts of the targets.

Nucleus	Thickness (mg/cm^2)	Enrichment
^{152}Sm	2.03	98.29%
^{154}Sm	2.96	98.69%
^{160}Gd	2.00	98.10%
^{164}Dy	2.1	98.43%
^{166}Er	2.0	97.69%
^{168}Er	2.0	95.24%
^{176}Yb	1.0, 2.0	96.68%
^{182}W	1.6, 3.4	94.4 %
^{184}W	1.9	94.8 %
^{192}Os	1.4	99.40%

The solid angles and angular resolutions were 1.2 msr and ±0.46° for measurements at forward angles ($\theta_{lab.}<36°$) and 2.3 msr and ±0.71° for measurements at backward angles ($\theta_{lab.}\geqq 36°$), respectively. The angular distributions were measured from 10° to 70° in 1.0 degree steps at forward angles and in 2.0 degree steps at backward angles.

At the forward angles, in order to measure the inelastic scattering more efficiently, separate measurements were carried out where the elastically scattered protons were stopped by a slit placed in front of the focal plane counter. At the beginning of the experiment, the uniformity of the efficiency along the focal plane was checked by measuring the elastic scattering with various $B\rho$ values, and was consistent to 1%.

All the data from the counters were recorded on magnetic tapes event-by-event in a list mode by a PDP-11/44 computer through the raw data processor.[46] We kept the counting rate lower than 800 cps, which corresponded to 5% dead time. This dead time was mainly due to the conversion time of the analog-to-digital converters.

After obtaining the final spectra by sorting the list mode raw data, overall dead-time corrections were carried out but did not exceed 5%. In Fig. 1, we show typical momentum spectra for ^{152}Sm at $\theta_{lab.}=48°$. The 0^+-6^+ states of the ground state ratational band, 2^+ and 4^+ states of the γ-vibrational band, 1^-, 3^- and 5^- states of the

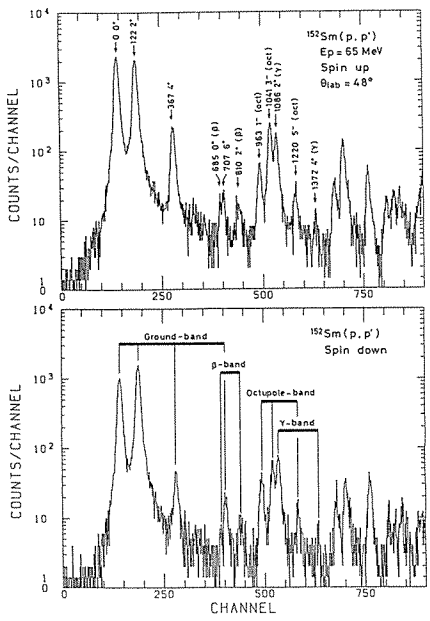

FIG. 1. Typical momentum spectra of the focal plane counter for ^{152}Sm (p,p') scattering at 65 MeV. Spin-up and spin-down spectra are shown at θ_{tab}=48°.

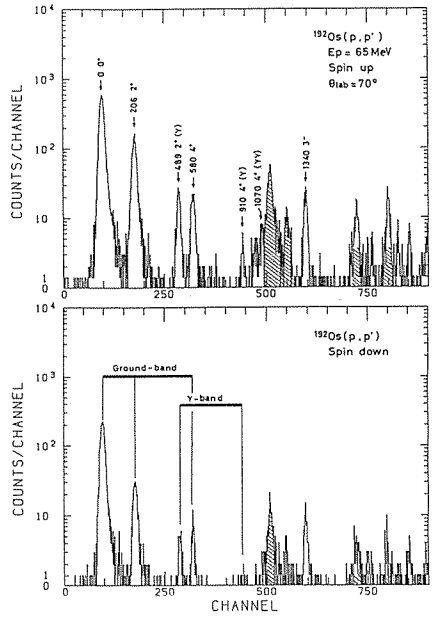

FIG. 2. Typical momentum spectra of the focal plane counter for ^{192}Os (p,p') scattering at 65 MeV. Spin-up and spin-down spectra are shown at θ_{tab}=70°. The cross hatched regions indicate the scattering from impurities in the target.

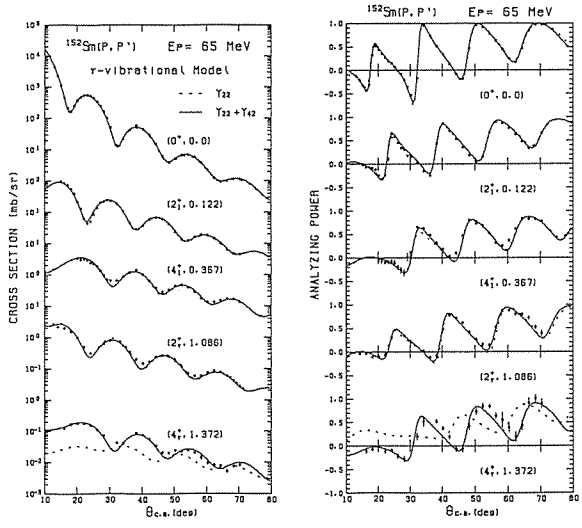

FIG. 3. Measured cross sections and analyzing powers for the 0^+, 2^+, and 4^+ states of the ground band and 2^+ and 4^+ states of the γ-band of ^{152}Sm by inelastic scattering of polarized protons at 65 MeV. The dotted (solid) curves show the best-fit result of the coupled-channel calculation assuming the Y_{22}-mode ($Y_{22}+Y_{42}$-mode) γ-vibration.

octupole-vibrational band, and 0^+ and 2^+ states of the β-vibrational band are strongly excited as shown in the spectra. In Fig. 2, we show typical momentum spectra for ^{192}Os at $\theta_{lab.}=70°$. The excitation energy of the 2^+ state of the γ-vibrational band is lower than that of the 4^+ state of the ground band in ^{192}Os. Typical spectra for ^{166}Er and ^{174}Yb are shown in Ref.5 and those for ^{184}W are shown in Ref. 6.

All the peak areas were extracted using a peak-fitting code[5,7] assuming that the peak shapes were identical for all the states except for the peaks from contaminations. The correction for the inelastic cross sections has been carried out taking account of the isotopic enrichment of the targets. The experimental cross sections and analysing powers for 0^+, 2^+, and 4^+ states of the ground band and 2^+, and 4^+ states of the γ-band

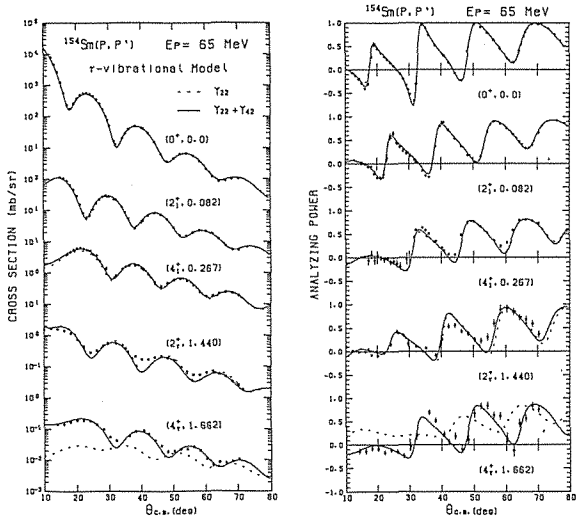

FIG. 4. The same as Fig. 3 except for ^{154}Sm.

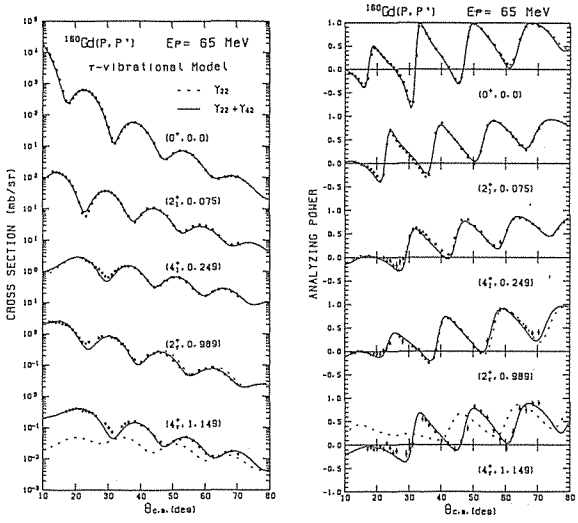

FIG. 5. The same as Fig. 3 except for ^{160}Gd.

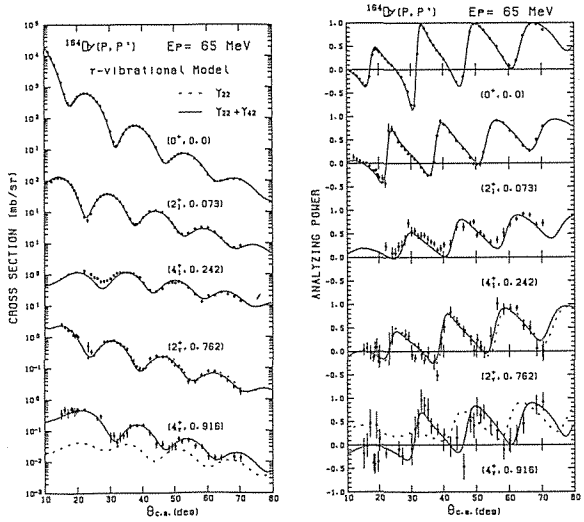

FIG. 6. The same as Fig. 3 except for ^{164}Dy.

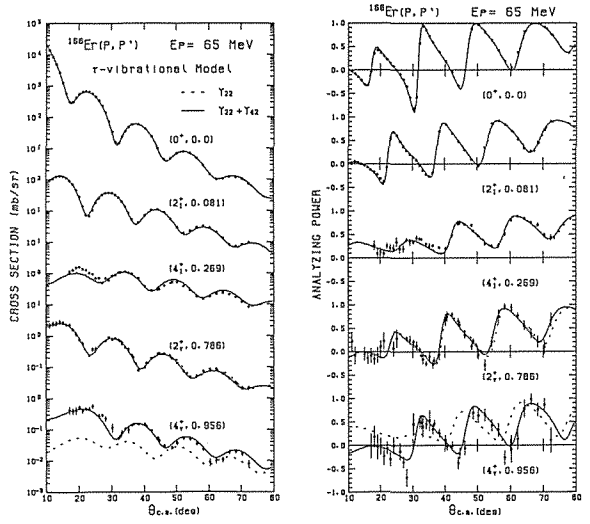

FIG. 7. The same as Fig. 3 except for ^{166}Er.

are plotted in Figs 3–12. The error bars of the experimental data include the statistical errors and the errors due to the peak-fitting, which have been estimated by solving the error correlation matrix in the peak-fitting procedure.

III. Form Factors for Surface Vibration of Deformed Nuclei

The basic formalism of the coupled-channel calculation in the rotational model and in the vibrational model is described by Tamura in detail.[47] The expansion to the γ-vibration has been presented by Ray *et al.*[27], Harakeh[48], and Van der Borg *et al.*[28] The expansion to the octupole-vibration has been also reported by Harakeh[48] and Govil *et*

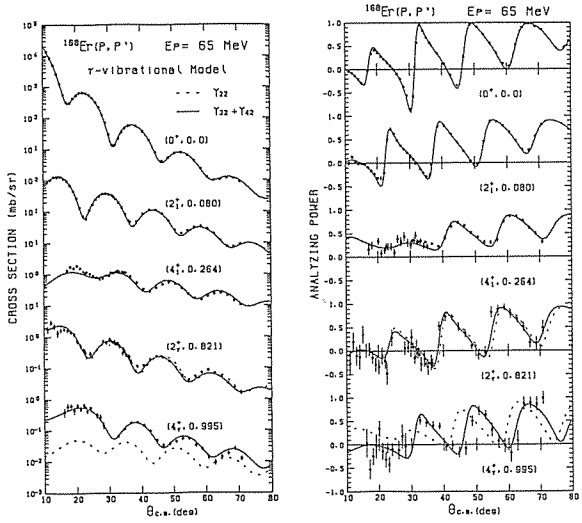

FIG. 8. The same as Fig. 3 except for ^{168}Er.

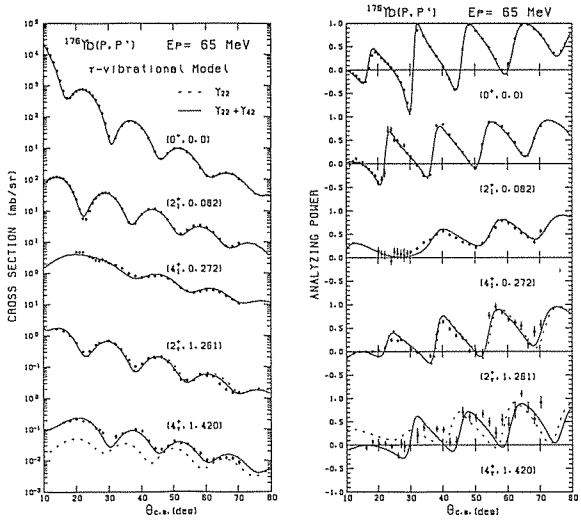

FIG. 9. The same as Fig. 3 except for ^{176}Yb.

al.[2] In this section, we follow these results for the case of the surface vibrations in deformed nuclei in a general form for the later discussion.

The optical potential for the proton scattering is given by

$$U_{sph}(r) = V_{Coul}(r, rc) - V_R f(r; r_R, a_R) - iW_v f(r; r_{wv}, a_{wv})$$

$$+4ia_{ws}W_s \frac{d}{dr} f(r; r_{ws}, a_{ws}) + V_{ls}\left[\frac{\hbar}{m_\pi c}\right]^2 \frac{1}{r}\frac{d}{dr} f(r; r_{ls}, a_{ls})(\vec{\sigma}\cdot\vec{l}), \qquad (1)$$

where

$$f(r; r_0, a_0) = \{1+\exp[(r-r_0A^{1/3})/a_0]\}^{-1}, \qquad (2)$$

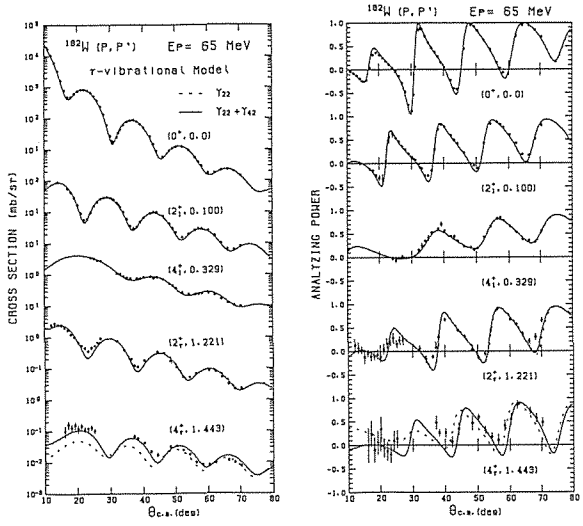

FIG. 10. The same as Fig. 3 except for ^{182}W.

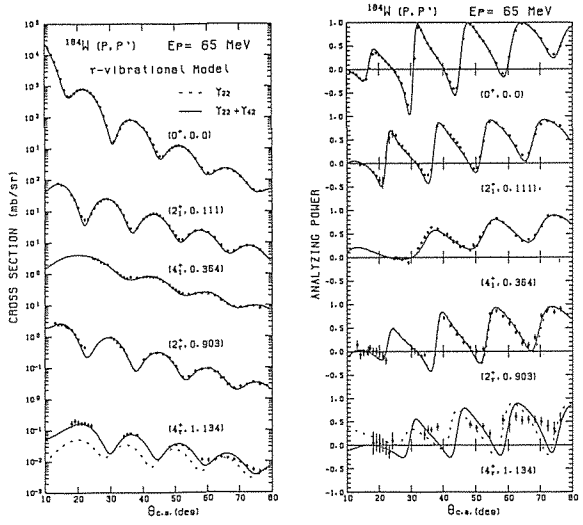

FIG. 11. The same as Fig. 3 except for ^{184}W.

and $V_{Coul}(r, r_C)$ is the Coulomb potential for a uniformly charged sphere.

In deformed nuclei, the elastic and inelastic scattering exciting the collective states is described by the deformed optical potential. The potential surface can be expanded according to the notation of Bohr and Mottelson as[49]:

$$R^j(\Omega') = R_0^j\left[1+\sum_{\lambda\mu}\beta^j_{\lambda\mu}(\Omega')+\sum_{lm}\alpha^j_{lm}Y_{lm}(\Omega')\right], \tag{3}$$

where $\Omega'=(\theta', \psi')$ represents the angles in the intrinsic frame and the suffix j represents each part of the optical potentials- the real central part, volume imaginary part, and so on. From now on, we avoid the suffix j in the equations for convenience. The second

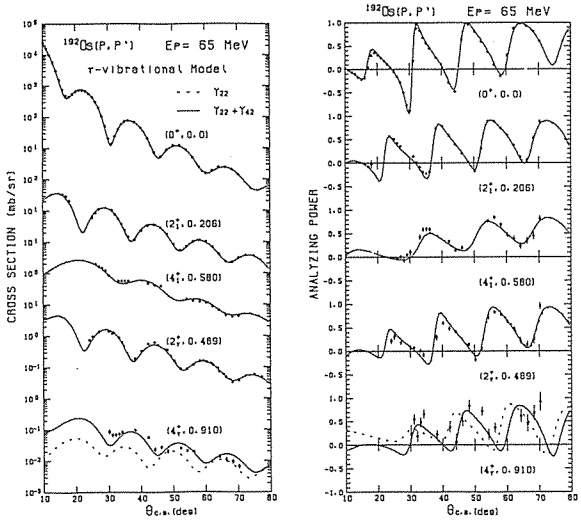

FIG. 12. The same as Fig. 3 except for ^{192}Os.

term in the right-hand side of Eq. (3) represents the *static* deformation and the third term represents the *dynamic* deformation (vibration).

We assume that the static deformation is axially symmetric.
The Eq. (3) can be reduced to:

$$R(\Omega') = R_0\left[1+\sum_{\lambda}\beta_{\lambda 0}\,Y_{\lambda 0}(\Omega')+\sum_{lm}\alpha_{lm}\,Y_{lm}(\Omega')\right], \tag{4}$$

Since the α_{lm} are q-numbers, the deformed optical potential U is expanded in first order in terms of α_{lm} as:

$$U(r-R,\,\Omega') = U_0(r-R_\beta,\,\Omega')+\sum_{lm}\alpha_{lm}\,Y_{lm}(\Omega')\,U_1(r-R_\beta,\,\Omega'), \tag{5}$$

where

$$R_\beta = R_0\left[1+\sum_{\lambda}\beta_{\lambda 0}\,Y_{\lambda 0}(\Omega')\right], \tag{6}$$

$$U_1(r-R_\beta,\,\Omega') = R_0\frac{\partial U(r-R,\,\Omega')}{\partial R}\Bigg|_{R=R_\beta}. \tag{7}$$

For a β-vibrational band, γ-vibrational band, and octupole-vibrational band, we could basically chose the pairs of $(l,\,m)$ in Eq. (4) as $(l,\,m)=(2,\,0)$[$+(0,\,0)$ for volume-conservation correction], $(l,\,m)=(2,\,2)+(2,\,-2)$[$+(4,\,2)+(4,\,-2)$ for hexadecapole γ-vibration], and $(l,\,m)=(3,\,0)$[$+(1,\,0)$ for center-of-mass motion correction], respectively.

Following Tamura,[47] the potentials U_0 and U_1 in Eq. (5) are expanded in multipoles as

$$U(r,\,\Omega') = \sum_{\lambda} v_\lambda^{\langle 0\rangle}(r)\,Y_{\lambda 0}(\Omega')+\sum_{\lambda}\sum_{lm}\left[\tilde{v}_\lambda^{\langle 1\rangle\,lm}(r)\alpha_{lm}\,Y_{\lambda m}(\Omega')\right], \tag{8}$$

where

$$\tilde{v}_{\lambda}^{\langle 1\rangle,\, lm}(r) = \sum_{\lambda'} v_{\lambda'}^{\langle 1\rangle}(r) \left[\frac{(2l+1)(2\lambda'+1)}{4\pi(2\lambda+1)}\right]^{\frac{1}{2}} \langle l0\lambda'0 \,|\, \lambda 0\rangle \langle lm\lambda'0 \,|\, \lambda m\rangle \,, \tag{9}$$

$$v_{\lambda'}^{\langle 1\rangle}(r) = 4\pi \int_0^1 d(\cos\theta')\, Y_{\lambda'0}(\theta')\, U_i(r,\, \theta') \,. \tag{10}$$

Finally, the potential (8) can be rotated to space-fixed coordinates using the rotation matrix $D_{\mu v}^{*\lambda}$,

$$U(r,\, \Omega) = \sum_{\lambda\mu} v_{\lambda}^{\langle 0\rangle}(r)\, Y_{\lambda\mu}(\Omega') D_{\mu 0}^{*\lambda} + \sum_{\lambda\mu} \sum_{lm} \left[\tilde{v}_{\lambda}^{\langle 1\rangle\, lm}(r) \alpha_{lm}\, Y_{\lambda m}(\Omega') D_{\mu m}^{*\lambda}\right] . \tag{11}$$

The optical potential U in Eq. (11) can be divided into two parts as follows:

$$U(r,\, \Omega) = U_{dias}(r) + U_{coupl}(r,\, \Omega) \,, \tag{12}$$

where

$$U_{dias}(r) = v_0^{\langle 0\rangle}(r)\, Y_{00} D_{00}^{*0} \tag{13}$$

$$U_{coupl}(r,\, \Omega) = \sum_{\lambda\mu(\lambda\neq 0)} v_{\lambda}^{\langle 0\rangle}(r)\, Y_{\lambda\mu}(\Omega') D_{\mu 0}^{*\lambda} + \sum_{\lambda\mu} \sum_{lm} \left[\tilde{v}_{\lambda}^{\langle 1\rangle\, lm}(r) \alpha_{lm}\, Y_{\lambda m}(\Omega') D_{\mu m}^{*\lambda}\right] . \tag{14}$$

The first term in the right-hand side of Eq. (14) represents the rotational coupling and the second term represents the vibrational coupling in the deformed nuclei. The Hamiltonian of this system is given by

$$H = T + H_t + U_{dias} + U_{coupl} \,, \tag{15}$$

where T is the kinetic energy of the incident particle and H_t is the Hamiltonian for the internal motion of the target nucleus. Then the Schrodinger equation can be written as

$$H\Psi = E_1 \Psi \tag{16}$$

where the wave function of the whole system is written as

$$\Psi = r^{-1} \sum_{J_n l_n j_n} R_{J_n l_n j_n}(r) \sum_{m_j M_n} \langle j_n I_n m_j M_n \,|\, JM\rangle\, y_{l_n j_n m_j} \Phi_{l_n M_n K_n} \,, \tag{17}$$

where

$$y_{l_n j_n m_j} = \sum_{m_l m_s} \langle l s m_l m_s \,|\, j m_j\rangle\, i^l Y_{l_n m_l} \chi_{s m_s} \,. \tag{18}$$

The spin function of the projectile is χ_{sm_s}, and $\Phi_{l_n M_n K_n}$ represents the wave function of the target nucleus of each nuclear state. The wave function of the target nucleus is given by

$$\Phi_{IMK} = \Psi_K(\xi) \left[\frac{2J+1}{16\pi^2(1+\delta_{K0})}\right]^{1/2} \times \left[D_{MK}^{*I} + (-1)^I D_{M-K}^{*I}\right] , \tag{19}$$

where $\Psi_K(\xi)$ is the intrinsic wave function of the nucleus in the K band.

The matrix element for the coupling potential is then given by

$$\langle (y_{lj}\otimes \Phi_{IK})_{JM}|\, U_{couple}\,|(y_{l'j'}\otimes \Phi_{l'K'})_{JM}\rangle = \sum_{\lambda}\Big(v_{\lambda}^{(0)}(r)\delta_{KK'}(2I'+1)^{1/2}(I'K\lambda 0\,|\,IK)(1-\delta_{\lambda 0}) + \delta_{K+K',m}\sum_{\bar{\lambda}} v_{\lambda}^{(1)\,lm}(r)\sum_{l} B^{lm}(I, I'; \lambda, \bar{\lambda})\Big) A(ljI, l'j'I'; \lambda Js)\,, \tag{20}$$

where[27]

$$A(ljI, l'j'I'; \lambda Js) = (4\pi)^{-1/2}(-1)^{J-s-I'+l+I'+(I'-l)/2} ll'\hat{j}\hat{J}'\langle ll'00\,|\,\lambda 0\rangle \cdot W(jIj'I', J\lambda)W(ljl'j'; s\lambda)\,, \tag{21}$$

using the Wigner coefficients and

$$B^{lm}(I, I'; \lambda, \bar{\lambda}) = \left(\frac{(2l+1)(2\bar{\lambda}+1)}{4\pi(2\lambda+1)}\right)^{1/2}\langle l0\bar{\lambda}0\,|\,\lambda 0\rangle\langle lm\bar{\lambda}0\,|\,\lambda m\rangle \cdot (2I'+1)^{1/2}\langle I'm\lambda -m\,|\,I0\rangle\eta_{lm}\,. \tag{22}$$

The quantity η_{lm} represents the amplitude of the oscillation associated with the α_{lm} and is given by:

$$\eta_{lm} = \sqrt{1+\delta_{m0}}\,\langle \Psi_0|\,\alpha_{lm}\,|\,\Psi_m\rangle\,. \tag{23}$$

The coupled-channel code ECIS79[50] has been modified to include the form factors of surface vibrations in deformed nuclei as described in this section. Therefore, any surface vibration in deformed nuclei can be calculated using this code so far as it can be expanded as Eq. (4).

IV. Analysis and Results

Two kinds of coupled-channel analyses have been performed for 0^+, 2^+ and 4^+ states of the ground state rotational band and 2^+ and 4^+ states of the $K^\pi=2^+$ γ-band assuming the γ-vibrational model and the asymmetric rotor model for ^{152,154}Sm, ^{160}Gd, ^{164}Dy, ^{166,168}Er, ^{176}Yb, ^{182,184}W, and ^{192}Os.

In the χ^2-fitting with the coupled-channel calculations, 3% errors were added to the statistical errors in order to include the unknown systematic errors and to avoid trapping in an unphysical local χ^2 minimum as follows:

$$\delta\sigma(\theta) = [\delta\sigma(\theta)^2_{stat} + \sigma(\theta)^2\times 0.03^2]^{1/2}\,, \tag{24}$$

$$\delta A_y(\theta) = [\delta A_y(\theta)^2_{stat} + 0.03^2]^{1/2}\,. \tag{25}$$

A. Analysis assuming the γ-vibrational model

Coupled-channel analyses assuming the γ-vibrational model have been performed using the modified version of the code ECIS79 as described in the Sec. III.

Deformed optical potentials of real central, volume imaginary, surface imaginary, real spin-orbit, and Coulomb forms were employed. In this coupled-channel calculation, the deformation parameters of each part of the optical potential are set to be equal for simplicity. The quadrupole moments of the real central part of the deformed optical

potential obtained by this method agree with those obtained by the moment-scaling method[5,6] to within 2%. The deformed full-Thomas term was used for the spin-orbit potential.[51] The deformed optical potential was expanded in multipoles up to $\lambda=8$ in Eqs. (8)–(14). The matching radius was chosen as 20 fm, also taking account of the Coulomb excitation.

The potential surface is assumed to be as follows:

$$R(\Omega') = R_0\Big[1+\sum_{\lambda=2,4,6}\beta_{\lambda 0}\,Y_{\lambda 0}(\Omega')+\alpha_{22}\{Y_{22}(\Omega')+Y_{2-2}(\Omega')\} + \alpha_{42}\{Y_{42}(\Omega')+Y_{4-2}(\Omega')\}\Big], \tag{26}$$

where α_{22} and α_{42} represent the collective coordinates corresponding to the quadrupole (Y_{22}) and hexadecapole (Y_{42}) γ-vibration. The potential surfaces of the nucleus during the Y_{22}-mode and Y_{42}-mode γ-vibrations are shown in Fig. 13. 0^+, 2^+ and 4^+ states of the ground state rotational band and 2^+ and 4^+ states of the γ-vibrational band have been coupled simultaneously in this calculation. Since the 3^+ state of the γ-band is an unnatural parity state and the excitation of the 3^+ states is very week as shown in Figs. 1–2, we did not include the 3^+ state. It was confirmed that the influence of the coupling of 3^+ state on the other states is negligible in this calculation. The coupling scheme is presented in Fig. 14.

A least-χ^2 search for the optical potential parameters and deformation parameters was carried out. The β_6 deformation parameters were kept fixed to the values obtained by the previous coupled-channel calculation for the 0^+-6^+ states of the ground band.[5,6]

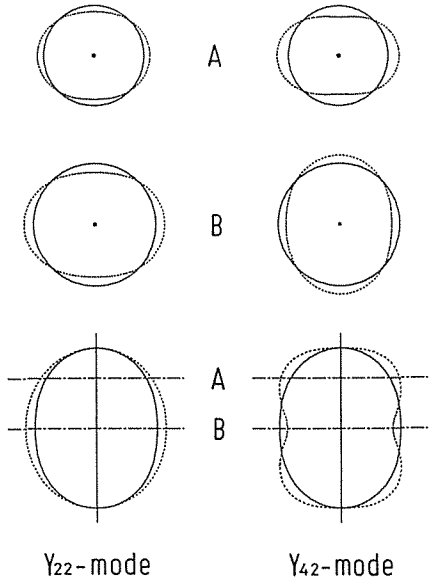

FIG. 13. Potential surface of the nucleus during the Y_{22}-mode and the Y_{42}-mode γ-vibration.

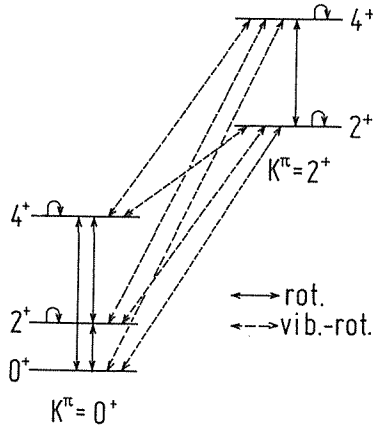

FIG. 14. Coupling scheme of the coupled-channel calculation assuming the γ-vibrational model. Solid lines with arrows indicate the rotational coupling and dashed lines with arrows indicate the vibration-rotation coupling.

A renormalization factor of the experimental cross sections was included to account for the uncertainty of the target thickness. The sloid(dashed) curves in Figs. 3–12 show the best-fit results of the coupled-channel calculation assuming the $Y_{22}+Y_{42}$ mode (only Y_{22} mode) γ-vibration. Without the hexadecapole (Y_{42}) term, the 4^+ state of the γ-vibrational band cannot be reproduced for all the measured nuclei. Excellent fits have been obtained for all the states if and only if we introduce the hexadecapole (Y_{42}) γ-vibration as shown in the figures. The best-fit optical potential parameters, the deformation parameters, the χ^2/f values, and the renormalization factors (N_0) of the experimental cross sections are listed in Table II.

In order to investigate the sensitivity of the data to the static and dynamic deformation parameters, χ^2 values were evaluated with a little variation of each deformation parameter. We defined the uncertainties of the deformation parameters by the values where the χ^2 increases 10% from the minimum one. These uncertainties are listed in Table II in parentheses.

Table II. The optical potential parameters and deformation parameters in the γ-vibrational model as obtained by varying these parametes to fit the 65 MeV (p, p′) data.

Nucleus	V_R (Mev)	r_R (fm)	a_R (fm)	W_v (Mev)	r_{V_0} (fm)	a_{V_0} (fm)	W_s (MeV)	r_{V_s} (fm)	a_{V_s} (fm)	V_{ls} (MeV)	r_{ls} (fm)	a_{ls} (fm)	β_{20}	β_{40}	β_{60}	η_{22}	η_{42}	χ^2/f	N_0
^{152}Sm	39.60	1.202	0.759	11.28	1.023	0.863	5.09	1.252	0.655	5.62	1.121	0.707	0.2398(41)	0.0623(20)	-0.007	0.0545(14)	0.0182(06)	3.7	1.00
^{154}Sm	41.70	1.180	0.745	9.37	1.228	0.344	4.42	1.345	0.498	6.04	1.116	0.685	0.2578(40)	0.0826(27)	-0.010	0.0487(19)	0.0214(07)	4.4	0.94
^{160}Gd	38.32	1.224	0.711	17.45	0.707	1.027	7.41	1.200	0.670	5.53	1.149	0.648	0.2798(58)	0.0471(25)	-0.013	0.0512(11)	0.0236(06)	3.6	0.91
^{164}Dy	37.79	1.222	0.716	11.97	0.908	0.894	6.81	1.209	0.650	5.49	1.160	0.628	0.2822(45)	0.0163(79)	-0.009	0.0481(13)	0.0238(12)	1.8	0.88
^{166}Er	38.66	1.223	0.731	9.20	0.979	0.673	7.44	1.219	0.650	5.67	1.162	0.618	0.2804(32)	0.0023(62)	-0.012	0.0495(10)	0.0229(11)	2.0	1.05
^{168}Er	36.61	1.234	0.714	9.05	1.038	0.681	7.09	1.223	0.628	5.67	1.173	0.603	0.2845(39)	-0.0107(41)	-0.020	0.0461(14)	0.0247(10)	2.3	1.00
^{176}Yb	39.30	1.222	0.718	15.89	0.714	1.054	7.70	1.200	0.660	5.43	1.164	0.645	0.2707(52)	-0.0541(29)	-0.005	0.0410(12)	0.0136(07)	3.8	0.87
^{182}W	37.88	1.234	0.709	9.02	0.968	0.795	7.33	1.224	0.612	5.37	1.174	0.644	0.2276(31)	-0.0581(13)	0.001	0.0460(15)	0.0069(13)	3.5	0.78
^{184}W	38.54	1.226	0.716	8.96	1.024	0.717	7.12	1.224	0.638	5.50	1.151	0.672	0.2183(29)	-0.0630(12)	0.005	0.0478(09)	0.0099(11)	2.6	1.19
^{192}Os	44.55	1.148	0.812	8.46	1.074	0.261	6.72	1.237	0.653	5.79	1.072	0.765	0.1568(21)	-0.0572(16)	-0.001	0.0643(20)	0.0143(12)	2.8	0.68

[a]Renormalization factors for the experimental cross sections to be divided.

B. Analysis assuming the asymmetric rotor model

Coupled-channel calculations assuming the asymmetric rotor model have also been performed using the code ECIS79. In this model, the nucleus is assumed to be a triaxial rigid rotor and the γ-band is generated from the rotation.[52] We have assumed the following deformation

$$R(\Omega') = R_0\Big[1+\sum_{\lambda=2,4,6}\beta_{\lambda 0}\,Y_{\lambda 0}(\Omega')+\beta_{22}\Big\{\frac{Y_{22}(\Omega')+Y_{2-2}(\Omega')}{\sqrt{2}}\Big\} +\beta_{42}\Big\{\frac{Y_{42}(\Omega')+Y_{4-2}(\Omega')}{\sqrt{2}}\Big\}\Big]. \tag{27}$$

The rotational Hamiltonian for the asymmetric rotor is

$$H_{rot} = \sum_{n=1}^{3} \frac{J_n^2}{2I_n}, \tag{28}$$

where I_n are the moments of inertia on each axis.[52-53] The moments of inertia in Eq. (28) have been determined by assuming the Davydov-Filippow model as:

$$I_n = \frac{4B\beta^2}{\hbar^2} \sin^2\left(\gamma - \frac{2\pi}{3} nm\right), \tag{29}$$

where $\hbar^2/4B\beta^2$ is a quantity which has the dimension of energy, and γ varies between 0 and $\pi/3$. Each nuclear state can be written as

$$\left| IM; \alpha > = \sum_K A^I_{\alpha(\beta,\gamma)K} \right| IMK> \tag{30}$$

with

$$\left| IMK> = \Psi(\beta, \gamma) \left[\frac{2J+1}{16\pi^2(1+\delta_{K0})}\right]^{1/2} \times [D^{*I}_{MK} + (-1)^I D^{*I}_{M-K},], \right. \tag{31}$$

where $\Psi(\beta, \gamma)$ is the intrinsic wave function.

The band mixing coefficients $A^I_{\alpha K}$ have been determined by solving the eigenequations

$$\sum_{K'} < IMK' | H_{rot} | IMK > A^I_{\alpha K'} = E^I_\alpha A^I_{\alpha K}, \tag{32}$$

where the E^I_α is the eigenvalue of the Hamiltonian of the asymmetric rotor.

We have set $\hbar^2/4B\beta^2$ and γ in Eq. (29) in order to reproduce the energy levels of the 2^+_1 state of the ground band and the 2^+_2 state of the γ-band. The asymmetric deformation parameters γ in Eq. (31) have been determined by the equation

Table III. Band mixing coefficients used for the coupled-channel calculations assuming the asymmetric rotor model.

Nucleus		0^+	2^+		2^+_γ		4^+			4^+_γ		
	γ(deg)	K=0	K=0	K=2	K=0	K=2	K=0	K=2	K=4	K=0	K=2	K=4
^{152}Sm	13.233	1.0000	0.9998	0.0195	-0.0195	0.9998	0.9972	0.0750	0.0006	-0.0750	0.9971	0.0099
^{154}Sm	9.538	1.0000	0.9999	0.0067	-0.0067	0.9999	0.9997	0.0259	0.0001	-0.0259	0.9997	0.0034
^{160}Gd	10.981	1.0000	0.9999	0.0105	-0.0105	0.9999	0.9992	0.0407	0.0002	-0.0407	0.9992	0.0054
^{164}Dy	12.304	1.0000	0.9999	0.0153	-0.0153	0.9999	0.9983	0.0590	0.0003	-0.0590	0.9982	0.0078
^{166}Er	12.676	1.0000	0.9999	0.0169	-0.0169	0.9999	0.9979	0.0650	0.0004	-0.0650	0.9978	0.0086
^{168}Er	12.354	1.0000	0.9999	0.0155	-0.0155	0.9998	0.9982	0.0598	0.0004	-0.0598	0.9982	0.0079
^{176}Yb	10.182	1.0000	1.0000	0.0083	-0.0083	1.0000	0.9995	0.0319	0.0001	-0.0319	0.9995	0.0040
^{182}W	11.382	1.0000	0.9999	0.0184	-0.0184	0.9999	0.9990	0.0457	0.0002	-0.0457	0.9989	0.0060
^{184}W	13.836	1.0000	0.9997	0.0227	-0.0227	0.9997	0.9962	0.0870	0.0008	-0.0870	0.9961	0.0115
^{192}Os	25.196	1.0000	0.9720	0.2349	-0.2349	0.9720	0.8468	0.5299	0.0450	-0.5307	0.8367	0.1348

$$\gamma = \frac{1}{3}\sin^{-1}\left(\frac{3}{y+1}\sqrt{y/2}\right), \tag{33}$$

with

$$y = \varepsilon_2(2)/\varepsilon_1(2), \tag{34}$$

where $\varepsilon_1(2)$ and $\varepsilon_2(2)$ represent the energy levels of the 2_1^+ state and 2_2^+ state, respectively. After γ was determined, the matrix elements of Eq. (31) have been evaluated and

Table IV. The optical potential parameters and deformation parameters in the asymmetric roter mode as obtained in the present coupled-channel calculations using the band mixing coefficients in Table III.

Nucleus	V_R (Mev)	r_R (fm)	a_R (fm)	W_v (Mev)	r_{V_v} (fm)	a_{V_v} (fm)	W_s (MeV)	r_{V_s} (fm)	a_{V_s} (fm)	V_{ls} (MeV)	r_{ls} (fm)	a_{ls} (fm)	β_{20}	β_{40}	β_{60}	β_{22}	β_{42}	χ^2/f	N_0^a
^{152}Sm	37.86	1.218	0.736	10.11	1.062	0.972	4.88	1.238	0.644	5.57	1.140	0.692	0.2371(42)	0.0608(19)	-0.007	0.0598(13)	0.0238(07)	3.8	1.01
^{154}Sm	40.08	1.187	0.756	10.65	1.134	0.728	4.42	1.274	0.581	5.71	1.116	0.687	0.2600(41)	0.0834(26)	-0.010	0.0500(17)	0.0239(07)	4.9	0.97
^{160}Gd	38.69	1.229	0.694	11.96	0.793	0.883	7.95	1.186	0.685	5.66	1.153	0.644	0.2781(54)	0.0480(27)	-0.013	0.0563(11)	0.0270(08)	3.8	0.91
^{164}Dy	36.69	1.228	0.702	11.28	0.904	0.872	6.93	1.207	0.660	5.45	1.155	0.636	0.2809(43)	0.0181(57)	-0.009	0.0535(14)	0.0265(13)	1.8	0.88
^{166}Er	38.32	1.220	0.735	8.19	1.037	0.599	7.30	1.226	0.632	5.74	1.157	0.618	0.2807(29)	0.0027(63)	-0.012	0.0555(10)	0.0251(09)	1.9	1.05
^{168}Er	37.35	1.226	0.717	8.66	1.063	0.594	7.03	1.234	0.619	5.62	1.161	0.616	0.2831(41)	-0.0037(46)	-0.020	0.0517(12)	0.0258(10)	2.1	1.00
^{176}Yb	37.71	1.233	0.697	10.61	0.825	0.874	8.05	1.194	0.676	5.45	1.168	0.631	0.2688(47)	-0.0538(28)	-0.005	0.0443(13)	0.0120(07)	3.7	0.88
^{182}W	37.15	1.239	0.700	9.04	0.943	0.756	7.60	1.222	0.613	5.22	1.178	0.634	0.2258(30)	-0.0578(14)	-0.001	0.0488(14)	0.0061(09)	3.6	0.78
^{184}W	38.36	1.225	0.717	8.70	1.056	0.708	6.80	1.234	0.625	5.47	1.147	0.670	0.2166(28)	-0.0633(13)	0.005	0.0535(11)	0.0072(10)	2.8	1.17
^{192}Os	41.00	1.174	0.783	7.46	1.083	0.187	6.95	1.228	0.667	5.73	1.081	0.745	0.1438(21)	-0.0602(06)	-0.001	0.1016(25)	-0.0172(19)	2.6	0.68

[a]Renormalization factors for the experimental cross sections to be divided.

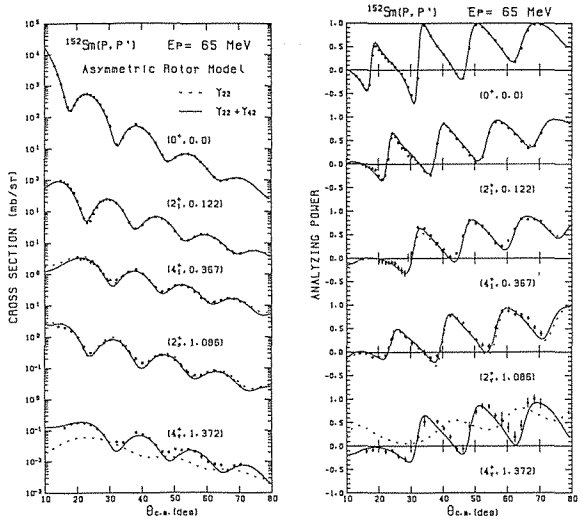

FIG. 15. Measured cross sections and analyzing powers for the 0^+, 2^+, and 4^+ states of the ground band and 2^+ and 4^+ states of the γ-band of ^{152}Sm by inelastic scattering of polarized protons at 65 MeV. The dotted (solid) curves show the best-fit result of the coupled-channel calculation assuming the static Y_{22} ($Y_{22}+Y_{42}$) γ-deformation.

then the band mixing parameters $A^l_{\alpha K}$ can be obtained. The band mixing parameters are listed in Table III.

The least-χ^2 fitting of the optical potential parameters and deformation parameters to the experimental data was carried out in the coupled-channel calculation assuming this asymmetric rotor model. The best-fit results of the coupled-channel calculation assuming this model are very similar to the results assuming the γ-vibrational model, except for ^{192}Os. Therefore, we show the results of the calculation only for ^{152}Sm, ^{176}Yb, and ^{192}Os. The result for ^{168}Er was reported in our previous paper.[1] The solid(dashed) curves in Figs. 15–17 show the best-fit results of the coupled-channel calculation assuming the $Y_{22}+Y_{42}$ (only Y_{22}) asymmetric deformation. Excellent fits have been

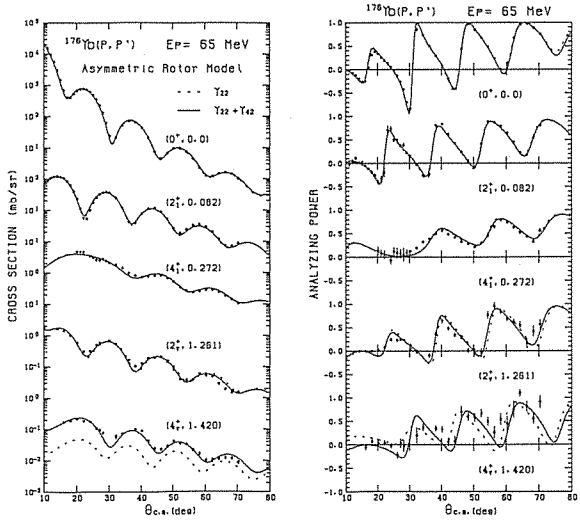

FIG. 16. The same as Fig. 15 except for ^{176}Yb.

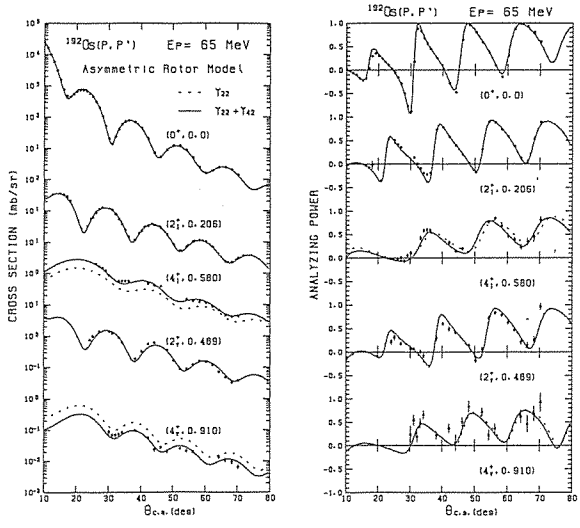

FIG. 17. The same as Fig. 15 except for ^{192}Os.

obtained for all the states by introducing the static Y_{42} deformation. The best-fit optical potential parameters, the deformation parameters, the χ^2/f values, and the renormalization factors of the experimental cross sections are listed in Table IV.

V. DISCUSSION

A. Quadrupole (Y_{22}) and hexadecapole (Y_{42}) transition strengths to the γ-vibrational band

In this section, we will first present the method of extracting the transition strength for a one-phonon vibration in a deformed nucleus from the form factors and deformation parameters of the nuclear matter density. Then we will discuss the relation of the form factors and deformation parameters between the nuclear matter density and the optical potential. Finally we will apply this method to the case of the γ-vibration.

1. *Transition strength to one-phonon state in a deformef nucleus*

In order to compare the results of hadronically induced excitation to electromagnetic transition rate, we present here the expressions for the reduced transition probabilities for matter multipole similar to the electric multipole. The isoscalar multipole operator $O(IS)$ is defined[54,55] similar to the electromagnetic transition operator[49] as follows:

$$O(IS) = Z/A \sum_{nucleons} r^l Y^*_{lm}(\Omega), \tag{35}$$

where the scaling factor Z/A has been introduced in order that if the relative neutron to proton contribution to the isoscalar transition operator is in the ratio N/Z, then the isoscalar and electromagnetic transition strengths will be numerically equal.

Within the framework of the collective model, the isoscalar matrix elements can be written in terms of the isoscalar mass transition density[54,55] as:

$$\begin{aligned} B(IS\lambda, 0 \to \lambda) &= (Z/A)^2 \left| <J_f| \,|\sum_{nucleons} r^l Y^*_{lm}|\,|J_i> \right|^2 . \\ &= (Z/A)^2 \left| \int r^l Y^*_{lm} \rho_{fi}(r) r^2 \mathrm{d}r \mathrm{d}\Omega \right|^2 . \end{aligned} \tag{36}$$

where $\rho_{fi}(r)$ represents the transition density which will be derived below. For collective vibrations in deformed nuclei, the nuclear matter surface is expanded similar to the potential surface in Eq. (4),

$$R^m(\Omega') = R_0^m \Big[1 + \sum_\lambda \beta^m_{\lambda 0} Y_{\lambda 0}(\Omega') + \sum_{\lambda' \mu'} \alpha^m_{\lambda' \mu'} Y_{\lambda' \mu'}(\Omega') \Big], \tag{37}$$

where $\beta^m_{\lambda 0}$ and $\alpha^m_{\lambda' \mu'}$ represent the static and dynamic deformation parameters for the nuclear matter density. The suffix m represents the quantity associated with the nuclear matter density. The nuclear matter density $\rho(r, \Omega)$ is expanded in first order in terms of $\alpha^m_{\lambda' \mu'}$ as:

$$\rho(r-R,\,\Omega')=\rho_0(r-R_\beta^m,\,\Omega')+\sum_{\lambda'\mu'}\alpha_{\lambda'\mu'}^m Y_{\lambda'\mu'}(\Omega')\rho_1(r-R_\beta^m,\,\Omega'),\tag{38}$$

where

$$R_\beta^m=R_0^m\Big[1+\sum_\lambda\beta_{\lambda0}^m Y_{\lambda0}(\Omega')\Big],\tag{39}$$

$$\rho_1(r-R_\beta,\,\Omega')=R_0^m\frac{\partial\rho(r-R,\,\Omega')}{\partial R}\Big|_{R=R_\beta^m}.\tag{40}$$

Then the transition density for the one-phonon vibration is given by

$$\rho_{fi}=\sum_{\lambda'\mu'}\eta_{\lambda'\mu'}^m Y_{\lambda'\mu'}R_0^m\frac{\partial\rho(r-R,\,\Omega')}{\partial\rho}\Big|_{R=R_\beta^m}.\tag{41}$$

where $\eta_{\lambda'\mu'}^m$ represents the amplitudes of the vibrations of the nuclear matter density associated with each $\alpha_{\lambda'\mu'}^m$. Substituting Eq. (41) in Eq. (36), we obtain the transition strength of the one-phonon vibration in a deformed nucleus as:

$$B(IS\lambda,\,0\to\lambda)=(Z/A)^2\Big\{\int\Big(\sum_{\lambda'\mu'}\eta_{\lambda'\mu'}^m Y_{\lambda'\mu'}\Big)R_0^m\frac{\partial\rho}{\partial R}Y_{\lambda\mu}^* r^{\lambda+2}\mathrm{d}r\mathrm{d}\Omega\Big\}^2.\tag{42}$$

If the nuclear matter density is spherical, then Eq. (42) can be reduced to a well-known formula using the orthonormality of the spherical harmonics:

$$B(IS\lambda,\,0\to\lambda)_{sph}=(Z/A)^2(\eta_{\lambda0}^m R_0^m)^2\Big\{\int\frac{\partial\rho(r)}{\partial\rho}r^{\lambda+2}\mathrm{d}r\Big\}^2\tag{43}$$

$$=(Z/A)^2(\eta_{\lambda0}^m R_0^m)^2\Big\{\frac{(\lambda+2)}{4\pi}<r^{\lambda-1}>_m\Big\}^2,\tag{44}$$

where $<r^{\lambda-1}>_m$ represents the radial moment of the nuclear matter density ρ of $(\lambda-1)$-th order. However, in surface vibration of deformed nuclei, Eqs. (43)–(44) are only the leading terms of Eq. (42), and it is necessary to use Eq. (42).

2. *Relation between the optical potential and the matter density*

We have obtained the form factors and the static and dynamic deformation parameters of the optical potential from the coupled-channel analysis. In order to calculate the transition strength, it is necessary to know the relation of the form factors and the deformation parameters between the optical potential and the nuclear matter density.

In the case of the static deformation, it is straightforward to obtain the relation.[56] According to a theorem due to Satchler[57], the (normalized) multipole moments of the optical potential ($q_{\lambda\mu}$) aer equal to those of the nuclear matter density, if the optical potential is given by folding the nuclear matter density with the effective interaction which is a function only of the distance of two interacting nucleons. That is,

$$q_{\lambda\mu}\equiv\frac{Z\int U(r,\,\Omega)Y_{\lambda\mu}(\Omega)r^{\lambda+2}\mathrm{d}r\mathrm{d}\Omega}{\int U(r,\,\Omega)r^2\mathrm{d}r\mathrm{d}\Omega}=\frac{Z\int\rho(r,\,\Omega)Y_{\lambda\mu}(\Omega)r^{\lambda+2}\mathrm{d}r\mathrm{d}\Omega}{\int\rho(r,\,\Omega)r^2\mathrm{d}r\mathrm{d}\Omega},\tag{45a}$$

if

$$U(r, \Omega) = \rho(r', \Omega')v_{eff}(|r-r'|)\,dr'd\Omega', \tag{45b}$$

where $v_{eff}(r)$ represents the effective two-body interaction between projectile and target nucleons. Using Eq. (45), we obtain the relation between the optical potential and the nuclear matter density. Note that Eq. (45b) is an approximation in actual nuclei, because the effective interaction is density dependent.[5-7,36-41]

In the case of the vibration, the story is not so simple. It is diffcult to drive the strict relations of the form factors and deformation parameters between the optical potential and nuclear matter density when the nuclear surface is oscillating. Up to now, it has been often assumed that the deformation length (βR) of the optical potential and nuclear matter density are equal, and that the nuclear matter density is uniform and has a sharp edge ($r_m=1.2fm$).[54] Nevertheless, we think it is better to assume Satchler's theorem[57] of Eq. (45) also in the case of vibrations, because Equation (45) includes the detailed difference of the form factors between the optical potential and matter density based on the folding model, while the simple βR scaling does not reflect the difference of the diffuseness of the surface of these two distributions. In addition, according to Owen and Satchler[58] serious errors may arise if an equivalent uniform distribution is used to compute the multipole moments of a distribution. Thus, we assume the relation of Eq. (45) in the case of the vibration. The optical potential U and the nuclear matter density ρ are expanded in first order in terms of $\alpha_{\lambda'\mu'}$ as shown in Eqs. (5)-(7) and Eqs. (37)–(39). Substituting these equations into Eq. (45), we have obtained the first-order expansion formula of Eq. (45) as follows:

$$\frac{\int \eta_{\lambda'\mu'} Y_{\lambda'\mu'} R_0 \frac{\partial U}{\partial R} Y^*_{\lambda\mu} r^{\lambda+2} dr d\Omega}{\int U r^2 dr d\Omega} = \frac{\int \eta^m_{\lambda'\mu'} Y_{\lambda'\mu'} R_0^m \frac{\partial U}{\partial R} Y^*_{\lambda\mu} r^{\lambda+2} dr d\Omega}{\int \rho r^2 dr d\Omega}, \tag{46}$$

where the suffix m represents the quantity associated with the nuclear matter density. Thus, we obtain the relation of the form factors and the deformation parameters between the optical potential and nuclear matter density in the case of vibration. Then the transition strength in Eq. (42) can be rewritten using Eq. (46) as follows:

$$B(IS\lambda, 0 \to \lambda) = (J_\rho/J_U)^2(Z/A)^2\left\{\int\left(\sum_{\lambda'\mu'} \eta_{\lambda'\mu'} Y_{\lambda'\mu'}\right) R_0 \frac{\partial U}{\partial R} Y^*_{\lambda\mu} r^{\lambda+2} dr d\Omega\right\}^2, \tag{47a}$$

where

$$(J_\rho/J_U) = \int \rho(r, \Omega) r^2 dr d\Omega / \int U(r, \Omega) r^2 dr d\Omega$$

$$= A/\int U(r, \Omega) r^2 dr d\Omega\,. \tag{47b}$$

Hence, we have obtained the formula for the isoscalar transition strength for the one-phonon vibration in deformed nuclei. This isoscalar transition strength obtained from inelastic hadron scattering is closely reoated to the electromagnetic transition strength as discussed above.

3. Y_{22} *and* Y_{42} *transition strenghs to the* γ*-vibrational band*

The quadrupole (Y_{22}) and hexadecapole (Y_{42}) transition strengths to the γ-vibrational band have been calculated using Eq. (47):

$$B(IS\lambda, 0\rightarrow\lambda) = (J_0/J_U)^2(Z/A)^2\left\{\int(\eta_{22}Y_{22}+\eta_{42}Y_{42})R_0\frac{\partial U}{\partial R}Y^*_{\lambda 2}r^{\lambda+2}drd\Omega\right\}^2, \quad (48)$$

where η_{22} and η_{42} represent the amplitudes of the vibration of the optical potential associated with the α_{22} and α_{42}, respectively, which have been determined by the coupled-channel analysis assuming the γ-vibrational model. We have used the real central part of the optical potential for U in Eq. (48), because the folding model of Eq. (45b) works well for the real central potential and the main part of the transition is generated by the real central potential. The calculated transition strengths are listed in Table V. In this table, the transition strengths in single particle units (spu) and their ratio to the total oscillator strength of each multipolarity by the sum rule[49] are also listed. The numbers in parentheses represent the uncertainties of each value calculated from the uncertainties of the deformation parameters in Table II.

Figures 18(c)–18(d) show the quadrupole (Y_{22}) and hexadecapole (Y_{42}) transition strengths to the γ-vibrational band as a function of mass number. The experimental Y_{22} strength increases with the mass number in the $152\leqq A\leqq 192$ region. The experimental Y_{42} transition strength increases with mass number in the $152\leqq A\leqq 168$ region and then decreases with mass number in the $168\leqq A\leqq 182$ region. The Y_{42} transition strengths again increase with mass number in the $182\leqq A\leqq 192$ region. The mass number dependence of the Y_{42} strength can be directly observed also in Figs. 3–12 by comparing the solid curves for the 4^+ states of the γ-vibrational band with dashed curves. The deviation of these two curves indicates the contribution of the Y_{42}-mode vibration to the γ-vibration.

Table V. The quadrupole (Y_{22}) and the hexadecapole (Y_{42}) transition strengths to the γ-vibrational band obtained by the present coupled-channel analysis for (p, p′) scattering at 65 MeV assuming the γ-vibrational model. These are also givin in terms of single-particle units and as a function of the classical sum rules.

Nucleus	$\hbar\omega_2$ (MeV)	$B(IS2;0\rightarrow 2_\gamma)$ (e^2b^2)	$\frac{B(IS2;0\rightarrow 2_\gamma)}{B_{sp}(IS2)}$	$\frac{\hbar\omega_2\cdot B(IS2;0\rightarrow 2_\gamma)}{S(IS2)_{class}}$	$\hbar\omega_4$ (MeV)	$B(IS4;0\rightarrow 4_\gamma)$ (e^2b^4)	$\frac{B(IS4;0\rightarrow 4_\gamma)}{B_{sp}(IS4)}$	$\frac{\hbar\omega_4\cdot B(IS4;0\rightarrow 4_\gamma)}{S(IS4)_{class}}$
^{152}Sm	1.086	1.101(57)×10^{-1}	4.57(24)	1.70(09)%	1.372	1.112(74)×10^{-2}	3.01(20)	0.122(08)%
^{154}Sm	1.440	0.832(65)×10^{-1}	3.36(27)	1.75(14)%	1.662	1.199(82)×10^{-2}	3.11(21)	0.172(12)%
^{160}Gd	0.989	1.158(50)×10^{-1}	4.49(19)	1.55(07)%	1.149	2.42(12) ×10^{-2}	5.69(29)	0.208(11)%
^{164}Dy	0.768	1.120(67)×10^{-1}	4.20(25)	1.10(07)%	0.916	2.93(27) ×10^{-2}	6.43(58)	0.186(02)%
^{166}Er	0.786	1.294(56)×10^{-1}	4.78(21)	1.23(05)%	0.956	3.30(26) ×10^{-2}	7.01(56)	0.197(16)%
^{168}Er	0.821	1.199(74)×10^{-1}	4.36(27)	1.19(07)%	0.995	3.98(32) ×10^{-2}	8.20(65)	0.256(20)%
^{176}Yb	1.261	0.966(63)×10^{-1}	3.37(21)	1.47(09)%	1.429	1.98(17) ×10^{-2}	3.61(31)	0.170(15)%
^{182}W	1.221	1.46(11) ×10^{-1}	4.75(35)	1.91(14)%	1.443	1.221(25)×10^{-2}	2.03(42)	0.094(20)%
^{184}W	0.903	1.609(73)×10^{-1}	5.18(23)	1.59(07)%	1.134	1.74(23) ×10^{-2}	2.82(37)	0.108(14)%
^{192}Os	0.480	2.89(19) ×10^{-1}	8.78(59)	1.58(11)%	0.910	2.33(31) ×10^{-2}	3.36(44)	0.114(15)%

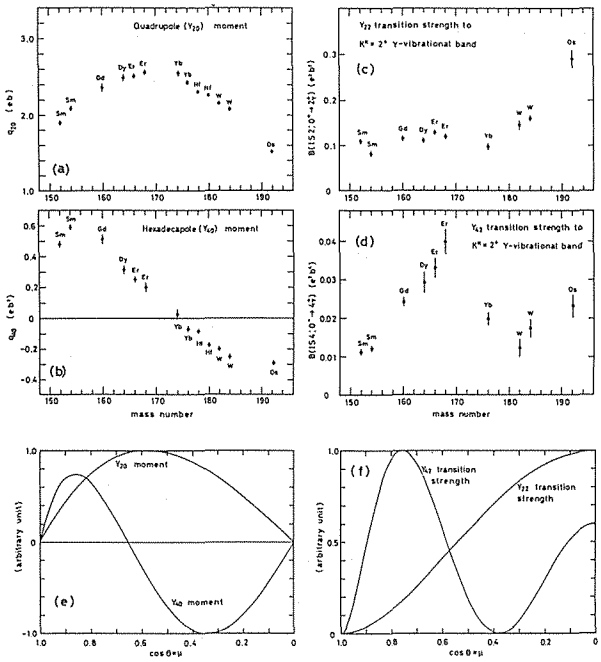

FIG. 18. (a) (b) The quadrupole (Y_{20}) and hexadecapole (Y_{40}) moments of the deformed optical potential obtained from the coupled-channel analysis of inelastic scattering of polarized protons at 65 MeV. (c) (d) The quadrupole (Y_{22}) and hexadecapole (Y_{42}) transition strengths to the γ-vibrational band obtained from the present coupled-channel analysis of inelestic scattering of polarized protons at 65 MeV. (e) The quadrupole (Y_{20}) and hexadecapole (Y_{40}) moments of a nucleus when the valence particles are filled from z-axis to $\mu=\cos\theta$ according to Bertsch. (ReF. 59) (f) The quadrupole (Y_{22}) and hexadecapole (Y_{42}) transition strengths to the γ-vibrational band according to the extension of the Bertsch's model.

Note that there are two regions in which the amplitude of the γ-vibration becomes large, *i.e.* the $A=168$ and $A=192$ regions. It is important that the characteristics of the γ-vibration are very different in these two regions. In the $A=168$ region, the $B(IS4)$ value is very large (7.0 spu for the ^{168}Er) and the $B(IS2)$ value is not so much large (4.8 spu for ^{168}Er). In the $A=192$ region, the $B(IS4)$ value is rather small (3.4 spu for ^{192}Os) and $B(IS2)$ value is large (8.8 spu for ^{192}Os). In other words, the hexadecapole (Y_{42}) γ-vibration is dominant in the $A=168$ region, while the quadrupole (Y_{22}) γ-vibration is dominant in the $A=192$ region.

B. Qualitative interpretation of the Y_{22} and Y_{42} transition strengths

The overall trend of the quadrupole (Y_{22}) and hexadecapole (Y_{42}) transition strength to the γ-vibrational band can be understood by expanding the polar cap model as described in our recent letter.[9]

The polar cap model for deformed nuclei was proposed by Bertsch[59] for a qualitative interpretation for the systematics of the hexadecapole (Y_{40}) moments of deformed nuclei reported by Hendrie *et al.*[21] At the beginning of the major shell, the

first four valence particles define a z-axis in the intrinsic frame. When filling the major shell, added particles are placed in orbits as close to the z-axis as possible. Eventually, the orbits are again filled to make a spherically symmetric distribution. Thus, the $q_{\lambda 0}$ moment of a nucleus in which the valence particles are filled from the z-axis to $\mu=\cos\theta$ is proportional to the integral

$$\int_{\mu}^{1} P_{\lambda 0}(x)\mathrm{d}x\,, \tag{49}$$

where $P_{\lambda 0}(x)$ is the λth Legendre polynomial, and $\mu=\cos\theta$ is the polar angle from the symmetry axis. Figure 18(e) shows the quadrupole (Y_{20}) and hexadecapole (Y_{40}) moments as predicted by this model. This model successfully explains the trends of the experimental values in Figs. 18(a)–18(b), which will be discussed in Sec. V C.

We have extended this model to the case of γ-vibrations. The quadrupole (Y_{22}) and hexadecapole (Y_{42}) transition strengths to the γ-vibraional band are given by $|<\gamma r^{\lambda} Y_{\lambda 2}|0>|^2$, where $\lambda=2,4$. When the valence particles are filled from the z-axis to $\mu=\cos\theta$, the Fermi surface lies around $\mu=\cos\theta$. Figure 19 shows this model schematically. The γ-vibration can be interpreted as the superposition of the particle-hole states with $K^{\pi}=2^{+}$ near the Fermi surface $(\mu\pm\Delta\mu)$. Then the transition strength is proportional to

$$\left[\int_{\mu-\Delta\mu}^{\mu+\Delta\mu} P_{\lambda 2}(x)dx\right]^2 \fallingdotseq (2\Delta\mu)^2\,[P_{\lambda 2}(\mu)]^2\,, \tag{50}$$

where the integration over φ has been replaced by a constant number because the φ-dependence of the $K^{\pi}=2^{+}$ γ-vibrational state is equal to that of $Y_{\lambda 2}$. Figure 18(f) shows the prediction of the quadrupole (Y_{22}) and hexadecapole (Y_{42}) transition strengths according to this model.

It is surprising that this simple model explains the overall trend of experimental values very well, especially for the Y_{42} transition strength. The success in explaining the Y_{22} and Y_{42} strengths by such a simple model means that the spatial location of the

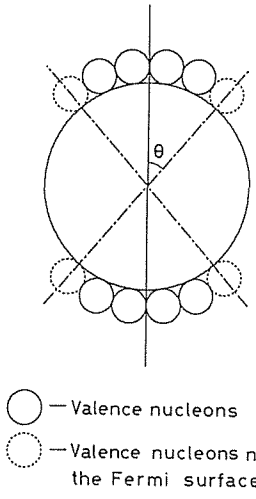

FIG. 19. Extended polar cap model for a deformed nucleus in which the valence nucleons are filled from the z-axis to $\mu=\cos\theta$.

particles occupying orbits near the Fermi surface changes gradually with the mass number owing to the very stable deformation in this mass region. This model is a simple representation of the shell-filling in the Nilsson potential for a single-j orbit. The energy of a single particle orbit becomes larger as the oscillator quanta n_z become smaller in a single-j orbit for a prolate deformation. This is the reason why the valence particles are placed in orbits as close to the z-axis as possible in the polar cap model. Although many single-j orbits exist in a major shell, the overall trend of the strengths are successfully predicted by the polar cap model.

C. Comparison of the Y_{22} and Y_{42} strengths with RPA calculation

In order to understand the systematic trend of quadrupole and hexadecapole transition strength to the γ-vibrational band microscopically and quantitatively, we compare the experimental results with RPA calculations by Matsuo.[60,61]

1. *RPA Model*

In the RPA calculation, the following Hamiltonian has been assumed.

$$H_{RPA} = H_{Nilsson} + H_{Pair} + H_{QQ}\,, \tag{51}$$

where $H_{Nilsson}$, H_{Pair}, and H_{QQ} represent the Nilsson Hamiltonian[62], the pairing interaction[63], and the quadrupole-quadrupole interaction in the doubly-stretched coordinate[64] ($Q''-Q''$ interaction), respectively. The strength of the pairing force was adjusted to reproduce the experimental odd-even mass difference and the strength of the $Q''-Q''$ force was adjusted to reproduce the experimental band-head energy of the γ-vibrational band, which is close to the self-consistent value given by Bohr and Mottelson.[49] Three major shells were employed for protons and neutrons as a model space.

In this model, the one-phonon state $|\gamma>$ is written as

$$\begin{aligned} |\gamma> &= \chi^{\dagger}|0>_{BCS} \\ &\doteqdot \sum_{\mu<\nu} \Psi(\mu,\nu) a_{\mu}^{\dagger} a_{\nu}^{\dagger} |0>_{BCS}\,, \end{aligned} \tag{52}$$

where $\chi^{\dagger}$ and $|0>_{BCS}$ represents the one-phonon creation operator and the BCS ground state, respectively, and $\Psi(\mu,\nu)$ represents the phonon amplitude. The $a_{\mu}^{\dagger}a_{\nu}^{\dagger}$ and μ, ν represent the two quasi-particle creation operator and the one particle orbits, respectively.

The phonon amplitude $\Psi(\mu,\nu)$ in Eq. (52) has the following functional form:

$$\Psi(\mu,\nu) \propto <\mu|\, r^2 Y_{22}\,|\,\nu>(u_{\mu}v_{\nu}+u_{\nu}v_{\mu})/(E_{\mu}+E_{\nu}-\omega_{\gamma}) \tag{53}$$

where $E_{\mu}=\sqrt{(\varepsilon_{\mu}-\varepsilon_F)^2+\Delta^2}$ represents the quasi-particle energy and ω_{γ} and u_{μ}, v_{ν} represent the excitation energy of the one-phonon state and the occupation factors, respectively.

The results of the RPA calculations are shown in Fig. 20 as various lines. The Y_{42} strengths of the RPA calculation were multiplied by 3.5 in this figure. Note that there is

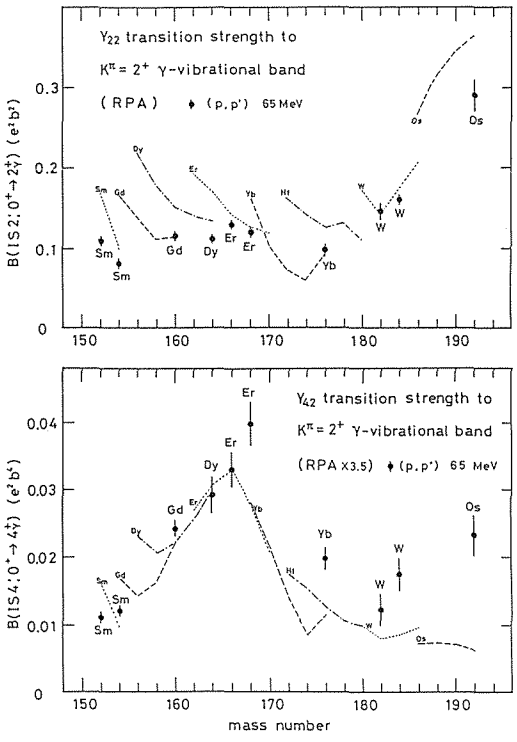

FIG. 20. The closed circles represent quadrupole (Y_{22}) and hexadecapole (Y_{42}) transition strengths to the γ-vibrational band obtained from the present coupled-channel analysis. Various lines indicate the results of the random phase approximation (RPA) calculation assuming the paring plus quadrupole-quadrupole (P+QQ) force. The results of the RPA calculation for the Y_{42} strength are multiplied by 3.5.

a little ambiguity in the absolute values of the RPA calculation owing to the restriction of the model space. The RPA calculation reproduces the mass number dependence of the experimental Y_{22} and Y_{42} strengths fairly well.

2. *Gross structure of the transition strength*

The gross structure of the RPA prediction is similar to the results of the polar cap model, although the RPA calculation reflects the detailed sub-shell structure. In the RPA calculation, the factor $(u_\mu v_\nu + u_\nu v_\mu)/(E_\mu + E_\nu - \omega_\gamma)$ in Eq. (53) becomes a maximum near the Fermi surface and the orbits near the Fermi surface change gradually with mass number according to the Nilsson model. This means that the following two assumptions in the polar cap model have been justified microscopically: (i) The transition strength to the γ-vibratioanl bands is dominated by the moments of the orbits near the Fermi surface. (ii) The location of the orbits near the Fermi surface changes gradually from the symmetry-axis to the equator with increasing mass number.

The experimental Y_{22} strengths are well explained by the RPA model for $152 \leqq A \leqq 192$. The experimental Y_{42} transition strengths increase with mass number in the $152 \leqq A \leqq 168$ region and then decrease with mass number in the $168 \leqq A \leqq 182$ region. The RPA calculation successfully reproduces the trend of the experimental Y_{42} transition strength in the $152 \leqq A \leqq 168$ region, while it fails to reproduce the data for the $168 \leqq A182$ region. Since these RPA calculations are based on an axially symmetric deformation, the resultant RPA predictions could be doubtful near the ^{192}Os region, where the nuclei are thought to be γ-unstable.

3. *Sub-shell structure effect*

According to Bohr and Mottelson[49,65], the strengths of γ-vibrations are affected by the sub-shell structure of the single-particle orbits in the deformed mean potential. In the region of ^{166}Er, the proton sub-shell $(N, n_z)=(4,1)$ (N; Principal quantum number, n_z; oscillator quantum number along the symmetry axis) and the neutron sub-shell $(N, n_z)=(5,3)$ which satisfy the selection rule of the γ-phonon excitation are half-filled and it is expected that the collectivity of the γ-vibration becomes large. The experimental Y_{22} strength has a broad local maximum near the ^{168}Er region. The RPA calculation successfully reproduces this trend, while the extended polar cap model do not reproduces this. In the extended polar cap model, we have assumed that the number of the particles near the Fermi surface which are responsible to the γ-phonon excitation is independent of the mass number [$\Delta\mu=const.$ in Eq. (50)]. However, this number changes with mass number in the actual nuclei. This effect is known as the sub-shell structure effect.[49,65] The collectivity of the γ-vibration is expected to be large in the ^{166}Er and ^{184}W regions, small in the ^{152}Sm and ^{172}Yb regions owing to the sub-shell structure effects. Therefore, the systematic behavior of the transition strengths to the γ-vibrational band is dominated by the moments of the orbits near the Fermi surface and modified a little by the sub-shell structure effects.

4. *The Y_{42} component in the γ-vibration*

The RPA calculation reproduces the trends of the Y_{42} strength, while it fails to reproduce the absolute values by about a factor of three. In the coupled-channel calculation, it is necessary to introduce the large Y_{42} vibration to reproduce the experimental data. Without the Y_{42} vibration, the calculated cross sections for the 4^+ states of the γ-vibrational band are about factors of 3–10 too small for all the measured nuclei, as shown in Figs. 3-12.

On the other hand, since this RPA calculation assumes only the $Q"-Q"$ force, only the Y_{22}-mode is induced in the γ-vibration. The Y_{42} transition strength of the RPA calculation is insufficient. Therefore, it will be necessary to introduce the Y_{42}-mode in the γ-vibration to explain the experimental Y_{22} and Y_{42} transition strengths consistently. In order to explain our experimental results for the Y_{42} strength to the γ-vibrational band in ^{168}Er, Nesterenko *et al.*[9] have also asserted the necessity of the hexadecapole-hexadecapole force.

D. Asymmetric rotor model

As described in the previous paper,[1] the coupled-channel calculation assuming the asymmetric rotor model yields very similar results to the γ-vibrational model, so long as the asymmetric deformation was not large. In the present analysis, the results of the coupled-channel calculation in the asymmetric rotor model are almost equal to those of the γ-vibrational model, except for ^{192}Os. For ^{192}Os, the asymmetric rotor model gives a better fit than does the γ-vibrational model, especially for the 4^+_γ state as shown in Figs. 12 and 17. The ^{192}Os nucleus is in the γ-unstable region and a Hartree-Fock calculation predicts a large static γ-deformation in this region.[65] The fact that the asymmetric rotor

model gives a better description of the experimental data than does the γ-vibrational model suggests the possible static γ-deformation of this nucleus.[53,65]

E. Multipole moments of deformed optical potential and a DDHF calculation

The (normalized) multipole moment of the deformed optical potential ($q_{\lambda\mu}$) is defined by Eq. (45a). The multipole moments of the real central part of the deformed optical potential (DOP) obtained by the coupled-channel analysis for our experimental data are listed in Table VI. In this table, multipole moments obtained by three kinds of coupled-channel analyses are presented, assuming the axially symmetric rigid rotor model, the γ-vibrational model, and the asymmetric rotor model. The multipole moments obtained by these three methods are almost equal within the mutual uncertainties as shown in Table VI. Therefore, the effect of the coupling to the γ-vibrational band on the multipole moments of the DOP is small as long as the amplitude of the γ-vibration is small. In the case of ^{192}Os, these statements are not applicable, because the amplitude of the γ-vibration is large in this nucleus. The quadrupole and hexadecapole moments of the DOP assuming the axially symmetric rigid rotor model are plotted in Fig. 21 as closed circles.

The overall trend of the quadrupole (Y_{20}) and hexadecapole (Y_{40}) moments can be understood by the polar cap model due to Bertsch[59] as described in Sec. V B. In order to investigate the systematic behavior of these multipole moments microscopically, we compare the multipole moments of the DOP with density-dependent Hartree-Fock(DDHF) calculations.

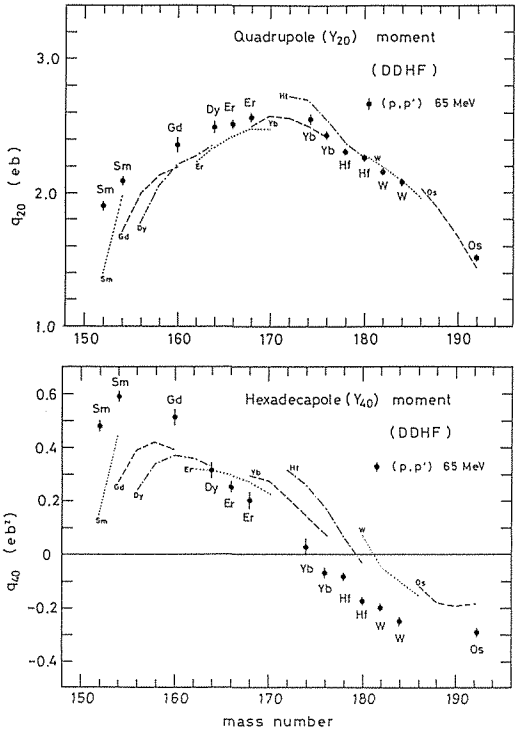

FIG. 21. The closed sircles represent quadrupole (Y_{20}) and hexadecapole (Y_{40}) moments of deformed optical potential obtained from the coupled-channel analysis. Various lines indicate the results of the density-dependent Hartree-Fock(DDHF) calculations in the framework of Negele and Rinker.

Table VI. The multipole moments of the deformed optical potential by (p, p′) scattering at 65 MeV in various models.

Nucleus	Symmetric rigid-rotor model[a]			γ-vibrational model[b]		Asymmetric rigid-rotor model[c]			
	Y_{20} (eb)	Y_{40} (eb^2)	Y_{60} (eb^3)	Y_{20} (eb)	Y_{40} (eb^2)	Y_{20} (eb)	Y_{40} (eb^2)	Y_{22} (eb)	Y_{42} (eb^2)
^{152}Sm	1.893(28)	0.486(13)	0.093(25)	1.889(35)	0.482(22)	1.895(36)	0.476(11)	0.373(08)	0.136(03)
^{154}Sm	2.094(41)	0.589(15)	0.094(14)	2.019(34)	0.580(21)	2.073(35)	0.619(15)	0.300(10)	0.124(03)
^{160}Gd	2.366(47)	0.512(19)	0.062(13)	2.387(54)	0.510(36)	2.382(51)	0.506(17)	0.373(07)	0.175(04)
^{164}Dy	2.487(46)	0.316(34)	-0.001(13)	2.448(43)	0.351(29)	2.454(41)	0.356(37)	0.375(09)	0.191(06)
^{166}Er	2.511(32)	0.252(20)	-0.025(07)	2.505(31)	0.269(21)	2.499(28)	0.263(42)	0.401(07)	0.200(05)
^{168}Er	2.564(38)	0.198(31)	-0.078(12)	2.567(38)	0.182(26)	2.528(40)	0.181(31)	0.382(08)	0.208(06)
^{176}Yb	2.436(32)	-0.071(20)	-0.104(07)	2.444(51)	-0.108(35)	2.452(47)	-0.111(19)	0.339(09)	0.137(05)
^{182}W	2.182(24)	-0.201(13)	-0.130	2.214(32)	-0.213(23)	2.206(31)	-0.216(10)	0.406(11)	0.110(07)
^{184}W	2.080(27)	-0.249(12)	-0.090	2.101(30)	-0.256(21)	2.074(31)	-0.263(09)	0.444(09)	0.121(07)
^{192}Os	1.509(25)	-0.295(12)		1.452(20)	-0.290(13)	1.310(20)	-0.314(13)	0.841(16)	-0.016(08)

[a]Multipole moments of the DOP obtained by the coupled-channel analysis for 0^+-6^+ members of the ground state rotational band assuming the axially symmetric rigid rotor model. (Present works for ^{152,154}Sm, ^{160}Gd, ^{164}Dy, and ^{192}Os. Others are taken from Refs. 5-6)

[b]Multipole moments of the DOP obtained by the coupled-channel analysis for 0^+-4^+ members of the ground band and 2^+-4^+ members of the γ-band assuming the γ-vibrational model. (Present works)

[c]Multipole moments of the DOP obtained by the coupled-channel analysis for 0^+-4^+ members of the ground band and 2^+-4^+ members of the γ-band assuming the asymmetric rotor model. (Present work)

The DDHF calculations were performed using the code HARFE developed by Vautherin and Brack in the framework of Negele and Rinker.[67-70] The calculations assume axially symmetric nuclear distributions and use the density matrix expansion (DME) effective Hamiltonian and the pairing approximation. The calculations were made using a basis consisting of 14 oscillator quanta. The DDHF calculations were performed on a vector processor (FACOM VP-200), and each iteration requires about 15 sec of CPU time. The calculation was performed for 34 nuclei in the $152 \leqq A \leqq 192$ region. For each nucleus, 75 iterations were carried out to guarantee the convergence of the results. The results for ^{154}Sm, ^{156}Gd, ^{166}Er, and ^{176}Yb are consistent with the values reported by Negele and Rinker.[67]

The quadrupole and hexadecapole moments of the proton, neutron, and matter distribution, and the root-mean-square radii of the proton, neutron, and charge distributions, and the binding energies per nucleon obtained from the DDHF calculations are listed in Table VII. These multipole moments are normalized by Z, as shown in Eq. (45a). The quadrupole and hexadecapole moments of the metter distributions are plotted as various lines in Fig. 21 for each isotope.

The quadrupole moments of the DOP increase with mass number in the $152 \leqq A \leqq 170$ region and then decrease with mass number in the $170 \leqq A \leqq 192$ region as shown in Fig. 21. The DDHF calculation reproduces the quadrupole moments quantitatively. The hexadecapole moments of the DOP decrease with mass number in the

Table VII. The (normalized) multipole moments and root-mean-square(rms) radii of proton(p), neutron(n), matter(m), and charge(c) distributions and the binding energies per nucleon from the DDHF calculations.

Nucleus	q^p_{20} (eb)	q^n_{20} (eb)	q^m_{20} (eb)	q^p_{40} (eb^2)	q^n_{40} (eb^2)	q^m_{40} (eb^2)	R^p_{rms} (fm)	R^n_{rms} (fm)	R^c_{rms} (fm)	E_B/A (MeV)
^{152}Sm	1.43	1.37	1.39	0.13	0.16	0.14	5.00	5.18	5.06	8.16
^{154}Sm	2.01	1.95	1.97	0.42	0.46	0.44	5.06	5.24	5.11	8.14
^{154}Gd	1.79	1.65	1.71	0.26	0.28	0.27	5.06	5.20	5.11	8.14
^{156}Gd	2.04	1.96	2.00	0.36	0.41	0.39	5.09	5.25	5.14	8.13
^{158}Gd	2.16	2.11	2.13	0.39	0.44	0.42	5.11	5.29	5.16	8.12
^{160}Gd	2.21	2.19	2.20	0.37	0.41	0.39	5.13	5.32	5.18	8.10
^{156}Dy	1.86	1.70	1.77	0.22	0.24	0.23	5.10	5.21	5.15	8.10
^{158}Dy	2.11	2.01	2.06	0.31	0.36	0.34	5.13	5.26	5.18	8.10
^{160}Dy	2.24	2.18	2.20	0.34	0.39	0.37	5.15	5.30	5.20	8.10
^{162}Dy	2.31	2.26	2.28	0.33	0.37	0.35	5.16	5.33	5.21	8.09
^{161}Dy	2.37	2.33	2.36	0.31	0.34	0.33	5.18	5.36	5.23	8.08
^{162}Er	2.28	2.21	2.24	0.28	0.34	0.32	5.18	5.30	5.23	8.07
^{164}Er	2.37	2.32	2.34	0.28	0.33	0.31	5.20	5.34	5.25	8.07
^{166}Er	2.44	2.41	2.42	0.27	0.31	0.29	5.21	5.37	5.26	8.07
^{168}Er	2.49	2.48	2.48	0.25	0.28	0.27	5.23	5.40	5.28	8.06
^{170}Er	2.48	2.48	2.48	0.21	0.23	0.22	5.24	5.43	5.29	7.96
^{168}Yb	2.52	2.48	2.50	0.26	0.31	0.29	5.25	5.38	5.30	8.04
^{170}Yb	2.60	2.57	2.58	0.25	0.28	0.27	5.26	5.41	5.31	8.04
^{172}Yb	2.58	2.55	2.56	0.20	0.22	0.21	5.27	5.44	5.32	8.03
^{174}Yb	2.52	2.51	2.51	0.13	0.14	0.14	5.28	5.46	5.33	8.02
^{176}Yb	2.44	2.43	2.43	0.070	0.062	0.065	5.29	5.48	5.33	8.00
^{172}Hf	2.76	2.70	2.72	0.31	0.33	0.32	5.30	5.42	5.35	8.00
^{174}Hf	2.73	2.68	2.70	0.25	0.26	0.26	5.31	5.45	5.36	8.00
^{176}Hf	2.55	2.55	2.55	0.16	0.16	0.16	5.31	5.47	5.36	8.00
^{178}Hf	2.36	2.39	2.38	0.062	0.057	0.059	5.31	5.48	5.56	7.99
^{180}Hf	2.26	2.28	2.27	−0.054	−0.032	−0.040	5.32	5.51	5.37	7.98
^{180}W	2.30	2.27	2.28	0.079	0.060	0.067	5.33	5.48	5.38	7.79
^{182}W	2.16	2.23	2.20	−0.079	−0.036	−0.053	5.34	5.50	5.39	7.96
^{184}W	2.05	2.12	2.10	−0.079	−0.12	−0.105	5.34	5.53	5.39	7.95
^{186}W	1.95	1.97	1.96	−0.13	−0.18	−0.16	5.34	5.55	5.40	8.86
^{186}Os	1.96	2.08	2.04	−0.10	−0.14	−0.12	5.36	5.52	5.41	7.92
^{188}Os	1.81	1.92	1.88	−0.16	−0.20	−0.18	5.37	5.54	5.41	7.92
^{190}Os	1.63	1.71	1.68	−0.17	−0.21	−0.20	5.37	5.56	5.42	7.91
^{192}Os	1.42	1.46	1.44	−0.17	−0.20	−0.19	5.37	5.57	5.42	7.90

$154 \leqq A \leqq 192$ region. The DDHF calculation explains the overall trend of the hexadecapole moments. However, there are quantitative discrepancies in the hexadecapole moments between the DOP and DDHF calculation. Similar discrepancies were also obtained[46] in describing the transitions to 4^+ and 6^+ states in electron scattering. These discrepancies may indicate the limit of this approximation.

F. Comparison with other measurements and density-dependence of the effective interaction

Let us now compare our experimental results with those obtained from the other experiments, especially Coulomb excitation and electron scattering. The multipole moments of the deformed optical potentials (DOP) obtained from the inelastic scattering of 65-MeV polarized protons and from other experiments are listed in Table VIII. The transition strengths to the γ-vibratioanl band obtained from the present experiment and from other experiments are listed in Table IX. Since the uncertainties of Y_{40} moments obtained by Coulomb excitation are too large and no data have been available for the Y_{42} strength by Coulomb excitation or electron scattering, we compare only our experimental results of Y_{20} moments and Y_{22} strengths with corresponding electromagnetic values. The Y_{20} moments and Y_{22} strengths obtained from the present experiment are plotted in FIg. 22 as closed circles and those obtained form the Coulomb excitation and the electron scattering are plotted as poen circles.[71-94]

Table VIII. The multipole moments of the deformed optical potentials obtained from the present experiment and from other experiments. Uncertainties are shown in parenthese.

Nucleus	Reactions		$q_{20}(eb)$	$q_{40}(eb^2)$	$q_{60}(eb^3)$	Ref.
^{152}Sm	(p,p')	65 MeV	1.893(28)	0.486(13)	0.093(25)	This work
	(d,d')	56 MeV	1.879	0.388		17
	(α,α')	50 MeV	2.12	0.52	0.05	21
	CE[a]		1.865(12)	0.373(70)		71
^{154}Sm	(p,p')	35 MeV	2.06(3)	0.54(2)		15
	(p,p')	51 MeV	2.15	0.36	0.07	16
	(p,p')	65 MeV	2.094(41)	0.589(15)	0.094(14)	This work
	(p,p')	134 MeV	2.31(8)	0.62(6)	0.19(4)	10
	(p,p')	800 MeV	2.12	0.58	0.099	12
	(d,d')	56 MeV	2.073	0.554	0.141	17
	(α,α')	50 MeV	2.38	0.61	0.04	21
	(α,α')	120 MeV	2.107	0.529	0.137	19
	CE		2.093(15)	0.540(74)		71
^{160}Gd	(p,p')	65 MeV	2.366(47)	0.512(19)	0.062(13)	This work
	CE		2.292(14)	0.15(±$\frac{3}{5}$)		71
^{164}Dy	(p,p')	65 MeV	2.487(46)	0.316(34)	-0.001(13)	This work
	CE		2.370(20)	0.075(±$\frac{18}{28}$)		71
^{166}Er	(p,p')	65 MeV	2.511(32)	0.252(20)	-0.025(7)	5
	(p,p')	134 MeV	2.50(8)	0.32(6)	-0.01(3)	10
	(α,α')	50 MeV	2.68	0.28	-0.10	21
	(e,e')	50-320 MeV	2.41	0.284	0.0101	23
	CE		2.378(11)	0.32(16)		72
	CE		2.432(5)	0.242(72)		73
	CE		2.419(9)	0.22(±$\frac{4}{6}$)		74
	CE		2.40(2)	0.06(±$\frac{4}{8}$)		75
^{168}Er	(p,p')	65 MeV	2.564(38)	0.198(31)	-0.078(12)	5
	(α,α')	36 MeV	2.61(16)	0.063(23)	0.085(11)	2
	CE		2.43(2)	0.11(±$\frac{6}{8}$)		72
	CE		2.40(2)	0.20(±$\frac{6}{8}$)		75
^{174}Yb	(p,p')	65 MeV	2.547(39)	0.025(31)	-0.099(29)	5
	(α,α')	50 MeV	2.75	-0.10	-0.09	21
	(e,e')	95-325 MeV	2.28	0.102	-0.060	24
	CE		2.439(12)	0.21(±$\frac{4}{8}$)		76
	CE		2.433(12)	0.23(17)		77
^{176}Yb	(p,p')	35 MeV	2.29(5)	-0.09(3)		15
	(p,p')	65 MeV	2.436(32)	-0.071(20)	-0.104(7)	5
	(p,p')	134 MeV	2.31(6)	0.052(44)	-0.071(20)	11
	(p,p')	800 MeV	2.31	0.36	-0.048	12
	(α,α')	50 MeV	2.76	-0.17	-0.15	21
	(e,e')	50-320 MeV	2.30	-0.128	-0.0054	23
	CE		2.325(19)	0.28(±$\frac{11}{20}$)		76
^{178}Hf	(p,p')	65 MeV	2.311(22)	-0.083(13)	-0.126	6
	(α,α')	50 MeV	2.50	-0.39	-0.14	21
	CE		2.204(12)	0.23(±$\frac{15}{27}$)		78
^{180}Hf	(p,p')	65 MeV	2.260(24)	-0.174(13)	-0.129	6
	CE		2.176(10)	0.21(±$\frac{11}{20}$)		78
^{182}W	(p,p')	65 MeV	2.182(24)	-0.201(13)	-0.130	6
	(p,p')	134 MeV	2.03(6)	0.025(±$\frac{13}{33}$)	-0.071(20)	11
	(α,α')	13-21 MeV	2.053	-0.30		72
	(α,α')	24 MeV	2.13(10)	-0.775(196)		20
	CE		2.053(15)	-0.63(±$\frac{24}{16}$)		72
^{184}W	(p,p')	65 MeV	2.080(27)	-0.249(12)	-0.090	6
	(α,α')	13-19 MeV	1.94	-0.243		72
	(α,α')	24 MeV	2.30(21)	-0.427(122)		20
	CE		1.94(2)	-0.68(25)		72
^{192}Os	(p,p')	65 MeV	1.509(25)	-0.295(12)		This work
	(e,e')	150-364 MeV	1.417(11)	-0.191(11)		4
	CE		1.457(17)	-0.585		79
	CE		1.428(21)			80
	CE		1.411(38)			81
^{232}Th	(p,p')	35 MeV	2.98(6)	0.98(5)		15
	(p,p')	35 MeV	2.82(4)	0.98(4)	0.30(4)	14
	(p,p')	65 MeV	3.132(42)	1.190(42)	0.348(7)	7
	(e,e')	50-320 MeV	3.07	1.04	0.31	23
	CE		3.01(2)	1.22(15)		82
^{238}U	(p,p')	35 MeV	3.30(6)	0.81(6)		15
	(p,p')	35 MeV	3.25(3)	0.88(3)	0.10(3)	14
	(p,p')	65 MeV	3.537(44)	1.159(34)	0.241(6)	7
	(e,e')	50-320 MeV	3.48	0.99	0.27	23
	CE		3.51(2)	0.83(22)		82

[a]Charge multipole moments obtained by Coulomb excitation.

Nucleus	$\hbar\omega_2$ (MeV)	$B(IS2;0\to2_\gamma)$ (e^2b^2)	$B(E2;0\to2_\gamma)$ (e^2b^2)	Ref.
^{152}Sm	1.086	$1.101(57)\times10^{-1}$	$0.081(6)\times10^{-1}$	83
			$0.092(5)\times10^{-1}$	84
^{154}Sm	1.440	$0.832(65)\times10^{-1}$	$0.069(10)\times10^{-1}$	85
			$0.059(9)\times10^{-1}$	86
			$0.066(15)\times10^{-1}$	87
^{160}Gd	0.989	$1.158(50)\times10^{-1}$	$0.088(4)\times10^{-1}$	88
			$0.101(3)\times10^{-1}$	89
			$0.104(4)\times10^{-1}$	90
^{164}Dy	0.768	$1.120(67)\times10^{-1}$	$0.114(6)\times10^{-1}$	88
			$0.122(\frac{+4}{-3})\times10^{-1}$	84
			$0.121(5)\times10^{-1}$	90
^{166}Er	0.786	$1.294(56)\times10^{-1}$	$0.140(8)\times10^{-1}$	91
			$0.140(6)\times10^{-1}$	90
^{168}Er	0.821	$1.199(74)\times10^{-1}$	$0.131(8)\times10^{-1}$	91
			$0.130(5)\times10^{-1}$	90
^{176}Yb	1.261	$0.986(63)\times10^{-1}$	$0.050(4)\times10^{-1}$	92
^{182}W	1.221	$1.46(11)\times10^{-1}$	$0.124(6)\times10^{-1}$	93
^{184}W	0.903	$1.609(73)\times10^{-1}$	$0.138(6)\times10^{-1}$	90
^{192}Os	0.480	$2.89(19)\times10^{-1}$	$0.189(32)\times10^{-1}$ [a]	4
			$0.215(19)\times10^{-1}$	94
			$0.196(12)\times10^{-1}$	93

Table IX. The quadrupole (Y_{22}) transition strengths to the 2^+ member of the γ-vibrational band obtained from the present (p, p′) experiments [$B(IS2)$] and from Coulomb excitation [$B(E2)$].

[a]This value is obtained from electron scattering.

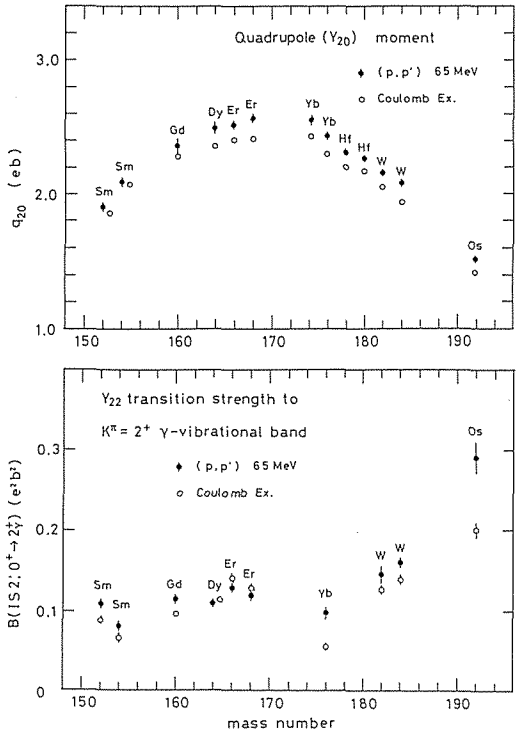

FIG. 22. The closed circles represent quadrupole (Y_{20}) moment of the deformed optical potential and quadrupole (Y_{22}) transition strength to the γ-vibrational band obtained from the coupled-channel analysis of this experiment. The open circles represent those obtained by electron scattering and Coulomb excitation.

1. *Quadrupole* (Y_{20}) *moment*

The quadrupole moments of the DOP are 4-6% larger than those of the charge distributions for all the measured nuclei except for ^{154}Sm as shown in Fig. 22. In the previous papers,[5-7] we have shown that the quadrupole moments of the DOP shoud be 4-6% larger than those of the nuclear matter densities, if we assume the density dependence of the effective interactions.[36-41] The quadrupole moments of the proton and neutron distributions predicted by the DDHF calculation are almost equal (within the 2% for the measured nuclei) as shown in Table VII. Therefore, the systematic difference (4-6%) of the quadrupole moments between the DOP at 65 MeV and charge distributions for almost all the measured nuclei is thought to be mainly due to the density dependence of the effective interaction.[3-5,36-41] In ^{154}Sm, the quadrupole moment of the neutron distribution is 3% smaller than that of the proton distribution according to the DDHF calculation. Therefore it could be possible that the exceptional small difference of the quadrupole moments of the DOP and charge distributions in ^{154}Sm is due to the different quadrupole deformations of protons and neutrons in this nucleus. In ^{232}Th and ^{238}U, the quadrupole moments of the DOP are only 1-2% larger than those of charge distributions.[7] This phenomenon could be explained by taking account of the Coulomb energy correction in the folding model together with the density dependece of the effective interaction.[7] The effect of the density dependence of the effective interaction has been also discussed in 134-MeV (p, p') scattering by Ronningen *et al.*[10] and Lay *et al.*[11] This effect is negligible at 800-MeV (p, p') scattering where the impulse approximation works well for the imaginary part of the optical potential, as discussed by Barlett *et al.*[12]

For almost all the nuclei for which we have measured inelastic proton scattering at 65 MeV, the difference between the quadrupole moment of the DOP and the charge quadrupole moment is explained quantitatively by the density dependence of the effective interaction. However, for the hexadecapole and hexacontatetrapole moments, there remain quantitative discrepancies if only density dependence is considered.[3-5] It is desired to investigate these theoretically in the view point of nuclear structure.

2. *Quadrupole* (Y_{22}) *transition strength*

The Y_{22} strengths obtained from the present experiment are generally 10-20% larger than those obtained from the Coulomb excitation, as shown in Fig. 22. If the transition matrix elements for protons and neutrons are equal and we assume the relation in Eq. (46), these transition strengths should be equal. The effect of the density dependence of the effective interaction is estimated by substituting the potential U, which has been obtained from Eq. (45b) assuming the density dependent effective interaction, into Eq. (47). This effect increases the Y_{22} transition strength by about 10–12% in comparison with the density independent case. Therefore the gross features of the systematic difference of the Y_{22} strength between the present measurements and Coulomb excitation are also due to the density dependence of the effective interaction. The detailed difference for each nucleus may reflect the differences of the proton and neutron transition matrix elements themselves.

VI. SUMMARY AND CONCLUSIONS

We have carried out a systematic investigation of the inelastic scattering of polarized protons at 65 MeV, exciting the 2^+ and 4^+ members of the $K^\pi=2^+$ γ-vibrational band in ^{152,154}Sm, ^{160}Gd, ^{164}Dy, ^{166,168}Er, ^{176}Yb, ^{182,184}W, and ^{192}Os.

Two kinds of coupled-channel analyses have been performed assuming the γ-vibrational model and the asymmetric rotor model. Excellent fits have been obtained for all the states by introducing both quadrupole (Y_{22}) and hexadecapole (Y_{42}) components in the γ-motion. The difference between the coupled-channel calculations assuming the γ-vibrational model and the asymmetric rotor model is very small except for ^{192}Os. The asymmetric rotor model gives slightly better descriptions than the γ-vibrational model for ^{192}Os, especially for the 4^+ states. This suggests the possible staic γ-deformation of ^{192}Os.

The quadrupole (Y_{22}) and hexadecapole (Y_{42}) transition strengths to the γ-vibrational band have been extracted from the optical potential parameters and the deformation parameters. They show a strong mass number dependence. This systematic behavior can be understood qualitatively by extending the polar cap model together with the systematics of the quadrupole (Y_{20}) and hexadecapole (Y_{40}) moments.

The Y_{22} and Y_{42} transition strengths to the γ-vibrational band have been compared with the prediction of an RPA calculation assuming the paring plus quadrupole-quadrupole interaction. The overall trends of the Y_{22} and Y_{42} transition strengths to the γ-vibrational band have been well reproduced by the RPA calculation. However, for the Y_{42} transition strength, the RPA calculation fails to reproduce the absolute values about by about a factor of three. In the coupled-channel calculation, it has been necessary to introduce large Y_{42} components to reproduce the exerimental data for the 4^+ state of the γ-band. This indicates the necessity of the Y_{42} vibration of the potential, *i.e.* a Y_{42}-mode in the γ-vibration, to reproduce the experimental Y_{42} transition strength.

The quadrupole (Y_{20}) and hexadecapole (Y_{40}) moments of the deformed optical potentials (DOP) have compared with the prediction of a density-dependent Hartree-Fock (DDHF) calculation using the density matrix expansion effective Hamiltonian in the framework of Negele and Rinker. The DDHF calculation reproduces the quadrupole moment of DOP very well, but it reproduces only the overall trend of the hexadecapole moments.

The quadrupole moments of the DOP are 4-6% larger than those obtained by Coulomb excitation for almost all the measured nuclei. This systematic difference can be understood by the density-dependence of the effective interaction assuming the equal quadrupole moments for proton and neutron distributions. Similar trends are also observed in the Y_{22} transition strength.

The present work has revealed the importance of the hexadecapole (Y_{42}) degree of freedom in the collective γ-motion over the whole range of deformed nuclei for the first time.

Acknowledgments

The experimental group consisted of Professor S. Kobayashi, Profeesor H. Sakaguchi, Dr. M. Nakamura, Mr. M. Yosoi, Mr. M. Ieiri, Mr. Y. Takeuchi, Mr. H. Togawa, and Mr. T. Tsutsumi, all of whom devoted a large amount of time and effort throughout the experiment. In the early stage of experiment, Dr. T. Noro, Dr. F. Ohtani, Dr. H. Sakamoto, Dr. H. Ogawa, and Mr. N. Issiki collaborated with us. Their excellent collaborations at the every stage of the experiment from the preparation of the experiment to the discussions are greatly appreciated. The author is particularly indebted to Professor S. Kobayashi, Professor H. Sakaguchi, and Dr. M. Nakamura for their efficient guidances and suggestions not only during the experiment but also in the satage of the discussions. The author is also grateful to the staff of the cyclotron at the RCNP for their cooperation during the experiment, and to Dr. Sugai at the Institute of Nuclear Study (INS), University of Tokyo for preparation of the ^{192}Os target. He is also indebted to to Dr. M. Matsuo at Kyoto University for his RPA calculation and discussions, and to Professor M. Matsuyanagi at Kyoto University and to Dr. Iida at RCNP for discussions and to Professor Negele and Professor Rinker for the usage of their DDHF code. Sincere thanks are expressed to Dr. J. Raynal for the usage of his code ECIS79, and to Dr. L. Ray for sending his modified version of the code JUPITOR and Dr. M. N. Harakeh for the modified version of the code CHUCK3, which were used for cross-checking the results of our modidied version of the code ECIS79. Sincere thanks are also expressed to Professor R. J. Peterson at University of Colorado for reading this manuscript and important suggestions. The authore is grateful to Professor M. Ishihara at the Institute of Physical and Chemical Research (RIKEN) for his encouragement. The coupled-channel calculation has been performed on a FACOM M-380 computer at RIKEN and partially on a FACOM M-340 computer at the Department of Physics, Kyoto University, and DDHF calculation has been performed on a vector processor (FACOM VP-200) at the Fujitsu System Laboratory.

APPENDIX A: Octupole-vibrational states

A strong enhancement for excitation of the 1^-, 3^-, and 5^- states has been obserbed in some deformed nuclei by (p, p') scattering at 65 MeV in this experiment. Typical spectra for these states are shown in Fig. 1 for ^{152}Sm case. In this appendix, we analyze these states for ^{152}Sm and ^{160}Gd. These 1^-, 3^-, and 5^- states are thought to be the members of the $K^\pi=0^-$ octupole-vibrational band.[93] Augular distributions of the experimental cross sections and analysing powers are shown in Figs. 23-24.

Coupled-channel analyses[13] for the 1^-, 3^-, and 5^- states of the octupole-vibrational band and the 0^+, 2^+, and 4^+ states of the ground state rotational band have been performed using the modified version of the code ECIS79 as described in Sec III. We took into account only the octupole (Y_{30}) vibration for the $K^\pi=0^-$ octupole-vibrational states. In this model, the potential surface is expanded using Eq. (4) as:

$$R(\Omega') = R_0\Big[1+\sum_{\lambda=2,4,6}\beta_{\lambda 0}\,Y_{\lambda 0}(\Omega')+\alpha_{30}\{Y_{30}(\Omega')+\varkappa Y_{10}(\Omega')\}\Big], \tag{A1}$$

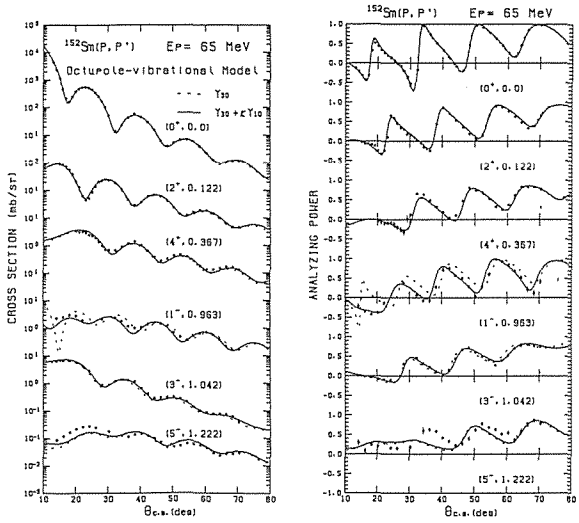

FIG. 23. Measured cross sections and analyzing powers for the 0^+, $^{2+}$, and 4^+ states of the ground band and 1^-, 3^-, and 5^- states of the octupole-band or ^{152}Sm by inelastic scattering of polarized protons at 65 MeV. The dotted (solid) curves show the best-fit result of the couped-channel calculation assuming the octupole-vibration with (without) the correction to remome the center-of mass motion.

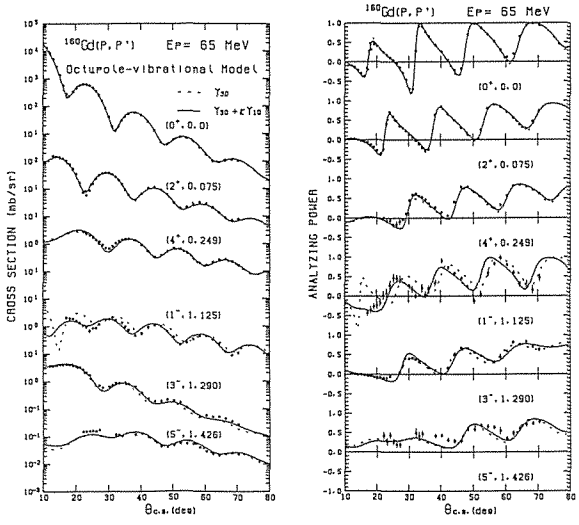

FIG. 24. The same as Fig. 23 except for ^{160}Gd.

where α_{30} is a collective coordinate corresponding to the octupole (Y_{30}) vibration, and the term κY_{10} has been introduced in order to remove the spurious center-of-mass motion due to the Y_{30} vibration in deformed nuclei. The constant k has been determined using the following equation:

$$\int U(r, \Omega') Y_{10}(\Omega') r^3 \mathrm{d}r \mathrm{d}\Omega' = 0 . \tag{A2}$$

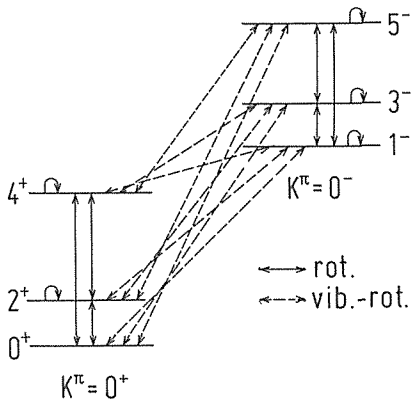

FIG. 25. Coupling scheme of the coupled-channel calculation assuming the octupole-vibrational model. Solid lines with arrows indicate the rotational coupling and dashed lines with arrows indicate the vibration-rotation coupling.

The form factors in the coupled-channel calculation assuming the potential surface in Eq. (A1) are described in Sec. III. The coupling scheme is presented in Fig. 25.

Solid curves in Figs. 23–24 show the best-fit results of the coupled-channel calculation assuming this octupole-vibrational model with the correction terms to remove the center-of-mass motion. Excellent fits have been obtained for all the states. In fitting the 5^- states it is not necessary to introduce the Y_{50}-vibration, contrary to the case of the γ-vibrational states, which require the Y_{42}-vibration in addition to the Y_{22}-vibration. The best-fit optical potential parameters, the deformation parameters, the χ^2/f values, and the renormalization factors of the experimental cross sections are listed in Table A1. Dashed curves in Figs. 23-24 show the best-fit results of the coupled-channel calculation without the correction term for the center-of-mass motion. Large unnatural oscillations in the cross sections and analysing poweres for the 1^- states in the 10°–25° region are obtained without the correction term; these features are initiated by the spurious center-of-mass motion.

Table AI. The optical potential parameters and deformation parameters in the octupole-vibrational model as obtained by present coupled channel analysis assuming the octupole-vibrational model.

Nucleus	V_R (Mev)	r_R (fm)	a_R (fm)	W_v (Mev)	r_{Wv} (fm)	a_{Wv} (fm)	W_s (MeV)	r_{Ws} (fm)	a_{Ws} (fm)	V_{ls} (MeV)	r_{ls} (fm)	a_{ls} (fm)	β_{20}	β_{40}	β_{60}	η_{30}	χ^2/f	N_0^a
^{152}Sm	38.86	1.220	0.744	7.07	1.105	0.750	6.60	1.223	0.631	5.58	1.164	0.627	0.2332(41)	0.0616(22)	-0.007	0.0778(13)	7.4	1.00
^{160}Gd	38.53	1.221	0.718	10.35	0.879	0.688	7.88	1.202	0.658	5.46	1.156	0.632	0.2745(53)	0.0496(25)	-0.013	0.0590(12)	5.3	0.91

[a]Renormalization factors for the experimental cross sections to be divided.

The success in reproducing the cross sections and analyzing powers for these octupole-vibrational states indicates that the very simple expansion of the potential surface in Eq. (A1) according to the Bohr-Mottelson picture is a very proper approximation for describing the transition to the octupole vibrational states. The systematics behavior of the transition strengths to the octupole-vibrational states remains as an interesting problem to be explored.

APPENDIX B: Numerical values of the measured differential cross sections and the analyzing poweres

^{152}Sm 0$^+$ elastic

Angle (θ_{cm})	Cross section (mb/sr)	Analyzing power (A_y)
13.09	4.424±0.012 ×10^3	-0.128±0.003
14.10	2.305±0.011 ×10^3	-0.209±0.005
15.11	1.142±0.012 ×10^3	-0.317±0.007
16.11	4.622±0.037 ×10^2	-0.428±0.008
17.12	2.118±0.014 ×10^2	-0.310±0.007
18.13	1.666±0.012 ×10^2	0.324±0.008
19.13	2.460±0.022 ×10^2	0.514±0.008
20.14	3.731±0.027 ×10^2	0.438±0.007
21.15	4.749±0.030 ×10^2	0.353±0.006
22.15	5.368±0.025 ×10^2	0.266±0.004
23.16	5.465±0.020 ×10^2	0.195±0.003
24.17	5.113±0.017 ×10^2	0.145±0.003
25.17	4.455±0.014 ×10^2	0.064±0.004
26.18	3.451±0.010 ×10^2	-0.010±0.003
27.18	2.552±0.010 ×10^2	-0.076±0.005
28.19	1.672±0.009 ×10^2	-0.208±0.006
29.20	1.022±0.008 ×10^2	-0.355±0.008
30.22	5.238±0.017 ×10^1	-0.529±0.005
32.23	1.366±0.006 ×10^1	-0.171±0.005
34.24	2.234±0.012 ×10^1	0.953±0.007
36.25	4.226±0.018 ×10^1	0.729±0.005
38.26	5.867±0.014 ×10^1	0.509±0.003
40.26	4.462±0.011 ×10^1	0.334±0.002
42.27	2.915±0.007 ×10^1	0.131±0.002
44.28	1.500±0.005 ×10^1	-0.080±0.004
46.29	6.138±0.029 ×10^0	-0.183±0.005
48.30	3.875±0.024 ×10^0	0.464±0.007
50.30	5.115±0.034 ×10^0	0.964±0.006
52.31	6.643±0.041 ×10^0	0.918±0.005
54.32	6.889±0.033 ×10^0	0.781±0.005
56.32	5.827±0.028 ×10^0	0.628±0.005
58.33	3.816±0.021 ×10^0	0.452±0.006
60.34	2.241±0.014 ×10^0	0.251±0.007
62.34	1.251±0.011 ×10^0	0.172±0.010
64.35	9.474±0.092 ×10^{-1}	0.465±0.010
66.35	1.020±0.011 ×10^0	0.843±0.008
68.36	1.146±0.012 ×10^0	0.974±0.007
70.36	1.145±0.012 ×10^0	0.972±0.007

^{152}Sm 2$^+$ (Ex = 0.122 MeV)

Angle (θ_{cm})	Cross section (mb/sr)	Analyzing power (A_y)
15.11	9.649±0.135 ×10^1	-0.017±0.018
16.11	8.497±0.092 ×10^1	-0.062±0.014
17.12	7.321±0.058 ×10^1	-0.063±0.010
18.13	5.427±0.053 ×10^1	-0.085±0.012
19.13	3.934±0.042 ×10^1	-0.116±0.014
20.14	2.170±0.026 ×10^1	-0.242±0.015
21.15	1.295±0.025 ×10^1	-0.322±0.023
22.15	6.230±0.121 ×10^0	-0.236±0.024
23.16	4.415±0.100 ×10^0	0.107±0.028
24.17	5.059±0.130 ×10^0	0.652±0.028
25.17	8.516±0.210 ×10^0	0.590±0.027
26.18	1.383±0.022 ×10^1	0.456±0.018
27.18	2.034±0.030 ×10^1	0.343±0.017
28.19	2.233±0.027 ×10^1	0.308±0.015
29.20	2.462±0.027 ×10^1	0.178±0.014
30.22	2.345±0.008 ×10^1	0.163±0.004
32.23	1.860±0.007 ×10^1	0.024±0.005
34.24	1.071±0.005 ×10^1	-0.149±0.005
36.25	4.438±0.031 ×10^0	-0.242±0.009
38.26	2.808±0.022 ×10^0	0.443±0.009
40.26	3.605±0.025 ×10^0	0.864±0.007
42.27	5.839±0.029 ×10^0	0.708±0.005
44.28	6.696±0.032 ×10^0	0.536±0.005
46.29	5.928±0.029 ×10^0	0.360±0.005
48.30	4.174±0.025 ×10^0	0.187±0.007
50.30	2.323±0.017 ×10^0	0.032±0.009
52.31	1.347±0.013 ×10^0	0.153±0.011
54.32	1.236±0.011 ×10^0	0.672±0.009
56.32	1.607±0.013 ×10^0	0.893±0.007
58.33	1.899±0.014 ×10^0	0.872±0.007
60.34	1.872±0.014 ×10^0	0.767±0.007
62.34	1.474±0.013 ×10^0	0.633±0.008
64.35	1.025±0.010 ×10^0	0.481±0.010
66.35	6.356±0.075 ×10^{-1}	0.335±0.013
68.36	4.742±0.063 ×10^{-1}	0.386±0.014
70.36	4.557±0.066 ×10^{-1}	0.657±0.013

^{152}Sm 4$^+$ (Ex = 0.366 MeV)

Angle (θ_{cm})	Cross section (mb/sr)	Analyzing power (A_y)
20.14	3.380±0.097 ×10^0	-0.051±0.037
21.15	3.056±0.117 ×10^0	-0.060±0.048
22.19	3.143±0.084 ×10^0	-0.095±0.037
23.16	2.882±0.080 ×10^0	-0.090±0.035
24.17	2.403±0.082 ×10^0	-0.076±0.044
25.17	2.199±0.099 ×10^0	-0.108±0.057
26.18	1.875±0.073 ×10^0	-0.201±0.049
27.18	1.349±0.071 ×10^0	-0.262±0.064
28.19	9.734±0.524 ×10^{-1}	-0.318±0.068
29.20	7.021±0.446 ×10^{-1}	0.018±0.081
30.22	6.648±0.114 ×10^{-1}	0.123±0.020
32.23	6.553±0.111 ×10^{-1}	0.657±0.017
34.24	8.786±0.129 ×10^{-1}	0.636±0.015
36.25	1.164±0.014 ×10^0	0.488±0.013
38.26	1.389±0.012 ×10^0	0.326±0.010
40.26	1.011±0.010 ×10^0	0.190±0.011
42.27	6.194±0.078 ×10^{-1}	0.041±0.015
44.28	3.682±0.060 ×10^{-1}	0.102±0.019
46.29	2.751±0.052 ×10^{-1}	0.474±0.020
48.30	3.217±0.057 ×10^{-1}	0.807±0.016
50.30	4.230±0.065 ×10^{-1}	0.737±0.014
52.31	4.564±0.067 ×10^{-1}	0.684±0.014
54.32	3.854±0.052 ×10^{-1}	0.521±0.014
56.32	2.791±0.044 ×10^{-1}	0.319±0.017
58.33	1.779±0.035 ×10^{-1}	0.255±0.022
60.34	1.322±0.030 ×10^{-1}	0.369±0.025
62.34	1.324±0.031 ×10^{-1}	0.619±0.023
64.35	1.497±0.032 ×10^{-1}	0.833±0.018
66.35	1.707±0.035 ×10^{-1}	0.824±0.016
68.36	1.648±0.034 ×10^{-1}	0.825±0.017
70.36	1.349±0.031 ×10^{-1}	0.779±0.019

^{152}Sm 6$^+$ (Ex = 0.707 MeV)

Angle (θ_{cm})	Cross section (mb/sr)	Analyzing power (A_y)
34.24	9.627±0.540 ×10^{-2}	0.541±0.074
36.25	8.354±0.701 ×10^{-2}	0.637±0.112
38.26	1.157±0.080 ×10^{-1}	0.752±0.085
40.26	1.245±0.079 ×10^{-1}	0.783±0.093
42.27	1.105±0.052 ×10^{-1}	0.573±0.064
44.28	1.134±0.054 ×10^{-1}	0.304±0.059
46.29	8.621±0.350 ×10^{-2}	0.223±0.050
48.30	4.747±0.319 ×10^{-2}	0.027±0.076
50.30	3.453±0.311 ×10^{-2}	0.277±0.107
52.31	2.881±0.310 ×10^{-2}	0.567±0.137
54.32	4.341±0.314 ×10^{-2}	0.687±0.099
56.33	4.602±0.310 ×10^{-2}	0.820±0.096
58.33	5.032±0.296 ×10^{-2}	0.720±0.082
60.34	3.834±0.247 ×10^{-2}	0.711±0.089
62.34	3.150±0.217 ×10^{-2}	0.532±0.090
64.35	2.198±0.171 ×10^{-2}	0.336±0.095
66.35	1.449±0.163 ×10^{-2}	0.330±0.133
68.36	1.529±0.161 ×10^{-2}	0.571±0.134
70.36	1.975±0.176 ×10^{-2}	0.614±0.117

^{152}Sm 2_1^+ (Ex = 1.086 MeV)

Angle (θ_{cm})	Cross section (mb/sr)	Analyzing power (A_y)
14.18	2.177±0.024 ×10^{0}	-0.030±0.013
16.18	1.973±0.023 ×10^{0}	-0.036±0.014
18.18	1.519±0.021 ×10^{0}	-0.106±0.016
20.19	9.672±0.175 ×10^{-1}	-0.103±0.022
22.19	4.945±0.134 ×10^{-1}	-0.068±0.033
24.20	3.117±0.106 ×10^{-1}	0.306±0.040
28.21	6.446±0.120 ×10^{-1}	0.344±0.021
30.22	8.109±0.348 ×10^{-1}	0.200±0.047
34.24	5.442±0.120 ×10^{-1}	0.018±0.026
36.25	3.356±0.092 ×10^{-1}	-0.122±0.032
38.26	1.985±0.064 ×10^{-1}	-0.078±0.037
40.27	1.436±0.048 ×10^{-1}	0.479±0.037
42.27	1.629±0.048 ×10^{-1}	0.773±0.028
44.28	2.329±0.054 ×10^{-1}	0.720±0.022
46.29	2.577±0.056 ×10^{-1}	0.619±0.021
48.30	2.399±0.054 ×10^{-1}	0.422±0.024
50.31	1.755±0.047 ×10^{-1}	0.261±0.030
52.31	1.176±0.040 ×10^{-1}	0.150±0.038
54.32	7.330±0.275 ×10^{-2}	0.133±0.043
56.33	5.929±0.235 ×10^{-2}	0.518±0.041
58.33	5.952±0.236 ×10^{-2}	0.870±0.034
60.34	7.484±0.253 ×10^{-2}	0.877±0.028
62.34	8.424±0.263 ×10^{-2}	0.799±0.026
64.35	7.563±0.248 ×10^{-2}	0.796±0.027
66.35	5.850±0.225 ×10^{-2}	0.720±0.034
68.36	4.102±0.187 ×10^{-2}	0.520±0.044
70.36	2.689±0.157 ×10^{-2}	0.391±0.060

^{152}Sm 4_1^+ (Ex = 1.372 MeV)

Angle (θ_{cm})	Cross section (mb/sr)	Analyzing power (A_y)
16.18	1.256±0.049 ×10^{-1}	-0.109±0.046
18.18	1.666±0.054 ×10^{-1}	-0.074±0.038
20.19	1.802±0.057 ×10^{-1}	-0.011±0.038
22.19	1.750±0.056 ×10^{-1}	-0.116±0.038
24.20	1.550±0.052 ×10^{-1}	-0.094±0.040
26.21	1.135±0.045 ×10^{-1}	-0.217±0.047
28.21	7.325±0.377 ×10^{-2}	-0.280±0.059
32.23	4.316±0.289 ×10^{-2}	0.204±0.075
34.24	4.136±0.390 ×10^{-2}	0.527±0.099
38.26	8.622±0.305 ×10^{-2}	0.522±0.037
40.27	7.505±0.260 ×10^{-2}	0.379±0.038
42.27	5.591±0.222 ×10^{-2}	0.194±0.045
44.28	3.449±0.184 ×10^{-2}	-0.057±0.061
46.29	2.115±0.145 ×10^{-2}	-0.053±0.077
48.30	2.021±0.141 ×10^{-2}	0.426±0.075
50.31	2.478±0.152 ×10^{-2}	0.738±0.058
52.31	2.343±0.148 ×10^{-2}	0.849±0.056
54.32	2.462±0.125 ×10^{-2}	0.844±0.044
56.33	2.105±0.117 ×10^{-2}	0.644±0.054
58.33	1.459±0.239 ×10^{-2}	0.555±0.158
60.34	9.712±0.863 ×10^{-3}	0.395±0.095
62.35	8.422±0.768 ×10^{-3}	0.198±0.101
64.35	7.814±0.775 ×10^{-3}	0.433±0.103
66.35	5.278±0.626 ×10^{-3}	0.916±0.099
68.36	7.506±0.738 ×10^{-3}	1.010±0.073
70.36	8.216±0.798 ×10^{-3}	0.901±0.094

^{152}Sm 1^- (Ex = 0.963 MeV)

Angle (θ_{cm})	Cross section (mb/sr)	Analyzing power (A_y)
14.18	2.299±0.079 ×10^{-1}	-0.207±0.040
16.18	2.498±0.084 ×10^{-1}	-0.349±0.039
18.18	3.051±0.088 ×10^{-1}	-0.424±0.033
20.19	2.775±0.081 ×10^{-1}	-0.384±0.034
22.19	1.939±0.069 ×10^{-1}	-0.136±0.042
28.21	2.115±0.078 ×10^{-1}	0.373±0.042
32.23	2.373±0.071 ×10^{-1}	0.066±0.035
34.24	1.792±0.063 ×10^{-1}	-0.067±0.040
36.25	1.166±0.048 ×10^{-1}	-0.069±0.048
38.26	9.913±0.372 ×10^{-2}	0.272±0.043
40.26	1.050±0.034 ×10^{-1}	0.726±0.032
42.27	1.363±0.038 ×10^{-1}	0.756±0.025
44.28	1.559±0.039 ×10^{-1}	0.568±0.026
46.29	1.450±0.038 ×10^{-1}	0.501±0.028
48.30	1.163±0.034 ×10^{-1}	0.283±0.033
50.30	6.946±0.265 ×10^{-2}	0.036±0.044
52.31	4.866±0.229 ×10^{-2}	0.283±0.053
54.32	3.627±0.162 ×10^{-2}	0.596±0.045
56.33	5.242±0.193 ×10^{-2}	0.978±0.025
58.33	6.533±0.215 ×10^{-2}	0.928±0.024
60.34	7.023±0.219 ×10^{-2}	0.850±0.026
62.34	5.730±0.200 ×10^{-2}	0.686±0.032
64.35	3.901±0.166 ×10^{-2}	0.512±0.044
66.35	2.225±0.122 ×10^{-2}	0.216±0.060
68.36	1.646±0.108 ×10^{-2}	0.121±0.073
70.36	1.727±0.110 ×10^{-2}	0.413±0.068

^{152}Sm 3^- (Ex = 1.041 MeV)

Angle (θ_{cm})	Cross section (mb/sr)	Analyzing power (A_y)
14.18	6.321±0.036 ×10^{0}	0.007±0.007
16.18	6.736±0.038 ×10^{0}	-0.021±0.007
18.18	6.699±0.037 ×10^{0}	-0.035±0.007
20.19	5.864±0.035 ×10^{0}	-0.074±0.007
22.19	4.364±0.029 ×10^{0}	-0.087±0.008
24.20	2.812±0.023 ×10^{0}	-0.103±0.010
28.21	8.718±0.136 ×10^{-1}	0.311±0.018
32.23	1.151±0.016 ×10^{0}	0.464±0.015
34.24	1.347±0.017 ×10^{0}	0.323±0.014
36.25	1.271±0.015 ×10^{0}	0.229±0.014
38.26	1.126±0.012 ×10^{0}	0.111±0.012
40.26	6.501±0.084 ×10^{-1}	0.012±0.015
42.27	4.161±0.068 ×10^{-1}	0.142±0.019
44.28	2.877±0.059 ×10^{-1}	0.447±0.022
46.29	2.998±0.061 ×10^{-1}	0.668±0.020
48.30	3.104±0.061 ×10^{-1}	0.723±0.019
50.31	3.192±0.061 ×10^{-1}	0.606±0.019
52.31	2.772±0.056 ×10^{-1}	0.494±0.021
54.32	2.098±0.040 ×10^{-1}	0.419±0.021
56.33	1.386±0.033 ×10^{-1}	0.276±0.026
58.33	1.005±0.029 ×10^{-1}	0.397±0.030
60.34	8.469±0.270 ×10^{-2}	0.524±0.032
62.34	7.673±0.260 ×10^{-2}	0.704±0.030
64.35	7.683±0.257 ×10^{-2}	0.775±0.028
66.35	7.427±0.248 ×10^{-2}	0.804±0.027
68.36	6.118±0.215 ×10^{-2}	0.768±0.031
70.36	4.427±0.188 ×10^{-2}	0.749±0.036

^{152}Sm 5$^-$ (Ex = 1.220 MeV)

Angle (θ_{cm})	Cross section (mb/sr)	Analyzing power (A_y)
14.18	8.583±0.502 ×10^{-2}	0.294±0.068
16.18	1.189±0.057 ×10^{-1}	0.079±0.056
18.18	1.637±0.061 ×10^{-1}	0.237±0.044
20.19	2.148±0.069 ×10^{-1}	0.197±0.038
22.19	2.565±0.071 ×10^{-1}	0.286±0.033
24.20	2.700±0.072 ×10^{-1}	0.153±0.031
26.21	2.420±0.069 ×10^{-1}	0.148±0.034
30.22	1.743±0.058 ×10^{-1}	0.185±0.038
34.24	1.242±0.101 ×10^{-1}	0.599±0.075
36.25	1.131±0.044 ×10^{-1}	0.625±0.040
38.26	1.347±0.042 ×10^{-1}	0.583±0.032
40.27	1.442±0.038 ×10^{-1}	0.413±0.029
42.27	1.222±0.034 ×10^{-1}	0.330±0.031
44.28	9.915±0.312 ×10^{-2}	0.217±0.036
46.29	7.201±0.268 ×10^{-2}	0.270±0.041
48.30	4.801±0.218 ×10^{-2}	0.401±0.050
50.31	4.885±0.216 ×10^{-2}	0.620±0.044
52.31	5.258±0.228 ×10^{-2}	0.773±0.039
54.32	6.261±0.207 ×10^{-2}	0.683±0.032
56.33	6.010±0.197 ×10^{-2}	0.630±0.032
58.33	5.373±0.188 ×10^{-2}	0.512±0.037
60.34	4.332±0.171 ×10^{-2}	0.546±0.041
62.35	2.857±0.142 ×10^{-2}	0.355±0.054
64.35	2.345±0.129 ×10^{-2}	0.560±0.057
66.35	2.652±0.134 ×10^{-2}	0.744±0.044
68.36	2.657±0.130 ×10^{-2}	0.862±0.041
70.36	2.905±0.140 ×10^{-2}	0.783±0.041

^{154}Sm 0$^+$ elastic

Angle (θ_{cm})	Cross section (mb/sr)	Analyzing power (A_y)
12.08	7.491±0.017 ×10^{3}	-0.067±0.003
13.09	4.374±0.014 ×10^{3}	-0.124±0.004
14.10	2.519±0.008 ×10^{3}	-0.198±0.004
15.10	1.170±0.007 ×10^{3}	-0.286±0.009
16.11	5.365±0.038 ×10^{2}	-0.404±0.009
17.12	2.177±0.023 ×10^{2}	-0.306±0.013
18.12	1.694±0.019 ×10^{2}	0.269±0.014
19.13	2.447±0.026 ×10^{2}	0.522±0.014
20.14	3.573±0.025 ×10^{2}	0.448±0.009
21.14	4.572±0.021 ×10^{2}	0.353±0.007
22.15	5.144±0.025 ×10^{2}	0.279±0.007
23.16	5.332±0.020 ×10^{2}	0.214±0.005
24.16	4.950±0.020 ×10^{2}	0.144±0.005
25.17	4.221±0.018 ×10^{2}	0.072±0.005
26.18	3.351±0.021 ×10^{2}	-0.002±0.007
27.18	2.475±0.014 ×10^{2}	-0.089±0.007
28.19	1.614±0.013 ×10^{2}	-0.198±0.010
29.19	9.643±0.110 ×10^{1}	-0.331±0.014
29.70	7.552±0.020 ×10^{1}	-0.419±0.004
30.20	4.884±0.070 ×10^{1}	-0.517±0.017
31.71	1.570±0.008 ×10^{1}	-0.655±0.007
32.23	1.247±0.005 ×10^{1}	-0.300±0.005
34.24	1.907±0.010 ×10^{1}	0.959±0.008
35.23	2.775±0.014 ×10^{1}	0.890±0.007
36.24	3.792±0.014 ×10^{1}	0.732±0.005
38.25	4.744±0.014 ×10^{1}	0.513±0.004
40.26	4.208±0.011 ×10^{1}	0.335±0.003
40.75	3.876±0.012 ×10^{1}	0.291±0.003
42.27	2.812±0.007 ×10^{1}	0.146±0.003
44.28	1.432±0.005 ×10^{1}	-0.077±0.003
46.28	5.948±0.030 ×10^{0}	-0.230±0.006
48.29	3.394±0.023 ×10^{0}	0.388±0.008
50.30	4.319±0.033 ×10^{0}	0.969±0.009
52.31	5.899±0.041 ×10^{0}	0.907±0.007
54.31	6.264±0.041 ×10^{0}	0.789±0.007
56.32	5.252±0.031 ×10^{0}	0.636±0.007
58.33	3.565±0.024 ×10^{0}	0.451±0.007
60.33	2.025±0.015 ×10^{0}	0.251±0.008
62.34	1.132±0.010 ×10^{0}	0.158±0.010
64.34	8.106±0.070 ×10^{-1}	0.409±0.009
66.35	8.511±0.075 ×10^{-1}	0.805±0.007
68.35	9.637±0.086 ×10^{-1}	0.975±0.007
70.35	9.667±0.086 ×10^{-1}	0.969±0.007

^{154}Sm 2$^+$ (Ex = 0.082 MeV)

Angle (θ_{cm})	Cross section (mb/sr)	Analyzing power (A_y)
15.10	1.077±0.025 ×10^{2}	0.000±0.028
16.11	9.820±0.156 ×10^{1}	-0.007±0.020
17.12	8.201±0.144 ×10^{1}	-0.064±0.021
18.12	6.125±0.116 ×10^{1}	-0.064±0.023
19.13	4.323±0.111 ×10^{1}	-0.211±0.031
20.14	2.767±0.071 ×10^{1}	-0.290±0.032
21.14	1.506±0.045 ×10^{1}	-0.299±0.037
22.15	7.679±0.435 ×10^{0}	-0.230±0.071
23.16	5.173±0.310 ×10^{0}	0.126±0.073
24.16	6.464±0.350 ×10^{0}	0.579±0.066
25.17	1.030±0.039 ×10^{1}	0.648±0.047
26.18	1.634±0.057 ×10^{1}	0.455±0.042
27.18	2.161±0.047 ×10^{1}	0.353±0.027
28.19	2.632±0.054 ×10^{1}	0.275±0.026
29.19	2.848±0.061 ×10^{1}	0.224±0.027
29.70	2.695±0.009 ×10^{1}	0.231±0.004
30.20	2.699±0.051 ×10^{1}	0.165±0.023
31.71	2.198±0.008 ×10^{1}	0.082±0.004
32.23	2.144±0.006 ×10^{1}	0.031±0.003
34.24	1.234±0.004 ×10^{1}	-0.152±0.004
35.23	8.188±0.048 ×10^{0}	-0.253±0.007
36.24	5.156±0.029 ×10^{0}	-0.281±0.007
38.25	2.524±0.027 ×10^{0}	0.369±0.011
40.26	3.942±0.033 ×10^{0}	0.883±0.010
40.75	4.482±0.044 ×10^{0}	0.881±0.011
42.27	6.549±0.039 ×10^{0}	0.714±0.007
44.28	7.796±0.039 ×10^{0}	0.534±0.006
46.29	6.976±0.035 ×10^{0}	0.368±0.006
48.29	4.831±0.027 ×10^{0}	0.179±0.007
50.30	2.674±0.020 ×10^{0}	0.025±0.009
52.31	1.500±0.016 ×10^{0}	0.158±0.012
54.31	1.439±0.017 ×10^{0}	0.674±0.011
56.32	1.861±0.018 ×10^{0}	0.900±0.009
58.33	2.193±0.020 ×10^{0}	0.848±0.010
60.33	2.126±0.017 ×10^{0}	0.753±0.008
62.34	1.715±0.014 ×10^{0}	0.626±0.008
64.34	1.153±0.009 ×10^{0}	0.466±0.008
66.35	7.127±0.064 ×10^{-1}	0.327±0.010
68.35	5.248±0.057 ×10^{-1}	0.402±0.011
70.35	5.158±0.058 ×10^{-1}	0.659±0.010

^{154}Sm 4$^+$ (Ex = 0.267 MeV)

Angle (θ_{cm})	Cross section (mb/sr)	Analyzing power (A_y)
17.12	3.778±0.296 ×10^{0}	-0.057±0.095
18.12	4.340±0.291 ×10^{0}	0.063±0.083
19.13	5.229±0.354 ×10^{0}	-0.053±0.082
20.14	5.750±0.277 ×10^{0}	0.028±0.059
22.15	5.624±0.188 ×10^{0}	-0.043±0.051
23.16	5.112±0.172 ×10^{0}	-0.021±0.041
24.16	4.811±0.146 ×10^{0}	-0.099±0.047
25.17	3.633±0.167 ×10^{0}	-0.085±0.056
26.18	3.464±0.209 ×10^{0}	-0.122±0.074
27.18	2.270±0.132 ×10^{0}	-0.185±0.071
29.19	1.342±0.125 ×10^{0}	-0.026±0.115
31.71	6.766±0.139 ×10^{-1}	0.433±0.024
32.23	7.806±0.120 ×10^{-1}	0.588±0.017
34.24	1.267±0.013 ×10^{0}	0.642±0.011
35.23	1.508±0.018 ×10^{0}	0.583±0.013
36.24	1.626±0.013 ×10^{0}	0.509±0.009
38.25	1.641±0.014 ×10^{0}	0.350±0.010
40.26	1.325±0.013 ×10^{0}	0.211±0.011
40.75	1.202±0.017 ×10^{0}	0.147±0.016
42.27	8.370±0.105 ×10^{-1}	0.069±0.014
44.28	4.692±0.080 ×10^{-1}	0.055±0.019
46.29	3.502±0.068 ×10^{-1}	0.484±0.021
48.29	4.418±0.074 ×10^{-1}	0.746±0.016
50.30	5.554±0.084 ×10^{-1}	0.763±0.015
52.31	6.065±0.086 ×10^{-1}	0.657±0.014
54.31	5.289±0.079 ×10^{-1}	0.527±0.015
56.32	3.814±0.062 ×10^{-1}	0.365±0.017
58.33	2.301±0.049 ×10^{-1}	0.242±0.023
60.33	1.702±0.039 ×10^{-1}	0.317±0.025
62.34	1.732±0.036 ×10^{-1}	0.581±0.021
64.34	2.061±0.032 ×10^{-1}	0.797±0.014
66.35	2.326±0.033 ×10^{-1}	0.808±0.012
68.35	2.145±0.031 ×10^{-1}	0.785±0.013
70.36	1.766±0.028 ×10^{-1}	0.733±0.014

^{154}Sm 6$^+$ (Ex = 0.544 MeV)

Angle (θ_{cm})	Cross section (mb/sr)	Analyzing power (A_y)
32.23	1.891±0.050 ×10^{-1}	0.192±0.030
34.24	1.697±0.042 ×10^{-1}	0.482±0.027
35.23	2.144±0.059 ×10^{-1}	0.528±0.030
36.24	2.240±0.044 ×10^{-1}	0.559±0.020
38.25	2.581±0.052 ×10^{-1}	0.495±0.021
40.26	2.576±0.052 ×10^{-1}	0.420±0.021
40.75	2.696±0.069 ×10^{-1}	0.393±0.028
42.27	2.226±0.049 ×10^{-1}	0.358±0.024
44.28	1.875±0.044 ×10^{-1}	0.234±0.026
46.29	1.385±0.038 ×10^{-1}	0.142±0.031
48.29	9.260±0.308 ×10^{-2}	0.218±0.037
50.30	7.994±0.284 ×10^{-2}	0.463±0.038
52.31	6.605±0.258 ×10^{-2}	0.671±0.037
54.31	6.923±0.266 ×10^{-2}	0.700±0.037
56.32	7.847±0.256 ×10^{-2}	0.818±0.028
58.33	8.007±0.258 ×10^{-2}	0.672±0.030
60.33	7.221±0.231 ×10^{-2}	0.600±0.032
62.34	5.450±0.181 ×10^{-2}	0.455±0.035
64.34	3.734±0.120 ×10^{-2}	0.417±0.034
66.35	2.550±0.097 ×10^{-2}	0.233±0.042
68.35	2.377±0.093 ×10^{-2}	0.489±0.042
70.36	2.820±0.101 ×10^{-2}	0.726±0.033

^{154}Sm 2$^+_1$ (Ex = 1.440 MeV)

Angle (θ_{cm})	Cross section (mb/sr)	Analyzing power (A_y)
10.14	1.454±0.015 ×10^{0}	0.096±0.012
12.19	1.550±0.021 ×10^{0}	0.014±0.016
14.18	1.484±0.021 ×10^{0}	-0.014±0.016
16.18	1.314±0.020 ×10^{0}	-0.011±0.017
18.18	1.089±0.017 ×10^{0}	-0.075±0.017
20.19	6.897±0.135 ×10^{-1}	-0.095±0.022
22.19	4.184±0.101 ×10^{-1}	-0.028±0.028
24.20	2.668±0.083 ×10^{-1}	0.154±0.037
26.21	3.137±0.092 ×10^{-1}	0.427±0.038
28.21	4.505±0.106 ×10^{-1}	0.345±0.031
29.70	5.215±0.279 ×10^{-1}	0.174±0.060
32.23	5.276±0.119 ×10^{-1}	0.108±0.027
34.24	4.469±0.091 ×10^{-1}	-0.005±0.024
35.23	3.698±0.105 ×10^{-1}	0.069±0.034
38.25	2.001±0.061 ×10^{-1}	-0.080±0.034
40.26	1.597±0.058 ×10^{-1}	0.254±0.044
42.27	1.595±0.060 ×10^{-1}	0.534±0.049
44.28	1.851±0.064 ×10^{-1}	0.552±0.046
46.29	2.027±0.064 ×10^{-1}	0.426±0.041
48.29	1.773±0.060 ×10^{-1}	0.374±0.043
50.30	1.508±0.054 ×10^{-1}	0.249±0.044
52.31	9.048±0.423 ×10^{-2}	0.221±0.055
54.32	6.497±0.349 ×10^{-2}	0.301±0.066
56.32	5.147±0.293 ×10^{-2}	0.601±0.076
58.33	5.188±0.317 ×10^{-2}	0.884±0.087
60.34	6.095±0.320 ×10^{-2}	0.910±0.078
62.34	6.537±0.312 ×10^{-2}	0.847±0.069
64.35	5.380±0.220 ×10^{-2}	0.720±0.057
66.35	4.524±0.195 ×10^{-2}	0.679±0.060
68.35	3.109±0.149 ×10^{-2}	0.590±0.065
70.36	2.379±0.126 ×10^{-2}	0.364±0.067

^{154}Sm 4$^+_1$ (Ex = 1.662 MeV)

Angle (θ_{cm})	Cross section (mb/sr)	Analyzing power (A_y)
14.18	1.383±0.072 ×10^{-1}	-0.139±0.058
16.18	1.365±0.071 ×10^{-1}	-0.138±0.058
18.18	1.579±0.070 ×10^{-1}	-0.078±0.050
20.19	1.816±0.070 ×10^{-1}	-0.088±0.044
22.19	1.819±0.066 ×10^{-1}	-0.163±0.041
24.20	1.752±0.061 ×10^{-1}	-0.112±0.039
26.21	1.376±0.052 ×10^{-1}	-0.140±0.042
28.21	9.642±0.429 ×10^{-2}	-0.233±0.051
30.22	5.408±0.326 ×10^{-2}	-0.031±0.067
32.23	4.140±0.356 ×10^{-2}	0.211±0.093
36.25	5.880±0.305 ×10^{-2}	0.694±0.052
38.26	8.069±0.381 ×10^{-2}	0.522±0.048
40.75	8.484±0.448 ×10^{-2}	0.233±0.056
42.27	6.546±0.306 ×10^{-2}	0.066±0.052
44.28	4.134±0.257 ×10^{-2}	0.192±0.068
46.29	2.715±0.195 ×10^{-2}	-0.098±0.080
48.30	1.820±0.168 ×10^{-2}	0.104±0.099
50.30	1.886±0.167 ×10^{-2}	0.670±0.081
52.31	2.159±0.182 ×10^{-2}	0.827±0.064
54.32	2.186±0.185 ×10^{-2}	0.836±0.072
56.32	2.545±0.168 ×10^{-2}	0.635±0.062
58.33	1.951±0.144 ×10^{-2}	0.619±0.071
60.34	1.070±0.106 ×10^{-2}	0.141±0.105
62.34	6.506±0.789 ×10^{-3}	-0.115±0.132
64.35	8.069±0.680 ×10^{-3}	0.463±0.081
66.35	7.637±0.607 ×10^{-3}	0.568±0.072
68.35	8.505±0.652 ×10^{-3}	0.841±0.060
70.36	9.969±0.666 ×10^{-3}	0.758±0.057

^{160}Gd 0$^+$ elastic

Angle (θ_{cm})	Cross section (mb/sr)	Analyzing power (A_y)
11.14	1.216±0.004 ×10^{4}	-0.091±0.004
12.14	7.686±0.023 ×10^{3}	-0.096±0.004
13.13	4.632±0.017 ×10^{3}	-0.141±0.005
14.14	2.492±0.011 ×10^{3}	-0.207±0.007
15.14	1.239±0.005 ×10^{3}	-0.294±0.006
16.14	5.195±0.024 ×10^{2}	-0.367±0.006
17.14	2.509±0.015 ×10^{2}	-0.194±0.007
18.14	2.153±0.015 ×10^{2}	0.317±0.008
19.15	3.085±0.013 ×10^{2}	0.453±0.005
20.15	4.191±0.021 ×10^{2}	0.410±0.008
21.15	5.236±0.017 ×10^{2}	0.328±0.004
22.16	5.744±0.017 ×10^{2}	0.251±0.004
23.16	5.663±0.014 ×10^{2}	0.176±0.003
24.17	5.157±0.013 ×10^{2}	0.112±0.003
25.17	4.303±0.012 ×10^{2}	0.043±0.003
26.18	3.204±0.015 ×10^{2}	-0.042±0.006
27.18	2.252±0.010 ×10^{2}	-0.138±0.006
28.18	1.396±0.003 ×10^{2}	-0.283±0.003
29.19	7.768±0.023 ×10^{1}	-0.459±0.004
30.19	3.682±0.016 ×10^{1}	-0.690±0.006
31.20	1.655±0.009 ×10^{1}	-0.699±0.007
32.20	1.142±0.007 ×10^{1}	0.285±0.007
33.21	1.644±0.010 ×10^{1}	0.920±0.007
34.21	2.729±0.015 ×10^{1}	0.903±0.007
35.22	3.714±0.017 ×10^{1}	0.766±0.006
36.23	4.599±0.015 ×10^{1}	0.654±0.004
38.24	5.175±0.013 ×10^{1}	0.435±0.003
40.25	4.113±0.008 ×10^{1}	0.258±0.003
42.26	2.421±0.007 ×10^{1}	0.040±0.003
44.27	1.149±0.004 ×10^{1}	-0.211±0.004
46.27	4.311±0.023 ×10^{0}	-0.171±0.006
48.28	3.609±0.018 ×10^{0}	0.702±0.005
50.29	5.412±0.034 ×10^{0}	0.978±0.006
52.29	6.653±0.029 ×10^{0}	0.868±0.005
54.30	6.224±0.038 ×10^{0}	0.704±0.007
56.31	4.844±0.021 ×10^{0}	0.525±0.005
58.31	2.899±0.028 ×10^{0}	0.309±0.011
60.32	1.582±0.009 ×10^{0}	0.123±0.007
62.32	9.275±0.082 ×10^{-1}	0.203±0.010
64.33	8.293±0.083 ×10^{-1}	0.649±0.010
66.33	9.513±0.091 ×10^{-1}	0.928±0.007
68.34	1.012±0.010 ×10^{0}	0.987±0.007
70.34	9.401±0.093 ×10^{-1}	0.933±0.007

^{160}Gd 2$^+$ (Ex = 0.075 MeV)

Angle (θ_{cm})	Cross section (mb/sr)	Analyzing power (A_y)
13.13	1.407±0.025 ×10^2	0.028±0.021
14.14	1.328±0.021 ×10^2	0.006±0.019
15.14	1.258±0.013 ×10^2	-0.022±0.012
16.14	1.119±0.009 ×10^2	-0.051±0.010
17.14	9.335±0.085 ×10^1	-0.065±0.011
18.14	7.017±0.076 ×10^1	-0.122±0.013
19.15	4.831±0.046 ×10^1	-0.181±0.012
20.15	3.101±0.033 ×10^1	-0.269±0.013
21.15	1.492±0.033 ×10^1	-0.378±0.028
22.16	6.680±0.265 ×10^0	-0.233±0.048
23.16	5.264±0.216 ×10^0	0.416±0.048
24.17	7.637±0.216 ×10^0	0.708±0.034
25.17	1.358±0.024 ×10^1	0.602±0.021
26.18	2.116±0.041 ×10^1	0.492±0.023
27.18	2.799±0.035 ×10^1	0.355±0.015
28.18	3.246±0.013 ×10^1	0.306±0.005
29.19	3.437±0.012 ×10^1	0.228±0.004
30.19	3.350±0.012 ×10^1	0.148±0.004
31.20	2.999±0.011 ×10^1	0.074±0.005
32.20	2.453±0.010 ×10^1	-0.017±0.005
33.21	1.833±0.009 ×10^1	-0.101±0.006
34.21	1.302±0.007 ×10^1	-0.203±0.007
35.22	7.970±0.059 ×10^0	-0.288±0.009
36.23	5.257±0.042 ×10^0	-0.248±0.010
38.24	3.384±0.030 ×10^0	0.643±0.010
40.25	5.925±0.033 ×10^0	0.858±0.007
42.26	9.260±0.048 ×10^0	0.664±0.006
44.27	1.006±0.004 ×10^1	0.506±0.005
46.27	8.127±0.034 ×10^0	0.305±0.005
48.28	5.503±0.021 ×10^0	0.129±0.005
50.29	2.763±0.019 ×10^0	-0.016±0.008
52.29	1.782±0.012 ×10^0	0.256±0.008
54.30	1.919±0.019 ×10^0	0.806±0.009
56.31	2.557±0.016 ×10^0	0.906±0.006
58.31	2.893±0.032 10^0	0.849±0.010
60.32	2.642±0.013 ×10^0	0.714±0.005
62.32	1.948±0.014 10^0	0.567±0.007
64.33	1.248±0.010 10^0	0.390±0.009
66.33	7.978±0.076 10^{-1}	0.284±0.011
68.34	6.425±0.072 ×10^{-1}	0.473±0.012
70.34	7.044±0.077 10^{-1}	0.742±0.009

^{160}Gd 4$^+$ (Ex = 0.249 MeV)

Angle (θ_{cm})	Cross section (mb/sr)	Analyzing power (A_y)
22.18	2.417±0.087 ×10^0	-0.147±0.043
23.16	2.073±0.075 ×10^0	-0.071±0.044
24.17	1.840±0.067 ×10^0	-0.063±0.045
25.17	1.654±0.064 ×10^0	-0.180±0.047
26.18	1.261±0.083 ×10^0	-0.165±0.075
27.18	1.098±0.061 ×10^0	-0.096±0.063
28.18	8.276±0.193 ×10^{-1}	-0.039±0.027
29.19	6.453±0.168 ×10^{-1}	0.106±0.031
30.19	5.986±0.158 ×10^{-1}	0.452±0.031
31.20	7.324±0.163 ×10^{-1}	0.593±0.025
32.20	9.504±0.178 ×10^{-1}	0.627±0.020
33.21	1.103±0.019 ×10^0	0.567±0.019
34.21	1.268±0.020 ×10^0	0.539±0.017
35.22	1.340±0.021 ×10^0	0.476±0.017
36.23	1.344±0.015 ×10^0	0.376±0.013
38.24	1.192±0.012 ×10^0	0.278±0.012
40.25	7.895±0.091 ×10^{-1}	0.146±0.014
42.26	4.651±0.088 ×10^{-1}	0.056±0.022
44.27	2.877±0.058 ×10^{-1}	0.409±0.024
46.27	3.372±0.062 ×10^{-1}	0.792±0.018
48.28	4.722±0.056 ×10^{-1}	0.798±0.012
50.29	5.992±0.079 ×10^{-1}	0.658±0.013
52.29	5.666±0.059 ×10^{-1}	0.539±0.012
54.30	4.148±0.071 ×10^{-1}	0.348±0.019
56.31	2.610±0.040 ×10^{-1}	0.251±0.018
58.31	1.822±0.060 ×10^{-1}	0.325±0.037
60.32	1.530±0.025 ×10^{-1}	0.574±0.017
62.32	1.975±0.035 ×10^{-1}	0.819±0.015
64.33	2.406±0.039 ×10^{-1}	0.840±0.014
66.33	2.486±0.039 ×10^{-1}	0.800±0.014
68.34	2.038±0.035 ×10^{-1}	0.712±0.016
70.34	1.463±0.029 ×10^{-1}	0.617±0.020

^{160}Gd 6$^+$ (Ex = 0.514 MeV)

Angle (θ_{cm})	Cross section (mb/sr)	Analyzing power (A_y)
32.20	1.687±0.067 ×10^{-1}	0.349±0.044
33.21	1.792±0.069 ×10^{-1}	0.331±0.044
34.21	1.905±0.071 ×10^{-1}	0.409±0.042
35.22	1.795±0.070 ×10^{-1}	0.304±0.043
36.22	1.993±0.073 ×10^{-1}	0.312±0.042
38.24	2.156±0.050 ×10^{-1}	0.322±0.026
40.25	1.739±0.040 ×10^{-1}	0.241±0.028
42.26	1.591±0.045 ×10^{-1}	0.199±0.033
44.27	1.060±0.031 ×10^{-1}	0.121±0.036
46.27	7.302±0.252 ×10^{-2}	0.160±0.040
48.28	4.956±0.168 ×10^{-2}	0.386±0.039
50.29	4.578±0.205 ×10^{-2}	0.663±0.046
52.30	5.095±0.170 ×10^{-2}	0.721±0.033
54.30	6.186±0.182 ×10^{-2}	0.593±0.030
56.31	6.146±0.184 ×10^{-2}	0.531±0.032
58.31	5.317±0.208 ×10^{-2}	0.388±0.044
60.32	4.248±0.123 ×10^{-2}	0.330±0.033
62.33	2.777±0.124 ×10^{-2}	0.318±0.049
64.33	2.380±0.113 ×10^{-2}	0.416±0.052
66.33	2.045±0.108 ×10^{-2}	0.643±0.052
68.34	2.485±0.115 ×10^{-2}	0.868±0.041
70.34	2.835±0.127 ×10^{-2}	0.811±0.039

^{160}Gd 2$_\gamma^+$ (Ex = 0.989 MeV)

Angle (θ_{cm})	Cross section (mb/sr)	Analyzing power (A_y)
12.14	2.205±0.033 ×10^0	-0.045±0.017
13.14	2.210±0.033 ×10^0	-0.038±0.017
14.14	2.094±0.032 ×10^0	0.006±0.018
15.14	2.084±0.032 ×10^0	0.001±0.018
16.14	1.866±0.030 ×10^0	-0.018±0.019
17.14	1.763±0.029 ×10^0	-0.019±0.020
18.15	1.589±0.028 ×10^0	-0.065±0.021
19.15	1.258±0.025 ×10^0	-0.044±0.023
20.15	9.622±0.215 ×10^{-1}	-0.049±0.026
21.16	6.980±0.181 ×10^{-1}	-0.056±0.031
22.16	5.184±0.158 ×10^{-1}	0.026±0.036
23.16	4.518±0.148 ×10^{-1}	0.065±0.038
24.17	5.114±0.154 ×10^{-1}	0.177±0.035
27.18	6.964±0.182 ×10^{-1}	0.312±0.030
28.19	7.743±0.485 ×10^{-1}	0.213±0.068
31.20	7.225±0.144 ×10^{-1}	0.100±0.024
32.20	6.737±0.136 ×10^{-1}	0.053±0.024
33.21	5.675±0.125 ×10^{-1}	0.033±0.026
34.21	4.370±0.108 ×10^{-1}	-0.087±0.029
35.22	3.612±0.100 ×10^{-1}	-0.159±0.032
36.24	2.654±0.063 ×10^{-1}	-0.241±0.029
38.24	1.378±0.040 ×10^{-1}	0.006±0.034
40.25	1.161±0.033 ×10^{-1}	0.602±0.031
42.26	1.914±0.050 ×10^{-1}	0.710±0.025
44.27	2.227±0.045 ×10^{-1}	0.614±0.022
46.28	2.357±0.046 ×10^{-1}	0.464±0.022
48.28	1.959±0.034 ×10^{-1}	0.296±0.021
50.29	1.304±0.034 ×10^{-1}	0.096±0.031
52.30	8.154±0.218 ×10^{-2}	-0.028±0.032
54.30	4.709±0.227 ×10^{-2}	0.225±0.056
56.31	4.691±0.164 ×10^{-2}	0.634±0.036
58.32	6.238±0.330 ×10^{-2}	0.888±0.043
60.32	7.116±0.161 ×10^{-2}	0.885±0.019
62.33	7.466±0.204 ×10^{-2}	0.788±0.024
64.33	6.090±0.182 ×10^{-2}	0.647±0.031
66.34	4.475±0.157 ×10^{-2}	0.517±0.037
68.34	3.007±0.129 ×10^{-2}	0.388±0.047
70.34	2.114±0.110 ×10^{-2}	0.406±0.057

^{160}Gd 4^{+} (Ex = 1.149 MeV)

Angle (θ_{cm})	Cross section (mb/sr)	Analyzing power (A_y)
17.14	3.090±0.126 ×10^{-1}	-0.077±0.047
18.15	3.381±0.129 ×10^{-1}	-0.053±0.045
19.15	3.539±0.133 ×10^{-1}	-0.095±0.043
20.15	3.765±0.136 ×10^{-1}	-0.077±0.042
22.16	3.158±0.125 ×10^{-1}	-0.081±0.046
23.16	3.118±0.122 ×10^{-1}	0.035±0.045
24.17	2.832±0.115 ×10^{-1}	-0.059±0.047
25.17	2.658±0.112 ×10^{-1}	-0.162±0.048
26.18	2.193±0.115 ×10^{-1}	-0.123±0.061
29.19	1.554±0.104 ×10^{-1}	-0.193±0.076
30.19	1.157±0.099 ×10^{-1}	0.022±0.097
31.20	8.431±0.580 ×10^{-2}	0.025±0.079
34.21	1.002±0.053 ×10^{-1}	0.556±0.057
35.22	1.231±0.060 ×10^{-1}	0.541±0.051
36.24	1.398±0.047 ×10^{-1}	0.424±0.039
38.24	1.447±0.041 ×10^{-1}	0.280±0.032
40.25	1.104±0.033 ×10^{-1}	0.091±0.036
42.26	8.352±0.338 ×10^{-2}	0.024±0.047
44.27	5.142±0.225 ×10^{-2}	-0.087±0.053
46.28	3.272±0.175 ×10^{-2}	0.056±0.062
48.28	2.538±0.122 ×10^{-2}	0.357±0.055
50.29	3.392±0.179 ×10^{-2}	0.817±0.049
52.30	3.866±0.150 ×10^{-2}	0.714±0.039
54.30	4.563±0.225 ×10^{-2}	0.590±0.052
56.31	3.520±0.144 ×10^{-2}	0.316±0.047
58.32	2.220±0.206 ×10^{-2}	0.131±0.105
60.32	1.390±0.075 ×10^{-2}	-0.061±0.064
62.33	1.085±0.079 ×10^{-2}	0.272±0.079
64.33	1.082±0.078 ×10^{-2}	0.777±0.071
66.34	1.415±0.090 ×10^{-2}	0.747±0.061
68.34	1.595±0.092 ×10^{-2}	0.888±0.050
70.34	1.278±0.086 ×10^{-2}	0.898±0.054

^{160}Gd 1^{-} (Ex = 1.125 MeV)

Angle (θ_{cm})	Cross section (mb/sr)	Analyzing power (A_y)
17.14	1.893±0.117 ×10^{-1}	-0.424±0.068
18.15	1.715±0.116 ×10^{-1}	-0.348±0.078
19.15	1.729±0.116 ×10^{-1}	-0.272±0.075
20.15	1.452±0.110 ×10^{-1}	-0.243±0.084
21.16	1.228±0.099 ×10^{-1}	-0.161±0.091
22.16	9.754±0.887 ×10^{-2}	0.032±0.102
23.16	8.653±0.823 ×10^{-2}	0.076±0.106
24.17	6.257±0.659 ×10^{-2}	0.275±0.116
25.17	7.788±0.724 ×10^{-2}	0.467±0.105
26.18	8.116±0.665 ×10^{-2}	0.452±0.087
27.18	1.089±0.093 ×10^{-1}	0.430±0.092
30.19	1.689±0.088 ×10^{-1}	0.260±0.060
31.20	1.933±0.141 ×10^{-1}	0.176±0.082
32.20	1.548±0.078 ×10^{-1}	0.003±0.059
34.21	1.195±0.107 ×10^{-1}	0.210±0.099
35.22	8.657±0.582 ×10^{-2}	0.033±0.077
36.24	6.574±0.388 ×10^{-2}	0.193±0.071
38.24	4.088±0.276 ×10^{-2}	0.341±0.076
40.25	4.742±0.250 ×10^{-2}	0.905±0.054
42.26	8.262±0.357 ×10^{-2}	0.732±0.040
44.27	9.485±0.315 ×10^{-2}	0.586±0.036
46.28	8.919±0.303 ×10^{-2}	0.460±0.036
48.28	5.880±0.204 ×10^{-2}	0.239±0.041
50.29	3.632±0.200 ×10^{-2}	-0.128±0.065
52.30	1.922±0.121 ×10^{-2}	0.050±0.074
54.30	2.197±0.124 ×10^{-2}	0.790±0.052
54.30	2.319±0.172 ×10^{-2}	0.589±0.074
56.31	3.119±0.145 ×10^{-2}	0.824±0.041
58.32	3.987±0.276 ×10^{-2}	0.974±0.057
60.32	4.021±0.126 ×10^{-2}	0.800±0.028
62.33	3.015±0.135 ×10^{-2}	0.598±0.045
64.33	2.081±0.113 ×10^{-2}	0.304±0.062
66.34	1.078±0.087 ×10^{-2}	0.305±0.088
68.34	7.898±0.713 ×10^{-3}	0.155±0.102
70.34	9.536±0.764 ×10^{-3}	0.467±0.084

^{160}Gd 3^{-} (Ex = 1.290 MeV)

Angle (θ_{cm})	Cross section (mb/sr)	Analyzing power (A_y)
12.14	3.324±0.040 ×10^{0}	0.020±0.014
13.14	3.323±0.040 ×10^{0}	0.012±0.014
14.14	3.492±0.041 ×10^{0}	-0.008±0.014
15.14	3.685±0.042 ×10^{0}	-0.003±0.013
16.14	3.655±0.042 ×10^{0}	-0.026±0.013
17.14	3.787±0.043 ×10^{0}	-0.044±0.013
18.15	3.685±0.042 ×10^{0}	-0.049±0.014
19.15	3.417±0.040 ×10^{0}	-0.075±0.014
20.15	3.233±0.040 ×10^{0}	-0.084±0.014
21.16	2.972±0.038 ×10^{0}	-0.070±0.015
22.16	2.441±0.034 ×10^{0}	-0.090±0.017
23.16	1.904±0.030 ×10^{0}	-0.101±0.019
24.17	1.533±0.027 ×10^{0}	-0.058±0.021
27.18	6.459±0.174 ×10^{-1}	0.046±0.031
28.19	5.369±0.287 ×10^{-1}	0.227±0.061
30.19	5.860±0.133 ×10^{-1}	0.398±0.025
31.20	6.613±0.137 ×10^{-1}	0.417±0.023
32.20	7.929±0.149 ×10^{-1}	0.378±0.021
33.21	7.731±0.151 ×10^{-1}	0.327±0.022
35.22	8.146±0.153 ×10^{-1}	0.258±0.022
36.24	7.168±0.106 ×10^{-1}	0.163±0.018
38.24	5.727±0.080 ×10^{-1}	0.095±0.017
40.25	3.395±0.056 ×10^{-1}	0.008±0.020
42.26	2.137±0.053 ×10^{-1}	0.157±0.029
44.27	1.704±0.041 ×10^{-1}	0.496±0.027
46.28	1.762±0.041 ×10^{-1}	0.674±0.023
48.28	1.978±0.034 ×10^{-1}	0.659±0.018
50.29	1.801±0.040 ×10^{-1}	0.556±0.024
52.30	1.563±0.030 ×10^{-1}	0.474±0.022
54.30	9.934±0.328 ×10^{-2}	0.363±0.037
56.31	7.305±0.205 ×10^{-2}	0.307±0.032
58.32	4.914±0.308 ×10^{-2}	0.438±0.067
60.32	5.343±0.142 ×10^{-2}	0.588±0.028
62.33	4.674±0.161 ×10^{-2}	0.817±0.029
64.33	4.691±0.163 ×10^{-2}	0.761±0.032
66.34	4.027±0.149 ×10^{-2}	0.833±0.031
68.34	3.219±0.133 ×10^{-2}	0.704±0.041
70.34	2.422±0.116 ×10^{-2}	0.632±0.048

^{160}Gd 5^{-} (Ex = 1.426 MeV)

Angle (θ_{cm})	Cross section (mb/sr)	Analyzing power (A_y)
22.16	1.374±0.106 ×10^{-1}	0.422±0.086
23.16	1.398±0.105 ×10^{-1}	0.257±0.085
24.17	1.417±0.099 ×10^{-1}	0.423±0.078
25.17	1.475±0.096 ×10^{-1}	0.262±0.072
26.18	1.411±0.085 ×10^{-1}	0.193±0.069
27.18	1.585±0.096 ×10^{-1}	0.187±0.068
32.20	1.052±0.108 ×10^{-1}	0.483±0.116
33.21	1.035±0.099 ×10^{-1}	0.414±0.100
34.21	9.260±0.686 ×10^{-2}	0.468±0.077
38.24	1.052±0.043 ×10^{-1}	0.411±0.046
40.25	1.152±0.039 ×10^{-1}	0.426±0.039
42.26	8.870±0.368 ×10^{-2}	0.310±0.046
44.27	6.261±0.271 ×10^{-2}	0.281±0.051
46.28	4.039±0.216 ×10^{-2}	0.290±0.058
48.28	3.797±0.180 ×10^{-2}	0.593±0.047
50.29	4.367±0.240 ×10^{-2}	0.583±0.053
52.30	5.073±0.204 ×10^{-2}	0.682±0.040
54.30	4.923±0.252 ×10^{-2}	0.651±0.050
56.31	4.839±0.183 ×10^{-2}	0.634±0.039
58.32	3.582±0.284 ×10^{-2}	0.543±0.083
60.32	2.598±0.108 ×10^{-2}	0.338±0.046
62.33	2.110±0.123 ×10^{-2}	0.478±0.059
64.33	1.860±0.113 ×10^{-2}	0.593±0.060
66.34	2.096±0.123 ×10^{-2}	0.700±0.053
68.34	2.241±0.118 ×10^{-2}	0.730±0.050
70.34	2.067±0.116 ×10^{-2}	0.780±0.049

^{164}Dy 0^{+} elastic

Angle (θ_{cm})	Cross section (mb/sr)	Analyzing power (A_y)
11.14	1.212±0.003 ×10^{4}	-0.026±0.003
12.13	7.462±0.024 ×10^{3}	-0.077±0.004
13.13	4.505±0.015 ×10^{3}	-0.129±0.004
14.13	2.414±0.010 ×10^{3}	-0.202±0.005
15.13	1.247±0.008 ×10^{3}	-0.289±0.008
16.14	5.305±0.043 ×10^{2}	-0.331±0.010
17.14	2.690±0.030 ×10^{2}	-0.150±0.014
18.14	2.328±0.018 ×10^{2}	0.316±0.010
18.64	2.659±0.023 ×10^{2}	0.416±0.010
19.14	3.123±0.035 ×10^{2}	0.437±0.014
19.65	3.727±0.027 ×10^{2}	0.422±0.009
20.15	4.405±0.024 ×10^{2}	0.380±0.007
21.15	5.173±0.044 ×10^{2}	0.307±0.011
22.15	5.606±0.021 ×10^{2}	0.242±0.005
23.16	5.488±0.044 ×10^{2}	0.161±0.010
24.16	4.851±0.025 ×10^{2}	0.101±0.006
25.17	4.028±0.017 ×10^{2}	0.017±0.005
26.17	3.041±0.012 ×10^{2}	-0.062±0.005
27.18	2.208±0.013 ×10^{2}	-0.155±0.007
28.18	1.317±0.010 ×10^{2}	-0.315±0.009
29.18	7.535±0.074 ×10^{1}	-0.466±0.011
30.19	3.320±0.048 ×10^{1}	-0.753±0.014
31.19	1.537±0.025 ×10^{1}	-0.764±0.015
32.20	1.147±0.022 ×10^{1}	0.340±0.023
33.20	1.642±0.031 ×10^{1}	0.952±0.017
34.21	2.678±0.032 ×10^{1}	0.889±0.011
35.21	3.794±0.052 ×10^{1}	0.778±0.013
36.21	4.566±0.042 ×10^{1}	0.618±0.010
37.22	5.009±0.036 ×10^{1}	0.522±0.008
38.22	5.012±0.029 ×10^{1}	0.415±0.007
39.23	4.627±0.038 ×10^{1}	0.329±0.010
40.23	3.979±0.025 ×10^{1}	0.228±0.008
42.24	2.316±0.026 ×10^{1}	-0.005±0.014
44.25	1.010±0.014 ×10^{1}	-0.258±0.016
46.26	3.938±0.091 ×10^{0}	-0.156±0.028
48.26	3.491±0.073 ×10^{0}	0.807±0.019
49.27	4.337±0.098 ×10^{0}	0.983±0.017
50.27	5.139±0.097 ×10^{0}	0.989±0.014
51.28	6.033±0.106 ×10^{0}	0.925±0.014
52.28	6.483±0.089 ×10^{0}	0.852±0.012
54.29	6.045±0.086 ×10^{0}	0.664±0.014
56.29	4.493±0.067 ×10^{0}	0.502±0.016
58.30	2.726±0.053 ×10^{0}	0.259±0.023
60.30	1.344±0.031 ×10^{0}	0.082±0.026
62.31	8.556±0.189 ×10^{-1}	0.195±0.026
64.32	8.578±0.210 ×10^{-1}	0.726±0.023
66.32	9.445±0.289 ×10^{-1}	0.973±0.021
68.32	9.877±0.299 ×10^{-1}	0.969±0.020
70.33	9.231±0.271 ×10^{-1}	0.850±0.024

^{164}Dy 2^{+} (Ex = 0.073 MeV)

Angle (θ_{cm})	Cross section (mb/sr)	Analyzing power (A_y)
12.13	8.355±0.366 ×10^{1}	0.134±0.054
13.13	1.052±0.028 ×10^{2}	0.091±0.032
14.13	1.070±0.022 ×10^{2}	0.057±0.025
15.13	1.074±0.020 ×10^{2}	0.020±0.023
16.14	1.004±0.015 ×10^{2}	0.013±0.019
17.14	8.679±0.164 ×10^{1}	-0.048±0.023
18.14	6.665±0.092 ×10^{1}	-0.148±0.017
18.64	5.529±0.096 ×10^{1}	-0.152±0.021
19.14	4.396±0.119 ×10^{1}	-0.141±0.033
19.65	3.543±0.082 ×10^{1}	-0.239±0.029
20.15	2.584±0.061 ×10^{1}	-0.294±0.030
21.15	1.454±0.084 ×10^{1}	-0.325±0.071
22.15	6.137±0.356 ×10^{0}	-0.426±0.074
23.16	4.754±0.636 ×10^{0}	0.706±0.149
24.16	7.781±0.446 ×10^{0}	0.742±0.066
25.17	1.400±0.039 ×10^{1}	0.649±0.033
26.17	2.154±0.035 ×10^{1}	0.463±0.019
27.18	2.789±0.043 ×10^{1}	0.376±0.018
28.18	3.169±0.045 ×10^{1}	0.296±0.017
29.18	3.378±0.046 ×10^{1}	0.205±0.016
30.19	3.237±0.046 ×10^{1}	0.149±0.017
31.19	2.949±0.035 ×10^{1}	0.091±0.015
32.20	2.388±0.034 ×10^{1}	0.015±0.017
33.20	1.868±0.032 ×10^{1}	-0.081±0.021
34.21	1.319±0.019 ×10^{1}	-0.180±0.017
35.21	8.483±0.217 ×10^{0}	-0.253±0.032
36.21	5.195±0.129 ×10^{0}	-0.239±0.030
37.22	3.650±0.103 ×10^{0}	0.034±0.034
38.22	3.599±0.080 ×10^{0}	0.590±0.023
39.23	4.040±0.129 ×10^{0}	0.899±0.034
40.23	5.798±0.097 ×10^{0}	0.831±0.017
42.24	8.950±0.163 ×10^{0}	0.666±0.019
44.25	9.735±0.138 ×10^{0}	0.484±0.016
46.26	8.492±0.147 ×10^{0}	0.317±0.020
48.26	5.474±0.092 ×10^{0}	0.120±0.020
49.27	3.925±0.088 ×10^{0}	-0.008±0.027
50.27	2.748±0.063 ×10^{0}	-0.022±0.028
51.28	1.939±0.055 ×10^{0}	-0.022±0.034
52.28	1.715±0.042 ×10^{0}	0.234±0.029
54.29	1.811±0.046 ×10^{0}	0.765±0.023
56.29	2.458±0.051 ×10^{0}	0.913±0.017
58.30	2.828±0.058 ×10^{0}	0.870±0.017
60.30	2.682±0.049 ×10^{0}	0.693±0.017
62.31	1.961±0.031 ×10^{0}	0.557±0.016
64.32	1.250±0.026 ×10^{0}	0.373±0.023
66.32	7.844±0.247 ×10^{-1}	0.267±0.036
68.32	6.208±0.234 ×10^{-1}	0.504±0.038
70.33	7.129±0.245 ×10^{-1}	0.785±0.029

^{164}Dy 4^{+} (Ex = 0.242 MeV)

Angle (θ_{cm})	Cross section (mb/sr)	Analyzing power (A_y)
22.15	1.152±0.082 ×10^{0}	0.237±0.085
24.16	8.939±0.962 ×10^{-1}	0.093±0.120
25.17	7.226±0.667 ×10^{-1}	0.085±0.107
26.17	6.651±0.518 ×10^{-1}	0.232±0.089
27.18	5.256±0.470 ×10^{-1}	0.254±0.102
28.18	5.316±0.505 ×10^{-1}	0.371±0.107
29.18	5.693±0.494 ×10^{-1}	0.727±0.082
30.19	6.513±0.541 ×10^{-1}	0.552±0.092
31.19	8.199±0.483 ×10^{-1}	0.561±0.063
32.20	9.700±0.484 ×10^{-1}	0.458±0.057
33.20	1.019±0.063 ×10^{0}	0.462±0.072
34.21	1.007±0.045 ×10^{0}	0.468±0.050
35.21	1.016±0.064 ×10^{0}	0.385±0.072
36.21	9.829±0.442 ×10^{-1}	0.331±0.052
37.22	9.138±0.359 ×10^{-1}	0.292±0.046
38.22	7.676±0.272 ×10^{-1}	0.160±0.042
39.23	7.036±0.365 ×10^{-1}	0.193±0.064
40.23	4.692±0.215 ×10^{-1}	0.268±0.054
42.24	2.718±0.223 ×10^{-1}	0.277±0.093
44.25	2.460±0.181 ×10^{-1}	0.654±0.077
46.26	2.984±0.227 ×10^{-1}	0.648±0.080
48.26	4.522±0.220 ×10^{-1}	0.719±0.048
49.27	4.712±0.260 ×10^{-1}	0.757±0.051
50.27	4.554±0.215 ×10^{-1}	0.474±0.052
51.28	5.086±0.225 ×10^{-1}	0.526±0.048
52.28	4.552±0.175 ×10^{-1}	0.451±0.044
54.29	3.237±0.150 ×10^{-1}	0.319±0.054
56.29	2.016±0.114 ×10^{-1}	0.370±0.065
58.30	1.154±0.095 ×10^{-1}	0.517±0.091
60.30	1.794±0.099 ×10^{-1}	0.700±0.054
62.31	1.824±0.077 ×10^{-1}	0.814±0.038
64.32	2.318±0.095 ×10^{-1}	0.921±0.033
66.32	2.003±0.106 ×10^{-1}	0.893±0.046
68.32	1.649±0.096 ×10^{-1}	0.685±0.058
70.33	1.195±0.082 ×10^{-1}	0.727±0.064

^{164}Dy 6^{+} (Ex = 0.501 MeV)

Angle (θ_{cm})	Cross section (mb/sr)	Analyzing power (A_y)
31.19	7.206±1.414 ×10^{-2}	0.385±0.207
32.20	1.172±0.193 ×10^{-1}	0.575±0.168
32.20	6.565±1.240 ×10^{-2}	0.089±0.207
34.21	1.315±0.161 ×10^{-1}	0.239±0.136
35.21	1.043±0.197 ×10^{-1}	0.362±0.202
36.21	1.111±0.147 ×10^{-1}	0.150±0.147
37.22	1.101±0.121 ×10^{-1}	0.165±0.126
38.22	1.013±0.097 ×10^{-1}	0.161±0.110
39.23	8.269±1.232 ×10^{-2}	0.259±0.171
40.23	8.825±0.930 ×10^{-2}	0.192±0.120
42.24	5.292±1.019 ×10^{-2}	-0.137±0.209
44.25	6.022±0.888 ×10^{-2}	0.272±0.162
46.26	3.149±0.557 ×10^{-2}	0.625±0.174
49.27	2.512±0.576 ×10^{-2}	0.593±0.223
50.27	2.929±0.526 ×10^{-2}	1.093±0.108
51.28	2.996±0.538 ×10^{-2}	0.521±0.184
52.28	3.140±0.453 ×10^{-2}	0.779±0.132
54.29	2.755±0.425 ×10^{-2}	0.771±0.141
56.29	2.880±0.420 ×10^{-2}	0.446±0.155
58.30	2.451±0.403 ×10^{-2}	0.367±0.176
60.31	1.584±0.280 ×10^{-2}	0.545±0.181
62.31	1.587±0.212 ×10^{-2}	0.130±0.150
64.32	1.090±0.190 ×10^{-2}	0.711±0.163
66.32	1.337±0.257 ×10^{-2}	0.786±0.172
68.33	1.541±0.277 ×10^{-2}	0.766±0.163
70.33	1.984±0.314 ×10^{-2}	0.871±0.132

^{164}Dy 2_1^+ (Ex = 0.762 MeV)

Angle (θ_{cm})	Cross section (mb/sr)	Analyzing power (A_y)
15.14	2.248±0.223 ×10^{0}	0.040±0.114
16.14	1.838±0.171 ×10^{0}	0.072±0.110
17.14	1.466±0.180 ×10^{0}	-0.021±0.141
18.14	1.389±0.113 ×10^{0}	-0.120±0.096
18.64	1.026±0.103 ×10^{0}	0.079±0.115
19.15	9.505±1.493 ×10^{-1}	0.089±0.177
19.65	1.006±0.111 ×10^{0}	-0.105±0.125
20.15	9.064±0.797 ×10^{-1}	-0.232±0.103
23.16	4.486±1.510 ×10^{-1}	0.057±0.337
24.16	2.928±0.542 ×10^{-1}	0.345±0.186
28.18	6.213±0.568 ×10^{-1}	0.353±0.104
29.18	6.437±0.542 ×10^{-1}	0.325±0.092
30.19	6.592±0.504 ×10^{-1}	-0.078±0.090
31.19	6.843±0.455 ×10^{-1}	-0.145±0.078
32.20	5.781±0.452 ×10^{-1}	0.087±0.093
33.20	5.098±0.418 ×10^{-1}	-0.068±0.097
34.21	4.291±0.294 ×10^{-1}	-0.183±0.079
35.21	3.628±0.370 ×10^{-1}	-0.034±0.119
37.22	1.486±0.209 ×10^{-1}	-0.232±0.155
38.23	9.825±1.022 ×10^{-2}	-0.517±0.110
39.23	8.466±1.301 ×10^{-2}	0.170±0.180
40.23	8.081±0.919 ×10^{-2}	0.523±0.119
42.24	1.779±0.201 ×10^{-1}	0.831±0.114
44.25	2.138±0.170 ×10^{-1}	0.639±0.087
46.26	1.998±0.187 ×10^{-1}	0.428±0.108
48.27	1.705±0.135 ×10^{-1}	0.232±0.089
49.27	1.403±0.132 ×10^{-1}	0.013±0.109
50.27	1.085±0.102 ×10^{-1}	0.248±0.110
51.28	9.537±0.897 ×10^{-2}	0.101±0.108
52.28	7.534±0.748 ×10^{-2}	-0.022±0.115
54.29	3.235±0.516 ×10^{-2}	0.328±0.177
56.29	3.206±0.461 ×10^{-2}	1.016±0.127
58.30	5.044±0.586 ×10^{-2}	0.892±0.113
60.31	6.934±0.640 ×10^{-2}	0.916±0.080
62.31	6.792±0.454 ×10^{-2}	0.921±0.056
64.32	4.767±0.386 ×10^{-2}	0.547±0.085
66.32	3.482±0.428 ×10^{-2}	0.496±0.136
68.33	2.201±0.320 ×10^{-2}	0.058±0.162
70.33	1.502±0.283 ×10^{-2}	-0.000±0.206

^{164}Dy 4_1^+ (Ex = 0.916 MeV)

Angle (θ_{cm})	Cross section (mb/sr)	Analyzing power (A_y)
15.14	3.168±1.016 ×10^{-1}	-0.184±0.316
16.14	4.229±0.959 ×10^{-1}	-0.011±0.245
17.14	3.386±1.016 ×10^{-1}	0.464±0.291
18.14	4.358±0.747 ×10^{-1}	-0.380±0.181
18.64	4.067±0.813 ×10^{-1}	-0.406±0.201
19.15	3.770±1.066 ×10^{-1}	0.425±0.285
19.65	3.820±0.786 ×10^{-1}	-0.355±0.210
20.15	4.176±0.670 ×10^{-1}	0.141±0.180
22.16	4.340±0.340 ×10^{-1}	-0.178±0.090
26.17	2.196±0.317 ×10^{-1}	-0.093±0.158
27.18	2.537±0.403 ×10^{-1}	-0.235±0.170
30.19	5.790±1.927 ×10^{-2}	-0.090±0.331
31.19	6.101±1.561 ×10^{-2}	0.341±0.263
32.20	3.727±1.118 ×10^{-2}	0.468±0.293
33.20	5.804±1.741 ×10^{-2}	0.960±0.228
34.21	6.216±1.319 ×10^{-2}	0.850±0.175
35.21	7.427±1.994 ×10^{-2}	0.758±0.237
36.22	1.221±0.185 ×10^{-1}	0.408±0.160
38.23	1.282±0.131 ×10^{-1}	0.334±0.114
40.23	1.323±0.137 ×10^{-1}	0.229±0.117
42.24	7.642±1.468 ×10^{-2}	-0.031±0.210
44.25	3.277±0.786 ×10^{-2}	0.151±0.253
46.26	3.147±0.866 ×10^{-2}	-0.459±0.269
48.27	2.366±0.580 ×10^{-2}	0.520±0.242
49.27	2.785±0.729 ×10^{-2}	0.417±0.264
50.27	2.755±0.614 ×10^{-2}	0.818±0.193
51.28	4.727±0.810 ×10^{-2}	0.636±0.168
52.28	3.929±0.609 ×10^{-2}	0.706±0.148
54.29	4.352±0.643 ×10^{-2}	0.412±0.158
56.29	2.767±0.495 ×10^{-2}	0.300±0.192
58.30	2.609±0.501 ×10^{-2}	-0.096±0.207
60.31	1.298±0.305 ×10^{-2}	0.094±0.250
62.31	1.161±0.218 ×10^{-2}	0.208±0.201
64.32	1.160±0.235 ×10^{-2}	0.455±0.208
68.33	1.241±0.298 ×10^{-2}	0.850±0.198
70.33	1.140±0.285 ×10^{-2}	0.920±0.191

^{166}Er 0^+ elastic

Angle (θ_{cm})	Cross section (mb/sr)	Analyzing power (A_y)
11.13	1.424±0.002 ×10^{4}	-0.026±0.002
12.13	8.765±0.017 ×10^{3}	-0.080±0.003
13.13	5.171±0.014 ×10^{3}	-0.144±0.004
14.13	2.811±0.011 ×10^{3}	-0.215±0.005
15.13	1.317±0.006 ×10^{3}	-0.303±0.006
16.13	6.018±0.030 ×10^{2}	-0.318±0.007
17.14	3.250±0.021 ×10^{2}	-0.039±0.008
18.14	3.220±0.018 ×10^{2}	0.355±0.007
19.14	4.434±0.027 ×10^{2}	0.420±0.008
20.15	5.793±0.022 ×10^{2}	0.370±0.006
21.15	6.727±0.023 ×10^{2}	0.297±0.005
22.15	7.050±0.016 ×10^{2}	0.221±0.003
23.16	6.730±0.017 ×10^{2}	0.150±0.003
24.16	5.926±0.015 ×10^{2}	0.083±0.003
25.16	4.737±0.013 ×10^{2}	0.000±0.003
26.17	3.571±0.011 ×10^{2}	-0.088±0.004
27.17	2.389±0.007 ×10^{2}	-0.206±0.004
28.18	1.472±0.008 ×10^{2}	-0.349±0.007
29.18	7.545±0.041 ×10^{1}	-0.583±0.008
30.19	3.554±0.040 ×10^{1}	-0.812±0.015
31.19	1.633±0.018 ×10^{1}	-0.575±0.013
32.20	1.534±0.021 ×10^{1}	0.569±0.016
33.20	2.420±0.023 ×10^{1}	0.933±0.010
34.20	3.738±0.035 ×10^{1}	0.849±0.011
35.21	4.983±0.033 ×10^{1}	0.719±0.009
36.21	5.953±0.039 ×10^{1}	0.589±0.008
38.23	6.041±0.015 ×10^{1}	0.386±0.003
40.24	4.446±0.013 ×10^{1}	0.185±0.004
42.25	2.487±0.008 ×10^{1}	-0.048±0.004
44.26	1.046±0.006 ×10^{1}	-0.332±0.008
46.26	4.647±0.033 ×10^{0}	-0.001±0.009
48.27	4.949±0.046 ×10^{0}	0.874±0.010
50.28	7.203±0.044 ×10^{0}	0.959±0.006
52.28	8.171±0.059 ×10^{0}	0.805±0.009
54.29	7.275±0.041 ×10^{0}	0.633±0.007
56.30	5.131±0.038 ×10^{0}	0.420±0.009
58.30	2.993±0.024 ×10^{0}	0.191±0.010
60.31	1.561±0.016 ×10^{0}	0.053±0.013
62.31	1.063±0.014 ×10^{0}	0.374±0.016
64.32	1.116±0.015 ×10^{0}	0.815±0.014
66.32	1.280±0.016 ×10^{0}	0.986±0.011
68.32	1.239±0.016 ×10^{0}	0.987±0.012
70.33	1.088±0.015 ×10^{0}	0.910±0.012
72.33	7.710±0.122 ×10^{-1}	0.754±0.017

^{166}Er 2^+ (Ex = 0.081 MeV)

Angle (θ_{cm})	Cross section (mb/sr)	Analyzing power (A_y)
11.13	9.987±0.307 ×10^{1}	0.016±0.038
12.13	1.128±0.028 ×10^{2}	0.056±0.031
13.13	1.318±0.028 ×10^{2}	0.032±0.026
14.13	1.364±0.025 ×10^{2}	0.000±0.023
15.13	1.317±0.018 ×10^{2}	-0.025±0.017
16.13	1.173±0.013 ×10^{2}	-0.062±0.014
17.14	9.509±0.117 ×10^{1}	-0.122±0.015
18.14	7.370±0.082 ×10^{1}	-0.171±0.014
19.14	4.881±0.088 ×10^{1}	-0.222±0.023
20.15	2.975±0.048 ×10^{1}	-0.308±0.020
21.15	1.460±0.038 ×10^{1}	-0.375±0.033
22.15	7.765±0.224 ×10^{0}	-0.066±0.036
23.16	7.173±0.250 ×10^{0}	0.548±0.042
24.16	1.094±0.028 ×10^{1}	0.679±0.031
25.16	1.901±0.032 ×10^{1}	0.606±0.021
26.17	2.654±0.035 ×10^{1}	0.476±0.017
27.17	3.386±0.027 ×10^{1}	0.365±0.010
28.18	3.869±0.039 ×10^{1}	0.284±0.013
29.18	3.901±0.027 ×10^{1}	0.207±0.009
30.19	3.847±0.038 ×10^{1}	0.144±0.012
31.19	3.348±0.025 ×10^{1}	0.083±0.009
32.20	2.766±0.027 ×10^{1}	-0.031±0.012
33.20	2.060±0.020 ×10^{1}	-0.137±0.012
34.20	1.427±0.020 ×10^{1}	-0.221±0.017
35.21	8.894±0.135 ×10^{0}	-0.265±0.019
36.21	5.618±0.121 ×10^{0}	-0.190±0.027
38.23	4.422±0.041 ×10^{0}	0.700±0.010
40.24	7.458±0.059 ×10^{0}	0.844±0.009
42.25	1.106±0.006 ×10^{1}	0.651±0.006
44.26	1.155±0.007 ×10^{1}	0.472±0.007
46.26	9.322±0.046 ×10^{0}	0.300±0.006
48.27	5.753±0.047 ×10^{0}	0.097±0.010
50.28	3.139±0.027 ×10^{0}	-0.043±0.011
52.28	1.985±0.029 ×10^{0}	0.350±0.018
54.29	2.404±0.024 ×10^{0}	0.862±0.010
56.30	3.072±0.031 ×10^{0}	0.916±0.010
58.30	3.407±0.026 ×10^{0}	0.837±0.008
60.31	3.032±0.023 ×10^{0}	0.701±0.008
62.31	2.185±0.020 ×10^{0}	0.522±0.011
64.32	1.400±0.016 ×10^{0}	0.333±0.015
66.32	8.694±0.130 ×10^{-1}	0.273±0.018
68.32	7.560±0.121 ×10^{-1}	0.462±0.019
70.33	8.744±0.131 ×10^{-1}	0.725±0.016
72.33	1.002±0.014 ×10^{0}	0.900±0.014

^{166}Er 4^+ (Ex = 0.269 MeV)

Angle ($\theta_{c.m.}$)	Cross section (mb/sr)	Analyzing power (A_y)
18.14	1.323±0.103 ×10^{0}	0.267±0.093
19.14	1.575±0.140 ×10^{0}	0.086±0.105
20.15	1.653±0.097 ×10^{0}	0.128±0.070
21.15	1.434±0.091 ×10^{0}	0.087±0.077
22.15	1.341±0.063 ×10^{0}	0.253±0.056
23.16	1.064±0.063 ×10^{0}	0.213±0.071
24.16	9.926±0.599 ×10^{-1}	0.209±0.072
25.16	7.243±0.535 ×10^{-1}	0.338±0.088
26.17	7.361±0.518 ×10^{-1}	0.191±0.082
27.17	5.179±0.313 ×10^{-1}	0.196±0.073
28.20	7.267±0.214 ×10^{-1}	0.383±0.035
29.18	6.204±0.344 ×10^{-1}	0.339±0.066
30.21	8.590±0.229 ×10^{-1}	0.338±0.032
31.19	9.192±0.428 ×10^{-1}	0.418±0.056
32.21	1.098±0.021 ×10^{0}	0.406±0.024
32.66	1.109±0.017 ×10^{0}	0.399±0.018
34.22	1.193±0.019 ×10^{0}	0.301±0.019
35.21	1.074±0.046 ×10^{0}	0.253±0.052
36.23	1.001±0.020 ×10^{0}	0.264±0.025
38.24	7.184±0.144 ×10^{-1}	0.220±0.025
40.24	3.909±0.124 ×10^{-1}	0.197±0.040
42.25	2.887±0.093 ×10^{-1}	0.481±0.036
44.26	3.063±0.111 ×10^{-1}	0.729±0.038
44.71	3.166±0.089 ×10^{-1}	0.744±0.029
46.26	4.132±0.098 ×10^{-1}	0.714±0.025
48.27	5.037±0.138 ×10^{-1}	0.695±0.030
48.72	5.401±0.112 ×10^{-1}	0.574±0.023
50.28	5.307±0.110 ×10^{-1}	0.469±0.024
52.28	3.964±0.121 ×10^{-1}	0.305±0.038
54.29	2.982±0.081 ×10^{-1}	0.244±0.033
56.30	1.899±0.074 ×10^{-1}	0.256±0.047
58.30	1.561±0.055 ×10^{-1}	0.508±0.039
60.31	1.857±0.056 ×10^{-1}	0.801±0.030
62.31	2.272±0.066 ×10^{-1}	0.883±0.026
64.32	2.467±0.069 ×10^{-1}	0.834±0.026
66.32	2.149±0.063 ×10^{-1}	0.748±0.030
68.32	1.736±0.058 ×10^{-1}	0.699±0.036
70.33	1.249±0.047 ×10^{-1}	0.481±0.043
72.33	8.500±0.404 ×10^{-2}	0.429±0.058

^{166}Er 6^+ (Ex = 0.545 MeV)

Angle ($\theta_{c.m.}$)	Cross section (mb/sr)	Analyzing power (A_y)
28.18	1.207±0.202 ×10^{-1}	-0.036±0.189
29.18	1.129±0.140 ×10^{-1}	-0.138±0.145
30.21	1.358±0.121 ×10^{-1}	0.166±0.104
30.21	1.478±0.089 ×10^{-1}	0.189±0.073
31.19	1.518±0.138 ×10^{-1}	-0.028±0.109
32.21	1.236±0.067 ×10^{-1}	0.033±0.068
32.66	1.049±0.048 ×10^{-1}	-0.128±0.056
33.20	8.451±1.211 ×10^{-2}	0.184±0.164
34.22	1.076±0.054 ×10^{-1}	-0.156±0.061
35.21	9.337±1.274 ×10^{-2}	0.143±0.158
36.23	1.083±0.063 ×10^{-1}	0.055±0.072
36.68	1.180±0.051 ×10^{-1}	0.028±0.053
38.24	9.123±0.496 ×10^{-2}	0.038±0.066
40.24	7.177±0.510 ×10^{-2}	0.069±0.087
40.69	7.309±0.399 ×10^{-2}	0.157±0.067
42.25	4.551±0.350 ×10^{-2}	0.047±0.092
44.26	3.513±0.358 ×10^{-2}	0.279±0.120
44.71	3.505±0.274 ×10^{-2}	0.370±0.091
46.26	3.311±0.300 ×10^{-2}	0.534±0.097
48.27	2.951±0.323 ×10^{-2}	0.762±0.107
48.72	3.189±0.263 ×10^{-2}	0.792±0.079
50.28	3.689±0.282 ×10^{-2}	0.877±0.066
52.29	3.039±0.329 ×10^{-2}	0.972±0.091
54.29	3.246±0.258 ×10^{-2}	0.686±0.081
56.30	2.854±0.275 ×10^{-2}	0.420±0.111
58.30	2.810±0.222 ×10^{-2}	0.350±0.091
60.31	1.773±0.203 ×10^{-2}	0.575±0.110
60.31	1.934±0.230 ×10^{-2}	0.372±0.133
62.31	1.787±0.179 ×10^{-2}	0.555±0.106
64.32	1.919±0.185 ×10^{-2}	0.691±0.101
66.32	1.891±0.183 ×10^{-2}	0.765±0.095
68.33	2.059±0.191 ×10^{-2}	0.714±0.097
70.33	1.799±0.179 ×10^{-2}	0.838±0.090
72.33	1.974±0.188 ×10^{-2}	0.958±0.084

^{166}Er 2_γ^+ (Ex = 0.786 MeV)

Angle ($\theta_{c.m.}$)	Cross section (mb/sr)	Analyzing power (A_y)
11.13	2.268±0.406 ×10^{0}	0.220±0.201
12.13	2.570±0.415 ×10^{0}	-0.081±0.180
15.13	2.762±0.308 ×10^{0}	-0.045±0.133
16.14	2.365±0.243 ×10^{0}	-0.134±0.121
17.14	2.305±0.306 ×10^{0}	-0.082±0.150
18.14	1.644±0.156 ×10^{0}	-0.157±0.114
19.14	1.195±0.167 ×10^{0}	-0.071±0.162
20.15	7.984±0.904 ×10^{-1}	0.106±0.131
21.15	5.921±0.869 ×10^{-1}	0.230±0.171
24.16	3.892±0.517 ×10^{-1}	0.072±0.152
25.17	3.926±0.724 ×10^{-1}	0.280±0.187
28.20	7.219±0.294 ×10^{-1}	0.276±0.048
29.18	9.301±0.628 ×10^{-1}	0.256±0.086
30.21	7.947±0.287 ×10^{-1}	0.209±0.044
31.19	8.557±0.624 ×10^{-1}	0.123±0.090
32.21	7.704±0.321 ×10^{-1}	0.037±0.052
32.66	7.034±0.181 ×10^{-1}	-0.083±0.032
33.20	5.776±0.423 ×10^{-1}	-0.165±0.087
34.22	4.415±0.167 ×10^{-1}	-0.256±0.045
35.21	3.906±0.348 ×10^{-1}	-0.108±0.107
36.23	2.495±0.179 ×10^{-1}	-0.268±0.081
36.68	2.132±0.107 ×10^{-1}	-0.188±0.062
38.24	8.307±0.715 ×10^{-2}	-0.064±0.103
40.24	1.047±0.101 ×10^{-1}	0.681±0.119
40.69	1.408±0.128 ×10^{-1}	0.752±0.098
42.25	2.013±0.116 ×10^{-1}	0.785±0.051
44.26	2.745±0.166 ×10^{-1}	0.654±0.059
44.71	2.834±0.156 ×10^{-1}	0.564±0.069
46.26	2.761±0.133 ×10^{-1}	0.355±0.063
48.27	2.180±0.127 ×10^{-1}	0.118±0.072
48.72	1.991±0.091 ×10^{-1}	0.220±0.057
50.28	1.402±0.092 ×10^{-1}	-0.066±0.077
52.29	7.707±0.737 ×10^{-2}	-0.286±0.114
54.29	4.958±0.446 ×10^{-2}	0.214±0.105
56.30	5.339±0.601 ×10^{-2}	0.749±0.139
58.30	7.746±0.606 ×10^{-2}	0.959±0.054
60.31	8.495±0.505 ×10^{-2}	0.856±0.056
60.31	8.771±0.680 ×10^{-2}	0.937±0.066
62.31	8.818±0.694 ×10^{-2}	0.763±0.063
64.32	6.328±0.449 ×10^{-2}	0.542±0.081
66.32	4.463±0.387 ×10^{-2}	0.381±0.098
68.33	3.270±0.326 ×10^{-2}	0.209±0.117
70.33	2.158±0.266 ×10^{-2}	0.098±0.143
72.33	2.210±0.283 ×10^{-2}	0.669±0.138

^{166}Er 4_γ^+ (Ex = 0.956 MeV)

Angle ($\theta_{c.m.}$)	Cross section (mb/sr)	Analyzing power (A_y)
17.14	4.365±1.036 ×10^{-1}	-0.016±0.257
18.14	4.076±0.833 ×10^{-1}	0.183±0.223
19.14	4.390±1.029 ×10^{-1}	-0.036±0.256
20.15	5.345±0.809 ×10^{-1}	-0.018±0.171
21.15	4.284±0.736 ×10^{-1}	-0.232±0.190
22.18	4.841±0.524 ×10^{-1}	-0.058±0.128
23.16	4.822±0.563 ×10^{-1}	-0.293±0.138
24.16	5.878±0.869 ×10^{-1}	-0.006±0.168
26.17	2.834±0.437 ×10^{-1}	-0.127±0.172
27.17	3.042±0.302 ×10^{-1}	-0.353±0.114
28.18	2.367±0.402 ×10^{-1}	-0.686±0.183
30.21	1.214±0.342 ×10^{-1}	0.451±0.232
32.21	5.616±0.614 ×10^{-2}	0.503±0.123
32.66	6.374±0.652 ×10^{-2}	0.488±0.131
33.20	8.164±1.567 ×10^{-2}	0.394±0.211
34.22	1.104±0.100 ×10^{-1}	0.453±0.098
35.21	1.034±0.205 ×10^{-1}	0.533±0.215
36.23	1.439±0.128 ×10^{-1}	0.347±0.106
36.68	1.553±0.098 ×10^{-1}	0.465±0.070
38.24	1.576±0.107 ×10^{-1}	0.265±0.083
40.24	1.554±0.138 ×10^{-1}	0.107±0.109
40.69	1.351±0.083 ×10^{-1}	-0.029±0.076
42.25	9.815±0.739 ×10^{-2}	-0.019±0.090
44.26	5.632±0.636 ×10^{-2}	-0.380±0.131
44.71	4.723±0.458 ×10^{-2}	-0.172±0.116
46.26	3.190±0.393 ×10^{-2}	-0.056±0.144
48.72	2.773±0.363 ×10^{-2}	0.691±0.133
50.28	3.909±0.489 ×10^{-2}	0.637±0.154
52.29	5.543±0.626 ×10^{-2}	0.650±0.121
54.29	5.268±0.613 ×10^{-2}	0.424±0.121
56.30	3.721±0.441 ×10^{-2}	0.330±0.136
58.30	2.474±0.305 ×10^{-2}	-0.260±0.143
60.31	1.284±0.205 ×10^{-2}	0.029±0.184
62.31	1.087±0.216 ×10^{-2}	0.136±0.218
64.32	1.142±0.205 ×10^{-2}	0.782±0.177
66.32	1.939±0.260 ×10^{-2}	0.980±0.110
68.33	2.048±0.277 ×10^{-2}	0.761±0.133
70.33	1.740±0.254 ×10^{-2}	0.861±0.123
72.33	8.305±1.907 ×10^{-3}	0.110±0.261

^{168}Er 0$^+$ elastic

Angle (θ_{cm})	Cross section (mb/sr)	Analyzing power (A_y)
11.13	1.353±0.002 ×10^{4}	-0.034±0.002
12.13	8.497±0.017 ×10^{3}	-0.074±0.003
13.13	4.991±0.014 ×10^{3}	-0.135±0.004
14.13	2.645±0.010 ×10^{3}	-0.205±0.005
15.13	1.280±0.005 ×10^{3}	-0.268±0.006
16.13	5.553±0.030 ×10^{2}	-0.313±0.007
17.14	3.128±0.020 ×10^{2}	-0.026±0.008
18.14	2.981±0.017 ×10^{2}	0.336±0.007
19.14	4.225±0.026 ×10^{2}	0.410±0.009
20.15	5.221±0.021 ×10^{2}	0.361±0.005
21.15	6.327±0.022 ×10^{2}	0.281±0.005
22.15	6.532±0.015 ×10^{2}	0.222±0.003
23.15	6.132±0.015 ×10^{2}	0.147±0.003
24.16	5.355±0.014 ×10^{2}	0.073±0.003
25.16	4.352±0.013 ×10^{2}	-0.002±0.004
26.17	3.166±0.011 ×10^{2}	-0.099±0.004
27.17	2.183±0.009 ×10^{2}	-0.200±0.006
28.18	1.267±0.007 ×10^{2}	-0.366±0.008
29.18	7.050±0.056 ×10^{1}	-0.559±0.011
30.18	2.978±0.036 ×10^{1}	-0.844±0.015
31.19	1.378±0.023 ×10^{1}	-0.575±0.021
31.69	1.273±0.022 ×10^{1}	0.051±0.021
32.19	1.374±0.020 ×10^{1}	0.568±0.017
33.20	2.233±0.027 ×10^{1}	0.951±0.013
34.20	3.490±0.034 ×10^{1}	0.829±0.012
35.21	4.788±0.040 ×10^{1}	0.682±0.010
36.21	5.594±0.038 ×10^{1}	0.567±0.008
36.67	5.800±0.014 ×10^{1}	0.525±0.004
38.68	5.456±0.013 ×10^{1}	0.333±0.003
40.69	3.687±0.009 ×10^{1}	0.120±0.003
42.70	1.943±0.007 ×10^{1}	-0.124±0.004
44.70	7.748±0.044 ×10^{0}	-0.342±0.007
46.71	4.079±0.031 ×10^{0}	0.273±0.010
48.72	5.214±0.038 ×10^{0}	0.956±0.008
50.72	7.306±0.045 ×10^{0}	0.904±0.007
52.73	7.677±0.045 ×10^{0}	0.747±0.007
54.74	6.344±0.040 ×10^{0}	0.552±0.008
56.74	4.240±0.032 ×10^{0}	0.346±0.009
58.75	2.349±0.020 ×10^{0}	0.122±0.011
60.75	1.269±0.015 ×10^{0}	0.065±0.015
62.76	1.009±0.014 ×10^{0}	0.527±0.016
64.76	1.060±0.014 ×10^{0}	0.896±0.013
66.77	1.209±0.013 ×10^{0}	0.979±0.010
68.77	1.173±0.013 ×10^{0}	0.919±0.011
70.77	9.171±0.115 ×10^{-1}	0.853±0.013

^{168}Er 2$^+$ (Ex = 0.080 MeV)

Angle (θ_{cm})	Cross section (mb/sr)	Analyzing power (A_y)
11.13	8.648±0.317 ×10^{1}	0.005±0.045
12.13	1.024±0.027 ×10^{2}	0.132±0.033
13.13	1.268±0.026 ×10^{2}	0.015±0.026
14.13	1.251±0.024 ×10^{2}	-0.013±0.024
15.13	1.296±0.017 ×10^{2}	-0.013±0.017
16.13	1.108±0.013 ×10^{2}	-0.028±0.015
17.14	9.402±0.114 ×10^{1}	-0.092±0.015
18.14	6.902±0.079 ×10^{1}	-0.166±0.015
19.14	4.521±0.081 ×10^{1}	-0.229±0.023
20.15	2.674±0.048 ×10^{1}	-0.320±0.023
21.15	1.302±0.037 ×10^{1}	-0.317±0.036
22.15	7.239±0.222 ×10^{0}	-0.204±0.038
23.16	5.848±0.249 ×10^{0}	0.512±0.052
24.16	1.107±0.028 ×10^{1}	0.726±0.030
25.16	1.695±0.031 ×10^{1}	0.625±0.022
26.17	2.476±0.034 ×10^{1}	0.482±0.017
27.17	3.103±0.037 ×10^{1}	0.372±0.015
28.18	3.664±0.038 ×10^{1}	0.298±0.013
29.18	3.780±0.038 ×10^{1}	0.223±0.013
30.18	3.561±0.036 ×10^{1}	0.147±0.013
31.19	3.288±0.035 ×10^{1}	0.075±0.013
31.69	2.989±0.033 ×10^{1}	-0.010±0.014
32.19	2.570±0.026 ×10^{1}	0.000±0.013
33.20	1.928±0.023 ×10^{1}	-0.131±0.015
34.20	1.351±0.020 ×10^{1}	-0.207±0.018
35.21	8.361±0.159 ×10^{0}	-0.292±0.024
36.21	5.126±0.117 ×10^{0}	-0.256±0.028
36.67	4.696±0.039 ×10^{0}	-0.038±0.011
38.68	4.763±0.039 ×10^{0}	0.782±0.010
40.69	8.488±0.051 ×10^{0}	0.791±0.007
42.70	1.124±0.006 ×10^{1}	0.620±0.006
44.70	1.111±0.005 ×10^{1}	0.434±0.006
46.71	8.535±0.045 ×10^{0}	0.246±0.007
48.72	5.134±0.035 ×10^{0}	0.047±0.009
50.72	2.615±0.025 ×10^{0}	-0.014±0.012
52.73	2.016±0.023 ×10^{0}	0.459±0.014
54.74	2.474±0.026 ×10^{0}	0.891±0.011
56.74	3.169±0.029 ×10^{0}	0.881±0.010
58.75	3.376±0.025 ×10^{0}	0.792±0.008
60.75	2.875±0.023 ×10^{0}	0.656±0.009
62.76	2.011±0.019 ×10^{0}	0.471±0.011
64.76	1.198±0.015 ×10^{0}	0.286±0.015
66.77	7.882±0.107 ×10^{-1}	0.274±0.017
68.77	7.625±0.106 ×10^{-1}	0.567±0.016
70.77	8.982±0.115 ×10^{-1}	0.816±0.013

^{168}Er 4$^+$ (Ex = 0.264 MeV)

Angle (θ_{cm})	Cross section (mb/sr)	Analyzing power (A_y)
17.14	1.324±0.128 ×10^{0}	0.163±0.112
18.14	1.727±0.114 ×10^{0}	0.247±0.076
20.15	1.853±0.109 ×10^{0}	0.337±0.068
21.15	1.552±0.093 ×10^{0}	0.082±0.072
22.15	1.226±0.062 ×10^{0}	0.147±0.061
22.63	1.056±0.055 ×10^{0}	0.223±0.062
23.16	1.165±0.067 ×10^{0}	0.215±0.069
24.16	1.020±0.061 ×10^{0}	0.221±0.071
25.16	8.894±0.555 ×10^{-1}	0.094±0.076
26.17	7.920±0.543 ×10^{-1}	0.387±0.078
27.17	7.053±0.487 ×10^{-1}	0.327±0.081
28.18	7.535±0.588 ×10^{-1}	0.438±0.085
29.18	9.145±0.568 ×10^{-1}	0.304±0.074
30.18	9.099±0.566 ×10^{-1}	0.257±0.074
30.65	1.143±0.017 ×10^{0}	0.350±0.018
31.19	1.104±0.064 ×10^{0}	0.352±0.068
31.69	1.125±0.065 ×10^{0}	0.460±0.066
32.19	1.191±0.057 ×10^{0}	0.320±0.056
32.66	1.294±0.018 ×10^{0}	0.326±0.017
33.20	1.222±0.056 ×10^{0}	0.334±0.054
34.20	1.192±0.056 ×10^{0}	0.233±0.057
34.67	1.153±0.017 ×10^{0}	0.318±0.018
35.21	1.116±0.054 ×10^{0}	0.225±0.058
36.67	8.409±0.145 ×10^{-1}	0.282±0.022
38.68	5.423±0.115 ×10^{-1}	0.224±0.026
40.69	3.327±0.091 ×10^{-1}	0.406±0.033
42.70	2.776±0.085 ×10^{-1}	0.648±0.033
44.70	3.628±0.096 ×10^{-1}	0.737±0.028
46.71	4.732±0.108 ×10^{-1}	0.667±0.025
48.72	5.462±0.113 ×10^{-1}	0.512±0.024
50.72	4.860±0.107 ×10^{-1}	0.420±0.026
52.73	3.575±0.091 ×10^{-1}	0.313±0.031
54.74	2.307±0.075 ×10^{-1}	0.301±0.039
56.74	1.671±0.063 ×10^{-1}	0.364±0.045
58.75	1.531±0.053 ×10^{-1}	0.758±0.035
60.75	2.002±0.060 ×10^{-1}	0.869±0.028
62.76	2.354±0.065 ×10^{-1}	0.864±0.026
64.76	2.490±0.067 ×10^{-1}	0.771±0.027
66.77	2.083±0.055 ×10^{-1}	0.618±0.030
68.77	1.412±0.045 ×10^{-1}	0.496±0.037
70.77	1.042±0.039 ×10^{-1}	0.320±0.046

^{168}Er 6$^+$ (Ex = 0.549 MeV)

Angle (θ_{cm})	Cross section (mb/sr)	Analyzing power (A_y)
30.65	2.660±0.077 ×10^{-1}	0.102±0.036
32.66	2.542±0.075 ×10^{-1}	0.075±0.037
34.67	2.367±0.073 ×10^{-1}	0.138±0.038
36.67	2.097±0.070 ×10^{-1}	0.104±0.042
38.68	1.576±0.059 ×10^{-1}	0.134±0.047
40.69	1.125±0.051 ×10^{-1}	0.195±0.056
42.70	7.787±0.414 ×10^{-2}	0.367±0.063
44.70	6.887±0.394 ×10^{-2}	0.487±0.066
46.71	6.168±0.367 ×10^{-2}	0.749±0.061
48.72	6.812±0.387 ×10^{-2}	0.805±0.056
50.73	6.339±0.374 ×10^{-2}	0.872±0.054
52.73	5.825±0.357 ×10^{-2}	0.488±0.070
54.74	4.814±0.325 ×10^{-2}	0.489±0.077
56.74	4.748±0.323 ×10^{-2}	0.416±0.079
58.75	3.328±0.233 ×10^{-2}	0.266±0.084
60.75	2.436±0.201 ×10^{-2}	0.622±0.089
62.76	2.011±0.182 ×10^{-2}	0.549±0.100
64.76	2.313±0.196 ×10^{-2}	0.803±0.081
66.77	2.730±0.189 ×10^{-2}	0.829±0.068
68.77	2.552±0.184 ×10^{-2}	0.752±0.073
70.77	2.131±0.168 ×10^{-2}	0.739±0.080

^{168}Er 2_1^+ (Ex = 0.821 MeV)

Angle (θ_{cm})	Cross section (mb/sr)	Analyzing power (A_y)
11.13	1.750±0.381 ×10^{0}	-0.264±0.239
12.13	2.877±0.478 ×10^{0}	0.197±0.190
13.13	2.197±0.380 ×10^{0}	-0.110±0.194
14.13	1.350±0.326 ×10^{0}	-0.130±0.255
15.13	1.634±0.259 ×10^{0}	0.351±0.179
16.13	1.793±0.218 ×10^{0}	0.015±0.142
17.14	1.584±0.187 ×10^{0}	0.038±0.136
18.14	1.401±0.142 ×10^{0}	-0.144±0.120
19.14	1.191±0.139 ×10^{0}	-0.269±0.143
20.15	7.127±0.937 ×10^{-1}	-0.332±0.149
21.15	5.191±0.753 ×10^{-1}	-0.108±0.166
22.15	3.753±0.487 ×10^{-1}	-0.222±0.145
22.63	3.101±0.604 ×10^{-1}	-0.479±0.230
24.16	2.865±0.450 ×10^{-1}	0.281±0.171
28.18	7.234±0.835 ×10^{-1}	0.058±0.136
29.18	6.494±0.575 ×10^{-1}	0.069±0.106
30.18	8.066±1.069 ×10^{-1}	0.288±0.152
30.65	7.439±0.242 ×10^{-1}	0.083±0.041
31.19	6.775±0.659 ×10^{-1}	-0.147±0.117
31.69	6.807±1.114 ×10^{-1}	0.037±0.184
32.19	6.063±0.555 ×10^{-1}	-0.044±0.108
32.66	5.824±0.174 ×10^{-1}	-0.082±0.037
33.20	5.086±0.657 ×10^{-1}	-0.280±0.145
34.20	3.054±0.405 ×10^{-1}	-0.171±0.150
34.67	3.477±0.156 ×10^{-1}	-0.272±0.056
35.21	2.636±0.363 ×10^{-1}	-0.343±0.156
36.21	2.208±0.304 ×10^{-1}	-0.249±0.157
36.68	1.726±0.128 ×10^{-1}	-0.270±0.095
38.68	1.136±0.116 ×10^{-1}	0.525±0.092
40.69	1.193±0.086 ×10^{-1}	0.729±0.092
42.70	1.854±0.095 ×10^{-1}	0.718±0.053
44.70	2.350±0.118 ×10^{-1}	0.488±0.067
46.71	2.138±0.134 ×10^{-1}	0.371±0.078
48.72	1.642±0.083 ×10^{-1}	0.110±0.063
50.73	1.040±0.078 ×10^{-1}	-0.096±0.093
52.73	5.625±0.531 ×10^{-2}	-0.029±0.113
54.74	4.086±0.438 ×10^{-2}	0.821±0.108
56.74	5.413±0.473 ×10^{-2}	0.883±0.072
58.75	7.182±0.556 ×10^{-2}	0.922±0.061
60.75	8.544±0.741 ×10^{-2}	0.785±0.089
62.76	6.867±0.497 ×10^{-2}	0.674±0.070
64.76	5.228±0.420 ×10^{-2}	0.506±0.093
66.77	3.247±0.286 ×10^{-2}	0.170±0.106
68.77	2.291±0.241 ×10^{-2}	0.155±0.125
70.77	1.609±0.208 ×10^{-2}	0.490±0.142

^{168}Er 4_1^+ (Ex = 0.995 MeV)

Angle (θ_{cm})	Cross section (mb/sr)	Analyzing power (A_y)
16.13	3.917±1.118 ×10^{-1}	0.038±0.301
17.14	5.915±1.190 ×10^{-1}	-0.528±0.201
18.14	6.136±0.967 ×10^{-1}	-0.247±0.180
19.14	4.448±1.013 ×10^{-1}	-0.038±0.251
20.15	6.194±0.845 ×10^{-1}	0.343±0.157
21.15	4.975±0.752 ×10^{-1}	-0.137±0.173
22.15	6.430±0.834 ×10^{-1}	-0.318±0.154
22.63	5.549±0.505 ×10^{-1}	-0.071±0.107
23.16	4.210±0.619 ×10^{-1}	-0.427±0.160
24.16	5.317±0.586 ×10^{-1}	-0.107±0.129
26.17	3.112±0.521 ×10^{-1}	-0.114±0.185
27.17	2.708±0.597 ×10^{-1}	0.179±0.250
28.18	1.490±0.359 ×10^{-1}	-0.027±0.260
32.66	6.543±0.482 ×10^{-2}	0.521±0.082
34.67	1.125±0.081 ×10^{-1}	0.474±0.082
36.68	1.769±0.125 ×10^{-1}	0.409±0.081
38.68	1.834±0.097 ×10^{-1}	0.397±0.065
40.69	1.453±0.104 ×10^{-1}	-0.038±0.087
42.70	9.765±0.642 ×10^{-2}	-0.010±0.081
44.71	4.796±0.447 ×10^{-2}	-0.156±0.113
46.71	3.339±0.394 ×10^{-2}	-0.075±0.140
48.72	3.737±0.335 ×10^{-2}	0.507±0.106
50.73	4.450±0.439 ×10^{-2}	0.728±0.096
52.73	5.440±0.441 ×10^{-2}	0.638±0.088
54.74	5.468±0.582 ×10^{-2}	0.321±0.138
56.74	3.378±0.390 ×10^{-2}	0.076±0.137
58.75	2.561±0.292 ×10^{-2}	-0.019±0.136
60.75	1.410±0.238 ×10^{-2}	-0.172±0.188
62.76	9.688±1.811 ×10^{-3}	0.086±0.211
64.76	1.429±0.214 ×10^{-2}	0.874±0.134
66.77	1.840±0.227 ×10^{-2}	0.891±0.114
68.77	2.625±0.354 ×10^{-2}	0.866±0.145
70.77	1.271±0.190 ×10^{-2}	0.992±0.126

^{174}Yb 0^+ elastic

Angle (θ_{cm})	Cross section (mb/sr)	Analyzing power (A_y)
11.13	1.584±0.003 ×10^{4}	-0.033±0.003
12.13	9.931±0.025 ×10^{3}	-0.079±0.003
13.13	5.718±0.016 ×10^{3}	-0.136±0.004
14.13	3.086±0.012 ×10^{3}	-0.201±0.006
15.13	1.445±0.007 ×10^{3}	-0.274±0.007
16.13	6.871±0.035 ×10^{2}	-0.241±0.007
17.14	4.192±0.025 ×10^{2}	0.060±0.008
18.14	4.361±0.025 ×10^{2}	0.346±0.008
19.14	5.948±0.038 ×10^{2}	0.380±0.010
20.15	7.139±0.033 ×10^{2}	0.325±0.007
21.15	8.262±0.028 ×10^{2}	0.259±0.005
22.15	8.392±0.023 ×10^{2}	0.189±0.004
23.15	7.796±0.025 ×10^{2}	0.118±0.004
24.16	6.592±0.027 ×10^{2}	0.047±0.005
25.16	5.167±0.019 ×10^{2}	-0.042±0.005
26.17	3.763±0.023 ×10^{2}	-0.100±0.008
27.17	2.430±0.014 ×10^{2}	-0.249±0.008
28.18	1.415±0.015 ×10^{2}	-0.427±0.015
29.18	6.529±0.065 ×10^{1}	-0.700±0.014
30.18	2.728±0.018 ×10^{1}	-0.892±0.009
31.19	1.570±0.026 ×10^{1}	-0.049±0.021
32.19	2.151±0.032 ×10^{1}	0.880±0.017
33.20	3.831±0.045 ×10^{1}	0.896±0.013
34.20	5.524±0.026 ×10^{1}	0.749±0.006
35.21	6.849±0.059 ×10^{1}	0.627±0.011
36.21	7.750±0.061 ×10^{1}	0.518±0.010
36.67	7.729±0.022 ×10^{1}	0.454±0.004
37.68	7.518±0.021 ×10^{1}	0.358±0.004
38.68	6.801±0.029 ×10^{1}	0.265±0.006
40.69	4.216±0.013 ×10^{1}	0.044±0.004
42.70	1.984±0.014 ×10^{1}	-0.219±0.009
44.70	7.401±0.059 ×10^{0}	-0.331±0.010
46.71	5.424±0.063 ×10^{0}	0.611±0.014
48.72	7.883±0.065 ×10^{0}	0.964±0.009
50.72	1.013±0.007 ×10^{1}	0.833±0.008
51.73	1.037±0.007 ×10^{1}	0.754±0.008
52.73	9.911±0.070 ×10^{0}	0.638±0.008
54.74	7.521±0.059 ×10^{0}	0.442±0.010
56.74	4.459±0.039 ×10^{0}	0.205±0.011
58.75	2.314±0.028 ×10^{0}	0.000±0.016
60.75	1.396±0.020 ×10^{0}	0.196±0.018
62.76	1.403±0.020 ×10^{0}	0.733±0.015
64.76	1.579±0.021 ×10^{0}	0.977±0.012
66.77	1.698±0.022 ×10^{0}	0.970±0.012
68.77	1.483±0.020 ×10^{0}	0.898±0.013
70.77	1.063±0.017 ×10^{0}	0.740±0.017

^{174}Yb 2_1^+ (Ex = 0.076 MeV)

Angle (θ_{cm})	Cross section (mb/sr)	Analyzing power (A_y)
11.13	1.140±0.099 ×10^{2}	0.138±0.052
12.13	1.323±0.104 ×10^{2}	0.110±0.037
13.13	1.492±0.099 ×10^{2}	0.049±0.026
14.13	1.448±0.025 ×10^{2}	0.053±0.022
15.13	1.406±0.020 ×10^{2}	-0.033±0.019
16.13	1.200±0.014 ×10^{2}	-0.050±0.015
17.14	9.520±0.124 ×10^{1}	-0.094±0.017
18.14	7.169±0.094 ×10^{1}	-0.175±0.017
19.14	4.613±0.091 ×10^{1}	-0.235±0.025
20.15	2.618±0.064 ×10^{1}	-0.344±0.031
21.15	1.310±0.042 ×10^{1}	-0.428±0.041
22.15	6.982±0.309 ×10^{0}	-0.017±0.055
23.16	8.283±0.368 ×10^{0}	0.688±0.055
24.16	1.380±0.050 ×10^{1}	0.767±0.045
25.16	2.285±0.048 ×10^{1}	0.567±0.025
26.17	2.925±0.072 ×10^{1}	0.478±0.032
27.17	3.954±0.057 ×10^{1}	0.404±0.018
28.18	4.182±0.082 ×10^{1}	0.276±0.025
29.18	4.451±0.050 ×10^{1}	0.218±0.014
30.18	4.222±0.021 ×10^{1}	0.135±0.007
31.19	3.614±0.039 ×10^{1}	0.046±0.014
32.19	2.903±0.035 ×10^{1}	-0.046±0.016
33.20	2.155±0.031 ×10^{1}	-0.111±0.018
34.20	1.414±0.013 ×10^{1}	-0.221±0.011
35.21	8.882±0.208 ×10^{0}	-0.287±0.030
36.21	5.488±0.170 ×10^{0}	-0.195±0.039
36.67	4.825±0.054 ×10^{0}	0.079±0.014
37.68	4.757±0.055 ×10^{0}	0.599±0.014
38.68	5.691±0.095 ×10^{0}	0.845±0.018
40.69	1.029±0.008 ×10^{1}	0.777±0.009
42.70	1.381±0.012 ×10^{1}	0.584±0.011
44.70	1.290±0.008 ×10^{1}	0.400±0.008
46.71	9.664±0.081 ×10^{0}	0.203±0.011
48.72	5.333±0.050 ×10^{0}	0.008±0.012
50.72	2.804±0.037 ×10^{0}	-0.026±0.017
51.73	2.296±0.034 ×10^{0}	0.232±0.018
52.73	2.342±0.034 ×10^{0}	0.577±0.017
54.74	3.150±0.040 ×10^{0}	0.892±0.013
56.74	3.931±0.038 ×10^{0}	0.877±0.010
58.75	4.071±0.038 ×10^{0}	0.770±0.010
60.75	3.250±0.030 ×10^{0}	0.614±0.011
62.76	2.176±0.024 ×10^{0}	0.401±0.014
64.76	1.269±0.019 ×10^{0}	0.257±0.018
66.77	8.493±0.156 ×10^{-1}	0.250±0.023
68.77	9.303±0.163 ×10^{-1}	0.570±0.020
70.77	1.096±0.018 ×10^{0}	0.829±0.016

^{174}Yb 4^{+} (Ex = 0.253 MeV)

Angle (θ_{cm})	Cross section (mb/sr)	Analyzing power (A_y)
18.14	2.722±0.169 ×10^{0}	0.087±0.079
19.14	2.697±0.195 ×10^{0}	0.245±0.087
20.15	3.709±0.198 ×10^{0}	0.207±0.066
21.15	2.812±0.141 ×10^{0}	0.237±0.061
22.15	2.993±0.126 ×10^{0}	0.259±0.052
23.16	3.575±0.160 ×10^{0}	0.131±0.056
24.16	3.215±0.185 ×10^{0}	0.075±0.073
25.16	2.615±0.136 ×10^{0}	0.033±0.064
26.17	2.146±0.173 ×10^{0}	0.224±0.100
27.17	2.144±0.123 ×10^{0}	0.172±0.071
28.18	2.079±0.171 ×10^{0}	0.090±0.100
29.18	2.043±0.103 ×10^{0}	0.118±0.062
30.18	1.978±0.045 ×10^{0}	0.175±0.029
31.19	1.984±0.090 ×10^{0}	0.312±0.055
32.19	1.619±0.082 ×10^{0}	0.264±0.062
33.20	1.453±0.077 ×10^{0}	0.295±0.064
34.20	1.251±0.036 ×10^{0}	0.286±0.035
34.67	1.074±0.054 ×10^{0}	0.247±0.061
35.21	9.562±0.626 ×10^{-1}	0.317±0.079
36.21	8.315±0.584 ×10^{-1}	0.332±0.083
36.67	6.722±0.171 ×10^{-1}	0.386±0.031
38.68	5.562±0.249 ×10^{-1}	0.461±0.052
40.69	5.386±0.152 ×10^{-1}	0.584±0.032
42.70	5.796±0.223 ×10^{-1}	0.575±0.044
44.70	7.015±0.174 ×10^{-1}	0.489±0.029
46.71	7.403±0.218 ×10^{-1}	0.458±0.035
48.72	6.247±0.164 ×10^{-1}	0.367±0.032
50.72	4.418±0.138 ×10^{-1}	0.215±0.039
52.73	3.121±0.116 ×10^{-1}	0.230±0.046
54.74	2.287±0.099 ×10^{-1}	0.364±0.052
56.74	1.964±0.079 ×10^{-1}	0.733±0.042
58.75	2.349±0.087 ×10^{-1}	0.789±0.037
60.75	2.515±0.091 ×10^{-1}	0.762±0.032
62.76	2.781±0.095 ×10^{-1}	0.717±0.033
64.76	2.437±0.079 ×10^{-1}	0.518±0.037
66.77	1.855±0.069 ×10^{-1}	0.408±0.044
68.77	1.255±0.057 ×10^{-1}	0.354±0.054
70.77	1.092±0.053 ×10^{-1}	0.462±0.056

^{174}Yb 6^{+} (Ex = 0.526 MeV)

Angle (θ_{cm})	Cross section (mb/sr)	Analyzing power (A_y)
30.18	2.168±0.149 ×10^{-1}	0.229±0.084
32.19	2.096±0.295 ×10^{-1}	0.230±0.164
34.20	2.258±0.370 ×10^{-1}	0.172±0.179
36.67	1.358±0.155 ×10^{-1}	0.180±0.130
38.68	1.309±0.263 ×10^{-1}	0.148±0.230
40.69	1.094±0.069 ×10^{-1}	0.463±0.073
42.70	9.389±0.898 ×10^{-2}	0.777±0.094
44.70	9.916±0.651 ×10^{-2}	0.601±0.072
46.71	9.371±0.778 ×10^{-2}	0.622±0.090
48.72	9.136±0.629 ×10^{-2}	0.510±0.078
50.73	7.638±0.572 ×10^{-2}	0.412±0.088
52.73	5.616±0.490 ×10^{-2}	0.458±0.099
54.74	3.987±0.414 ×10^{-2}	0.562±0.113
56.74	3.200±0.320 ×10^{-2}	0.484±0.113
58.75	2.757±0.298 ×10^{-2}	0.565±0.117
60.75	4.070±0.325 ×10^{-2}	0.803±0.076
62.76	3.440±0.298 ×10^{-2}	0.903±0.078
64.76	3.547±0.303 ×10^{-2}	0.676±0.089
66.77	2.974±0.278 ×10^{-2}	0.536±0.103
68.77	3.231±0.291 ×10^{-2}	0.444±0.102
70.77	2.167±0.238 ×10^{-2}	0.276±0.126

^{176}Yb 0^{+} elastic

Angle (θ_{cm})	Cross section (mb/sr)	Analyzing power (A_y)
11.13	1.359±0.003 ×10^{4}	-0.027±0.003
12.13	8.374±0.022 ×10^{3}	-0.072±0.004
13.13	4.925±0.017 ×10^{3}	-0.123±0.004
14.13	2.629±0.011 ×10^{3}	-0.197±0.005
15.13	1.302±0.007 ×10^{3}	-0.262±0.007
16.13	6.045±0.037 ×10^{2}	-0.252±0.008
17.13	3.515±0.026 ×10^{2}	0.039±0.009
18.13	3.538±0.024 ×10^{2}	0.308±0.009
19.13	4.674±0.030 ×10^{2}	0.382±0.008
20.14	5.844±0.034 ×10^{2}	0.335±0.007
21.14	6.576±0.030 ×10^{2}	0.254±0.006
22.14	6.732±0.030 ×10^{2}	0.189±0.006
23.15	6.318±0.029 ×10^{2}	0.133±0.006
24.15	5.411±0.027 ×10^{2}	0.052±0.006
25.15	4.231±0.022 ×10^{2}	-0.029±0.007
26.16	3.104±0.024 ×10^{2}	-0.133±0.010
27.16	1.971±0.016 ×10^{2}	-0.264±0.010
28.17	1.143±0.019 ×10^{2}	-0.429±0.020
29.17	5.424±0.058 ×10^{1}	-0.700±0.014
30.19	2.115±0.013 ×10^{1}	-0.840±0.011
32.20	1.862±0.011 ×10^{1}	0.851±0.007
34.21	4.550±0.020 ×10^{1}	0.728±0.007
36.21	6.276±0.021 ×10^{1}	0.496±0.005
38.22	5.747±0.017 ×10^{1}	0.294±0.003
40.23	3.833±0.011 ×10^{1}	0.080±0.003
42.24	1.827±0.008 ×10^{1}	-0.193±0.005
44.24	6.713±0.045 ×10^{0}	-0.415±0.008
46.25	3.968±0.034 ×10^{0}	0.445±0.010
48.26	5.905±0.052 ×10^{0}	0.971±0.009
50.26	8.341±0.063 ×10^{0}	0.842±0.007
52.27	8.421±0.060 ×10^{0}	0.675±0.008
54.27	6.501±0.049 ×10^{0}	0.478±0.008
56.28	3.951±0.035 ×10^{0}	0.234±0.010
58.28	2.041±0.021 ×10^{0}	0.003±0.012
60.29	1.135±0.015 ×10^{0}	0.136±0.016
62.29	1.080±0.016 ×10^{0}	0.672±0.014
64.30	1.305±0.019 ×10^{0}	0.959±0.011
66.30	1.428±0.019 ×10^{0}	0.971±0.009
68.30	1.276±0.017 ×10^{0}	0.882±0.010
70.31	9.077±0.137 ×10^{-1}	0.755±0.013

^{176}Yb 2^{+} (Ex = 0.082 MeV)

Angle (θ_{cm})	Cross section (mb/sr)	Analyzing power (A_y)
11.13	7.544±0.362 ×10^{1}	-0.007±0.060
12.13	9.582±0.316 ×10^{1}	0.044±0.041
13.13	1.035±0.028 ×10^{2}	0.109±0.033
14.13	1.068±0.024 ×10^{2}	0.019±0.029
15.13	1.005±0.019 ×10^{2}	0.032±0.024
16.13	9.378±0.152 ×10^{1}	-0.056±0.021
17.13	7.365±0.122 ×10^{1}	-0.120±0.021
18.13	5.540±0.098 ×10^{1}	-0.188±0.023
19.13	3.509±0.088 ×10^{1}	-0.258±0.032
20.14	2.060±0.073 ×10^{1}	-0.404±0.044
21.14	9.884±0.473 ×10^{0}	-0.331±0.061
22.15	4.989±0.405 ×10^{0}	-0.195±0.090
23.15	4.743±0.389 ×10^{0}	0.702±0.095
24.15	8.768±0.450 ×10^{0}	0.726±0.060
25.15	1.554±0.052 ×10^{1}	0.503±0.041
26.16	2.208±0.071 ×10^{1}	0.490±0.038
27.16	2.853±0.064 ×10^{1}	0.374±0.027
28.17	3.251±0.106 ×10^{1}	0.388±0.039
29.17	3.389±0.045 ×10^{1}	0.223±0.017
30.18	3.202±0.044 ×10^{1}	0.155±0.017
32.20	2.156±0.009 ×10^{1}	-0.032±0.005
34.21	1.017±0.006 ×10^{1}	-0.254±0.007
36.21	3.692±0.040 ×10^{0}	-0.235±0.014
38.22	3.495±0.041 ×10^{0}	0.810±0.013
40.23	6.826±0.053 ×10^{0}	0.835±0.009
42.24	9.807±0.061 ×10^{0}	0.623±0.007
44.24	1.022±0.006 ×10^{1}	0.427±0.007
46.25	7.773±0.050 ×10^{0}	0.242±0.007
48.26	4.583±0.036 ×10^{0}	0.054±0.009
50.26	2.299±0.026 ×10^{0}	-0.087±0.014
52.27	1.604±0.022 ×10^{0}	0.415±0.015
54.27	2.111±0.028 ×10^{0}	0.889±0.012
56.28	2.863±0.034 ×10^{0}	0.871±0.011
58.28	3.110±0.029 ×10^{0}	0.796±0.009
60.29	2.598±0.026 ×10^{0}	0.643±0.010
62.29	1.800±0.021 ×10^{0}	0.456±0.012
64.30	1.060±0.015 ×10^{0}	0.227±0.016
66.30	6.439±0.109 ×10^{-1}	0.177±0.019
68.30	6.308±0.108 ×10^{-1}	0.541±0.017
70.31	7.891±0.129 ×10^{-1}	0.807±0.013

^{176}Yb 4^+ (Ex = 0.272 MeV)

Angle (θ_{cm})	Cross section (mb/sr)	Analyzing power (A_y)
20.14	$4.184\pm0.276\times10^{0}$	0.141±0.079
21.14	$4.093\pm0.230\times10^{0}$	0.080±0.069
22.15	$4.077\pm0.228\times10^{0}$	0.055±0.080
24.15	$2.997\pm0.197\times10^{0}$	-0.069±0.081
25.15	$2.733\pm0.182\times10^{0}$	0.120±0.082
26.16	$2.290\pm0.204\times10^{0}$	0.083±0.107
27.16	$2.201\pm0.165\times10^{0}$	0.070±0.090
28.17	$2.427\pm0.274\times10^{0}$	0.053±0.133
29.17	$2.129\pm0.109\times10^{0}$	0.091±0.063
30.19	$1.840\pm0.019\times10^{0}$	0.124±0.014
32.20	$1.580\pm0.019\times10^{0}$	0.189±0.014
34.21	$1.254\pm0.017\times10^{0}$	0.323±0.016
36.21	$8.591\pm0.143\times10^{-1}$	0.385±0.019
38.22	$7.060\pm0.132\times10^{-1}$	0.496±0.020
40.23	$6.323\pm0.123\times10^{-1}$	0.565±0.021
42.24	$6.676\pm0.126\times10^{-1}$	0.484±0.020
44.24	$7.038\pm0.126\times10^{-1}$	0.419±0.020
46.25	$7.215\pm0.127\times10^{-1}$	0.330±0.020
48.26	$5.897\pm0.113\times10^{-1}$	0.283±0.022
50.26	$4.494\pm0.098\times10^{-1}$	0.215±0.025
52.27	$3.008\pm0.079\times10^{-1}$	0.300±0.029
54.27	$2.316\pm0.073\times10^{-1}$	0.456±0.033
56.28	$2.069\pm0.068\times10^{-1}$	0.643±0.032
58.28	$2.250\pm0.063\times10^{-1}$	0.786±0.024
60.29	$2.464\pm0.066\times10^{-1}$	0.739±0.024
62.29	$2.470\pm0.064\times10^{-1}$	0.630±0.026
64.30	$2.140\pm0.059\times10^{-1}$	0.525±0.029
66.30	$1.616\pm0.045\times10^{-1}$	0.441±0.030
68.30	$1.242\pm0.040\times10^{-1}$	0.329±0.035
70.31	$9.297\pm0.346\times10^{-2}$	0.562±0.038

^{176}Yb 6^+ (Ex = 0.565 MeV)

Angle (θ_{cm})	Cross section (mb/sr)	Analyzing power (A_y)
30.20	$1.897\pm0.068\times10^{-1}$	0.173±0.042
32.20	$1.932\pm0.062\times10^{-1}$	0.280±0.037
34.21	$1.947\pm0.062\times10^{-1}$	0.431±0.035
36.21	$2.009\pm0.065\times10^{-1}$	0.408±0.036
38.22	$1.718\pm0.058\times10^{-1}$	0.518±0.036
40.23	$1.356\pm0.052\times10^{-1}$	0.444±0.042
42.24	$1.198\pm0.049\times10^{-1}$	0.445±0.044
44.24	$1.036\pm0.045\times10^{-1}$	0.562±0.045
46.25	$9.653\pm0.447\times10^{-2}$	0.476±0.051
48.26	$9.577\pm0.435\times10^{-2}$	0.576±0.048
50.26	$7.861\pm0.394\times10^{-2}$	0.479±0.052
52.27	$5.987\pm0.348\times10^{-2}$	0.461±0.062
54.27	$4.915\pm0.322\times10^{-2}$	0.471±0.068
56.28	$4.265\pm0.295\times10^{-2}$	0.588±0.071
58.29	$4.010\pm0.247\times10^{-2}$	0.624±0.059
60.29	$3.960\pm0.247\times10^{-2}$	0.683±0.059
62.29	$3.504\pm0.233\times10^{-2}$	0.913±0.054
64.30	$3.186\pm0.220\times10^{-2}$	0.854±0.059
66.30	$2.838\pm0.191\times10^{-2}$	0.775±0.059
68.31	$2.372\pm0.177\times10^{-2}$	0.577±0.076
70.31	$1.637\pm0.141\times10^{-2}$	0.475±0.092

^{176}Yb 2_γ^+ (Ex = 1.261 MeV)

Angle (θ_{cm})	Cross section (mb/sr)	Analyzing power (A_y)
14.17	$1.434\pm0.019\times10^{0}$	-0.006±0.016
16.17	$1.230\pm0.018\times10^{0}$	-0.004±0.017
18.17	$8.724\pm0.155\times10^{-1}$	-0.002±0.021
20.17	$5.131\pm0.114\times10^{-1}$	0.022±0.026
22.17	$2.725\pm0.083\times10^{-1}$	0.075±0.036
24.18	$2.822\pm0.083\times10^{-1}$	0.242±0.034
26.18	$4.401\pm0.103\times10^{-1}$	0.231±0.027
27.19	$5.135\pm0.115\times10^{-1}$	0.250±0.026
30.20	$6.012\pm0.122\times10^{-1}$	0.043±0.024
32.20	$4.647\pm0.101\times10^{-1}$	-0.023±0.025
36.22	$1.452\pm0.054\times10^{-1}$	-0.097±0.044
38.22	$9.070\pm0.436\times10^{-2}$	0.361±0.053
40.23	$1.105\pm0.047\times10^{-1}$	0.640±0.043
42.24	$1.625\pm0.058\times10^{-1}$	0.481±0.038
44.24	$1.710\pm0.058\times10^{-1}$	0.340±0.038
46.25	$1.790\pm0.059\times10^{-1}$	0.286±0.038
48.26	$1.269\pm0.049\times10^{-1}$	0.011±0.045
50.26	$7.127\pm0.385\times10^{-2}$	-0.020±0.061
52.27	$3.488\pm0.274\times10^{-2}$	-0.039±0.088
54.27	$3.323\pm0.259\times10^{-2}$	0.764±0.072
56.28	$3.385\pm0.276\times10^{-2}$	0.949±0.073
58.29	$5.151\pm0.286\times10^{-2}$	0.840±0.048
60.29	$4.525\pm0.260\times10^{-2}$	0.686±0.053
62.30	$4.291\pm0.246\times10^{-2}$	0.618±0.055
64.30	$2.486\pm0.201\times10^{-2}$	0.544±0.081
66.30	$1.656\pm0.148\times10^{-2}$	0.161±0.098
68.31	$1.320\pm0.132\times10^{-2}$	0.420±0.109
70.31	$1.302\pm0.125\times10^{-2}$	0.564±0.100

^{176}Yb 4_γ^+ (Ex = 1.420 MeV)

Angle (θ_{cm})	Cross section (mb/sr)	Analyzing power (A_y)
16.17	$1.500\pm0.068\times10^{-1}$	-0.052±0.053
18.17	$1.693\pm0.074\times10^{-1}$	0.069±0.050
20.17	$1.919\pm0.075\times10^{-1}$	0.026±0.045
22.17	$1.639\pm0.068\times10^{-1}$	0.032±0.048
24.18	$1.549\pm0.065\times10^{-1}$	-0.023±0.048
26.18	$9.474\pm0.499\times10^{-2}$	-0.222±0.060
27.19	$8.431\pm0.662\times10^{-2}$	0.034±0.089
28.19	$6.806\pm0.662\times10^{-2}$	-0.028±0.108
32.20	$5.228\pm0.774\times10^{-2}$	0.200±0.159
34.21	$6.446\pm0.424\times10^{-2}$	0.370±0.070
38.22	$8.835\pm0.448\times10^{-2}$	0.344±0.056
40.23	$7.785\pm0.417\times10^{-2}$	0.328±0.060
42.24	$3.761\pm0.276\times10^{-2}$	0.057±0.082
44.24	$2.135\pm0.220\times10^{-2}$	0.067±0.115
46.25	$2.032\pm0.226\times10^{-2}$	0.702±0.113
48.26	$2.534\pm0.242\times10^{-2}$	0.610±0.091
50.26	$3.718\pm0.297\times10^{-2}$	0.586±0.080
52.27	$3.163\pm0.259\times10^{-2}$	0.669±0.075
54.28	$2.921\pm0.252\times10^{-2}$	0.499±0.088
56.28	$1.935\pm0.206\times10^{-2}$	0.263±0.117
58.29	$1.483\pm0.157\times10^{-2}$	0.540±0.110
60.29	$8.657\pm1.249\times10^{-3}$	0.449±0.145
62.30	$9.239\pm1.443\times10^{-3}$	0.750±0.174
64.30	$1.021\pm0.133\times10^{-2}$	1.102±0.065
66.30	$1.064\pm0.119\times10^{-2}$	0.812±0.106
68.31	$1.041\pm0.109\times10^{-2}$	0.558±0.105
70.31	$7.697\pm1.027\times10^{-3}$	0.915±0.123

^{178}Hf 0^{+} elastic

Angle ($\theta_{c.m.}$)	Cross section (mb/sr)	Analyzing power (A_y)
11.07	1.433±0.007 ×10^{4}	-0.021±0.006
12.07	8.781±0.037 ×10^{3}	-0.071±0.006
13.08	5.206±0.026 ×10^{3}	-0.127±0.007
14.08	2.661±0.011 ×10^{3}	-0.198±0.006
15.09	1.385±0.009 ×10^{3}	-0.254±0.009
16.10	6.239±0.044 ×10^{2}	-0.233±0.009
17.10	4.072±0.032 ×10^{2}	0.029±0.011
18.11	4.089±0.025 ×10^{2}	0.333±0.009
19.11	5.199±0.031 ×10^{2}	0.379±0.009
20.12	6.520±0.030 ×10^{2}	0.314±0.007
21.12	7.189±0.024 ×10^{2}	0.254±0.005
22.13	7.336±0.032 ×10^{2}	0.177±0.006
23.14	6.849±0.024 ×10^{2}	0.118±0.005
24.14	5.671±0.023 ×10^{2}	0.042±0.005
25.15	4.669±0.016 ×10^{2}	-0.032±0.005
26.15	3.192±0.015 ×10^{2}	-0.141±0.006
27.16	2.181±0.011 ×10^{2}	-0.271±0.007
28.16	1.186±0.008 ×10^{2}	-0.449±0.010
29.17	6.223±0.065 ×10^{1}	-0.679±0.014
30.17	2.502±0.030 ×10^{1}	-0.864±0.016
31.18	1.455±0.021 ×10^{1}	-0.178±0.020
32.18	2.059±0.023 ×10^{1}	0.823±0.015
33.19	3.457±0.027 ×10^{1}	0.868±0.013
34.19	5.221±0.030 ×10^{1}	0.736±0.011
35.20	6.475±0.037 ×10^{1}	0.605±0.010
36.20	6.914±0.021 ×10^{1}	0.483±0.007
38.21	6.330±0.016 ×10^{1}	0.267±0.005
40.22	4.360±0.012 ×10^{1}	0.081±0.004
42.23	2.037±0.009 ×10^{1}	-0.225±0.006
44.24	8.271±0.058 ×10^{0}	-0.428±0.010
45.24	5.120±0.076 ×10^{0}	-0.150±0.020
46.25	4.699±0.035 ×10^{0}	0.448±0.011
47.25	5.419±0.071 ×10^{0}	0.863±0.018
48.26	6.946±0.048 ×10^{0}	0.972±0.014
50.27	9.596±0.051 ×10^{0}	0.838±0.012
52.27	9.662±0.047 ×10^{0}	0.657±0.010
54.28	7.600±0.038 ×10^{0}	0.456±0.008
56.29	4.728±0.027 ×10^{0}	0.225±0.008
58.29	2.439±0.020 ×10^{0}	0.011±0.011
60.30	1.460±0.014 ×10^{0}	0.101±0.012
62.31	1.393±0.014 ×10^{0}	0.670±0.013
64.31	1.662±0.016 ×10^{0}	0.950±0.014
66.32	1.785±0.016 ×10^{0}	0.961±0.014
68.32	1.546±0.012 ×10^{0}	0.888±0.013
70.33	1.135±0.010 ×10^{0}	0.762±0.013

^{178}Hf 2^{+} (Ex = 0.093 MeV)

Angle ($\theta_{c.m.}$)	Cross section (mb/sr)	Analyzing power (A_y)
14.08	9.444±0.265 ×10^{1}	0.072±0.037
15.09	9.308±0.265 ×10^{1}	0.008±0.038
16.10	8.490±0.170 ×10^{1}	-0.012±0.027
17.10	6.817±0.146 ×10^{1}	-0.115±0.029
18.11	4.828±0.091 ×10^{1}	-0.146±0.025
19.11	3.177±0.084 ×10^{1}	-0.277±0.036
20.12	1.767±0.056 ×10^{1}	-0.370±0.042
21.12	1.001±0.036 ×10^{1}	-0.401±0.049
22.13	5.174±0.435 ×10^{0}	-0.005±0.112
23.14	6.533±0.325 ×10^{0}	0.513±0.065
24.14	1.009±0.067 ×10^{1}	0.676±0.080
25.15	1.667±0.042 ×10^{1}	0.600±0.039
26.15	2.293±0.048 ×10^{1}	0.428±0.028
27.16	2.931±0.046 ×10^{1}	0.392±0.021
28.16	3.242±0.041 ×10^{1}	0.280±0.017
29.17	3.406±0.144 ×10^{1}	0.192±0.058
30.17	3.156±0.069 ×10^{1}	0.149±0.029
31.18	2.466±0.049 ×10^{1}	0.053±0.026
32.18	2.041±0.029 ×10^{1}	-0.036±0.019
33.19	1.538±0.019 ×10^{1}	-0.119±0.017
34.19	1.061±0.014 ×10^{1}	-0.195±0.018
35.20	6.490±0.131 ×10^{0}	-0.322±0.027
36.20	3.879±0.045 ×10^{0}	-0.148±0.015
38.21	3.514±0.045 ×10^{0}	0.768±0.018
40.22	6.568±0.062 ×10^{0}	0.834±0.014
42.23	9.405±0.064 ×10^{0}	0.604±0.011
44.24	9.943±0.066 ×10^{0}	0.418±0.010
45.24	8.813±0.103 ×10^{0}	0.346±0.016
46.25	7.405±0.044 ×10^{0}	0.223±0.008
47.25	5.944±0.071 ×10^{0}	0.138±0.016
48.26	4.578±0.033 ×10^{0}	0.026±0.010
50.27	2.203±0.023 ×10^{0}	-0.101±0.014
52.27	1.562±0.019 ×10^{0}	0.426±0.016
54.28	2.058±0.022 ×10^{0}	0.865±0.015
56.29	2.691±0.023 ×10^{0}	0.897±0.014
58.29	3.026±0.025 ×10^{0}	0.785±0.012
60.30	2.626±0.020 ×10^{0}	0.641±0.011
62.31	1.805±0.016 ×10^{0}	0.437±0.011
64.31	1.081±0.012 ×10^{0}	0.241±0.014
66.32	6.652±0.098 ×10^{-1}	0.201±0.019
68.32	6.290±0.079 ×10^{-1}	0.498±0.016
70.33	7.659±0.082 ×10^{-1}	0.827±0.014

^{178}Hf 4^{+} (Ex = 0.307 MeV)

Angle ($\theta_{c.m.}$)	Cross section (mb/sr)	Analyzing power (A_y)
24.14	2.529±0.101 ×10^{0}	0.071±0.052
26.15	2.160±0.084 ×10^{0}	0.127±0.049
28.16	1.729±0.090 ×10^{0}	0.040±0.068
30.17	1.449±0.045 ×10^{0}	0.124±0.040
31.18	1.238±0.033 ×10^{0}	0.123±0.035
32.18	1.211±0.037 ×10^{0}	0.175±0.038
34.19	7.463±0.565 ×10^{-1}	0.187±0.092
36.20	4.427±0.164 ×10^{-1}	0.406±0.055
38.21	4.814±0.165 ×10^{-1}	0.500±0.042
40.22	4.796±0.183 ×10^{-1}	0.544±0.050
42.23	5.430±0.152 ×10^{-1}	0.480±0.036
44.24	5.732±0.175 ×10^{-1}	0.420±0.039
45.24	5.451±0.303 ×10^{-1}	0.461±0.067
46.25	5.185±0.139 ×10^{-1}	0.333±0.035
47.25	4.909±0.265 ×10^{-1}	0.230±0.071
48.26	5.333±0.264 ×10^{-1}	0.339±0.057
50.27	3.742±0.110 ×10^{-1}	0.269±0.037
52.27	2.783±0.186 ×10^{-1}	0.258±0.085
54.28	1.709±0.074 ×10^{-1}	0.472±0.050
56.29	1.845±0.063 ×10^{-1}	0.736±0.038
58.29	1.996±0.067 ×10^{-1}	0.792±0.035
60.30	2.121±0.059 ×10^{-1}	0.738±0.029
62.31	2.100±0.057 ×10^{-1}	0.639±0.029
64.31	1.785±0.053 ×10^{-1}	0.520±0.034
66.32	1.248±0.045 ×10^{-1}	0.399±0.044
68.32	9.555±0.329 ×10^{-2}	0.347±0.044
70.33	7.905±0.274 ×10^{-2}	0.382±0.042

^{178}Hf 6^{+} (Ex = 0.632 MeV)

Angle ($\theta_{c.m.}$)	Cross section (mb/sr)	Analyzing power (A_y)
42.23	6.232±0.530 ×10^{-2}	0.556±0.123
44.24	5.354±1.270 ×10^{-2}	0.622±0.220
45.24	7.756±2.230 ×10^{-2}	0.441±0.403
46.25	6.314±0.426 ×10^{-2}	0.466±0.095
47.25	5.540±1.480 ×10^{-2}	0.466±0.376
48.26	5.955±0.914 ×10^{-2}	0.320±0.248
50.27	5.442±0.319 ×10^{-2}	0.419±0.080
52.27	4.732±0.278 ×10^{-2}	0.444±0.081
54.28	3.212±0.236 ×10^{-2}	0.512±0.105
56.29	2.527±0.211 ×10^{-2}	0.766±0.129
58.29	2.522±0.215 ×10^{-2}	0.842±0.134
60.30	2.239±0.214 ×10^{-2}	0.819±0.150
62.31	2.679±0.202 ×10^{-2}	0.873±0.117
64.31	2.256±0.181 ×10^{-2}	0.731±0.123
66.32	1.947±0.167 ×10^{-2}	0.617±0.126
68.32	1.878±0.142 ×10^{-2}	0.488±0.108
70.33	1.543±0.142 ×10^{-2}	0.543±0.132

^{180}Hf 0$^+$ elastic*

Angle (θ_{cm})	Cross section (mb/sr)	Analyzing power (A_y)
11.07	1.270±0.006 ×10^{4}	-0.030±0.006
12.07	7.879±0.031 ×10^{3}	-0.083±0.005
13.08	4.568±0.017 ×10^{3}	-0.141±0.005
14.08	2.376±0.011 ×10^{3}	-0.200±0.006
15.09	1.183±0.006 ×10^{3}	-0.253±0.007
16.09	5.632±0.030 ×10^{2}	-0.203±0.007
17.10	3.638±0.022 ×10^{2}	0.083±0.008
18.11	3.838±0.025 ×10^{2}	0.340±0.009
19.11	4.944±0.022 ×10^{2}	0.367±0.007
20.12	6.077±0.021 ×10^{2}	0.308±0.006
21.12	6.640±0.019 ×10^{2}	0.243±0.005
22.13	6.676±0.017 ×10^{2}	0.164±0.004
23.13	6.181±0.017 ×10^{2}	0.104±0.004
24.14	5.124±0.015 ×10^{2}	0.032±0.004
25.14	4.003±0.015 ×10^{2}	-0.057±0.005
26.15	2.812±0.016 ×10^{2}	-0.158±0.007
27.16	1.813±0.011 ×10^{2}	-0.286±0.006
28.16	9.919±0.073 ×10^{1}	-0.468±0.011
29.17	4.746±0.045 ×10^{1}	-0.741±0.014
30.17	2.004±0.021 ×10^{1}	-0.874±0.015
31.18	1.334±0.014 ×10^{1}	0.112±0.014
32.18	1.985±0.036 ×10^{1}	0.862±0.021
33.19	3.422±0.029 ×10^{1}	0.829±0.013
34.19	4.872±0.033 ×10^{1}	0.705±0.011
35.20	6.113±0.033 ×10^{1}	0.579±0.009
36.20	6.475±0.019 ×10^{1}	0.463±0.006
38.21	5.629±0.019 ×10^{1}	0.274±0.005
40.22	3.759±0.012 ×10^{1}	0.037±0.004
42.23	1.732±0.009 ×10^{1}	-0.262±0.007
44.24	6.473±0.052 ×10^{0}	-0.436±0.011
45.24	4.490±0.038 ×10^{0}	-0.020±0.011
46.25	4.409±0.036 ×10^{0}	0.591±0.011
48.25	6.718±0.051 ×10^{0}	0.973±0.014
50.26	9.291±0.050 ×10^{0}	0.810±0.011
52.27	8.870±0.045 ×10^{0}	0.636±0.009
54.28	6.853±0.030 ×10^{0}	0.425±0.007
56.28	4.072±0.022 ×10^{0}	0.189±0.007
58.29	2.109±0.017 ×10^{0}	-0.048±0.011
60.30	1.301±0.013 ×10^{0}	0.195±0.013
62.30	1.345±0.013 ×10^{0}	0.763±0.013
64.31	1.584±0.016 ×10^{0}	0.949±0.014
66.31	1.678±0.013 ×10^{0}	0.947±0.013
68.32	1.409±0.012 ×10^{0}	0.855±0.012
70.32	1.010±0.010 ×10^{0}	0.723±0.013
72.33	6.263±0.087 ×10^{-1}	0.519±0.017

^{180}Hf 2$^+$ (Ex = 0.093 MeV)

Angle (θ_{cm})	Cross section (mb/sr)	Analyzing power (A_y)
14.08	8.746±0.255 ×10^{1}	0.045±0.038
15.09	8.227±0.179 ×10^{1}	-0.029±0.028
16.09	7.168±0.110 ×10^{1}	-0.084±0.019
17.10	5.614±0.090 ×10^{1}	-0.094±0.021
18.11	4.073±0.089 ×10^{1}	-0.178±0.028
19.11	2.550±0.056 ×10^{1}	-0.243±0.028
20.12	1.508±0.038 ×10^{1}	-0.381±0.032
21.12	7.356±0.284 ×10^{0}	-0.345±0.050
22.13	4.484±0.220 ×10^{0}	0.099±0.063
23.13	5.077±0.303 ×10^{0}	0.714±0.076
24.14	8.967±0.365 ×10^{0}	0.601±0.060
25.14	1.373±0.037 ×10^{1}	0.567±0.035
26.15	1.867±0.048 ×10^{1}	0.484±0.036
27.16	2.400±0.045 ×10^{1}	0.380±0.025
28.16	2.644±0.042 ×10^{1}	0.277±0.020
29.17	2.695±0.036 ×10^{1}	0.201±0.017
30.17	2.565±0.035 ×10^{1}	0.132±0.018
31.18	2.265±0.021 ×10^{1}	0.057±0.012
32.18	1.729±0.021 ×10^{1}	-0.059±0.016
33.19	1.347±0.018 ×10^{1}	-0.133±0.017
34.19	8.729±0.143 ×10^{0}	-0.203±0.022
35.20	5.489±0.100 ×10^{0}	-0.259±0.025
36.20	3.206±0.042 ×10^{0}	-0.118±0.017
38.21	3.159±0.054 ×10^{0}	0.814±0.020
40.22	5.896±0.057 ×10^{0}	0.785±0.014
42.23	8.345±0.067 ×10^{0}	0.596±0.011
44.24	8.452±0.059 ×10^{0}	0.416±0.010
45.24	7.586±0.050 ×10^{0}	0.297±0.009
46.25	6.366±0.043 ×10^{0}	0.215±0.009
48.25	3.749±0.034 ×10^{0}	0.005±0.012
50.26	1.883±0.021 ×10^{0}	-0.069±0.015
52.27	1.378±0.041 ×10^{0}	0.458±0.027
54.28	1.896±0.017 ×10^{0}	0.883±0.013
56.28	2.430±0.019 ×10^{0}	0.877±0.012
58.29	2.731±0.021 ×10^{0}	0.775±0.012
60.30	2.266±0.018 ×10^{0}	0.604±0.011
62.30	1.525±0.014 ×10^{0}	0.435±0.012
64.31	8.655±0.112 ×10^{-1}	0.220±0.016
66.31	5.812±0.076 ×10^{-1}	0.184±0.016
68.32	5.446±0.077 ×10^{-1}	0.587±0.016
70.32	6.966±0.084 ×10^{-1}	0.866±0.015
72.33	7.827±0.101 ×10^{-1}	0.932±0.015

^{180}Hf 4$^+$ (Ex = 0.309 MeV)

Angle (θ_{cm})	Cross section (mb/sr)	Analyzing power (A_y)
19.11	2.404±0.154 ×10^{0}	0.288±0.084
24.14	2.683±0.111 ×10^{0}	0.086±0.053
26.15	2.691±0.084 ×10^{0}	0.031±0.040
28.16	2.030±0.073 ×10^{0}	0.044±0.047
30.17	1.619±0.047 ×10^{0}	0.086±0.037
31.18	1.269±0.071 ×10^{0}	0.043±0.071
32.18	1.226±0.037 ×10^{0}	0.191±0.037
34.19	8.165±0.246 ×10^{-1}	0.314±0.039
36.20	5.573±0.192 ×10^{-1}	0.571±0.039
38.21	5.924±0.230 ×10^{-1}	0.566±0.042
40.22	6.082±0.187 ×10^{-1}	0.607±0.035
42.23	6.829±0.205 ×10^{-1}	0.478±0.034
44.24	6.772±0.181 ×10^{-1}	0.375±0.034
45.24	6.486±0.163 ×10^{-1}	0.228±0.031
46.25	5.378±0.148 ×10^{-1}	0.172±0.034
48.25	3.771±0.172 ×10^{-1}	0.122±0.057
50.26	2.768±0.116 ×10^{-1}	0.112±0.053
52.27	2.037±0.099 ×10^{-1}	0.334±0.056
54.28	2.067±0.059 ×10^{-1}	0.618±0.032
56.28	2.061±0.057 ×10^{-1}	0.814±0.027
58.29	2.383±0.065 ×10^{-1}	0.795±0.029
60.30	2.162±0.059 ×10^{-1}	0.689±0.029
62.30	2.105±0.053 ×10^{-1}	0.612±0.029
64.31	1.570±0.051 ×10^{-1}	0.437±0.038
66.31	1.203±0.036 ×10^{-1}	0.374±0.036
68.32	8.812±0.323 ×10^{-2}	0.374±0.044
70.32	7.775±0.295 ×10^{-2}	0.604±0.041
72.33	7.928±0.343 ×10^{-2}	0.748±0.041

^{180}Hf 6$^+$ (Ex = 0.641 MeV)

Angle (θ_{cm})	Cross section (mb/sr)	Analyzing power (A_y)
42.23	8.794±0.507 ×10^{-2}	0.358±0.072
44.24	7.939±1.250 ×10^{-2}	0.347±0.161
45.24	7.542±0.453 ×10^{-2}	0.515±0.079
46.25	6.775±0.349 ×10^{-2}	0.302±0.064
48.25	5.959±1.340 ×10^{-2}	0.224±0.333
50.26	4.436±0.339 ×10^{-2}	0.228±0.101
52.27	3.960±0.240 ×10^{-2}	0.271±0.078
54.28	3.265±0.308 ×10^{-2}	0.329±0.126
56.28	3.305±0.216 ×10^{-2}	0.720±0.089
58.29	2.857±0.203 ×10^{-2}	0.808±0.100
60.30	3.637±0.259 ×10^{-2}	0.628±0.099
62.30	3.094±0.206 ×10^{-2}	0.714±0.090
64.31	2.603±0.201 ×10^{-2}	0.657±0.113
66.31	2.229±0.144 ×10^{-2}	0.455±0.086
68.32	1.791±0.131 ×10^{-2}	0.323±0.100
70.32	1.425±0.132 ×10^{-2}	0.362±0.126
72.33	1.098±0.322 ×10^{-2}	0.539±0.389

^{182}W 0° elastic

Angle (θ_{cm})	Cross section (mb/sr)	Analyzing power (A_y)
11.06	1.499±0.005 ×10⁴	-0.034±0.004
12.07	9.346±0.024 ×10³	-0.076±0.003
13.08	5.361±0.017 ×10³	-0.128±0.004
14.08	2.972±0.009 ×10³	-0.192±0.004
15.09	1.443±0.006 ×10³	-0.244±0.005
16.09	7.088±0.030 ×10²	-0.222±0.006
17.10	4.325±0.021 ×10²	0.042±0.006
18.10	4.295±0.020 ×10²	0.312±0.006
19.11	5.462±0.022 ×10²	0.361±0.006
20.12	6.640±0.025 ×10²	0.313±0.006
21.12	7.441±0.021 ×10²	0.251±0.004
22.13	7.496±0.020 ×10²	0.183±0.004
23.13	6.959±0.014 ×10²	0.110±0.003
24.14	5.901±0.017 ×10²	0.032±0.004
25.14	4.602±0.010 ×10²	-0.047±0.003
26.15	3.298±0.011 ×10²	-0.140±0.005
27.15	2.106±0.010 ×10²	-0.290±0.006
28.16	1.186±0.008 ×10²	-0.475±0.009
29.16	5.441±0.043 ×10¹	-0.753±0.013
30.17	2.414±0.027 ×10¹	-0.884±0.015
30.67	1.687±0.027 ×10¹	-0.538±0.021
31.17	1.521±0.019 ×10¹	0.058±0.015
32.18	2.201±0.021 ×10¹	0.850±0.014
32.68	3.053±0.032 ×10¹	0.883±0.014
33.18	3.767±0.027 ×10¹	0.859±0.012
34.19	5.379±0.034 ×10¹	0.713±0.010
35.19	6.739±0.037 ×10¹	0.572±0.009
36.20	7.440±0.022 ×10¹	0.468±0.006
37.20	7.733±0.035 ×10¹	0.371±0.007
38.21	6.912±0.013 ×10¹	0.278±0.004
39.21	5.690±0.030 ×10¹	0.154±0.006
40.22	4.427±0.011 ×10¹	0.046±0.003
42.23	2.277±0.006 ×10¹	-0.221±0.004
43.23	1.296±0.011 ×10¹	-0.404±0.011
44.24	7.804±0.048 ×10⁰	-0.417±0.009
46.24	5.050±0.036 ×10⁰	0.446±0.009
48.25	7.921±0.052 ×10⁰	0.957±0.013
49.26	9.433±0.079 ×10⁰	0.918±0.013
50.26	1.056±0.004 ×10¹	0.836±0.010
52.27	1.074±0.005 ×10¹	0.626±0.009
54.27	8.358±0.032 ×10⁰	0.434±0.006
56.28	4.859±0.022 ×10⁰	0.154±0.006
57.28	3.534±0.027 ×10⁰	0.031±0.009
58.29	2.630±0.017 ×10⁰	-0.058±0.008
60.29	1.530±0.013 ×10⁰	0.163±0.010
62.30	1.564±0.012 ×10⁰	0.716±0.011
64.30	1.914±0.015 ×10⁰	0.952±0.013
66.31	2.043±0.012 ×10⁰	0.949±0.012
68.31	1.763±0.012 ×10⁰	0.848±0.012
70.32	1.263±0.009 ×10⁰	0.700±0.010

^{182}W 2⁺ (Ex = 0.100 MeV)

Angle (θ_{cm})	Cross section (mb/sr)	Analyzing power (A_y)
13.08	6.050±0.341 ×10¹	0.013±0.068
14.08	8.240±0.201 ×10¹	0.004±0.030
17.10	5.140±0.154 ×10¹	-0.124±0.037
18.10	3.915±0.068 ×10¹	-0.150±0.022
19.11	2.603±0.051 ×10¹	-0.255±0.024
20.12	1.549±0.047 ×10¹	-0.306±0.038
21.12	8.433±0.272 ×10⁰	-0.330±0.041
22.13	5.104±0.237 ×10⁰	0.050±0.056
23.13	5.493±0.188 ×10⁰	0.556±0.040
24.14	8.790±0.274 ×10⁰	0.634±0.035
25.14	1.443±0.024 ×10¹	0.542±0.021
26.15	1.926±0.032 ×10¹	0.464±0.019
27.15	2.410±0.035 ×10¹	0.364±0.017
28.16	2.659±0.036 ×10¹	0.296±0.017
29.16	2.745±0.033 ×10¹	0.200±0.014
30.17	2.588±0.027 ×10¹	0.132±0.013
30.67	2.412±0.032 ×10¹	0.095±0.017
31.17	2.265±0.023 ×10¹	0.071±0.013
32.18	1.807±0.019 ×10¹	-0.021±0.013
32.68	1.570±0.022 ×10¹	-0.091±0.017
33.18	1.331±0.015 ×10¹	-0.111±0.014
34.19	9.101±0.136 ×10⁰	-0.263±0.019
35.19	5.373±0.102 ×10⁰	-0.260±0.024
36.20	3.271±0.042 ×10⁰	-0.157±0.016
37.20	2.749±0.076 ×10⁰	0.298±0.031
38.21	3.014±0.028 ×10⁰	0.729±0.016
39.21	4.377±0.096 ×10⁰	0.828±0.023
40.22	5.936±0.049 ×10⁰	0.783±0.013
42.23	8.295±0.047 ×10⁰	0.600±0.009
43.23	8.920±0.091 ×10⁰	0.498±0.013
44.24	8.740±0.054 ×10⁰	0.427±0.008
46.24	6.783±0.041 ×10⁰	0.227±0.007
48.25	3.859±0.028 ×10⁰	-0.010±0.009
49.26	2.752±0.039 ×10⁰	-0.044±0.017
50.26	2.019±0.016 ×10⁰	-0.103±0.010
52.27	1.400±0.016 ×10⁰	0.429±0.013
54.27	1.825±0.016 ×10⁰	0.643±0.012
56.28	2.435±0.019 ×10⁰	0.684±0.013
57.28	2.707±0.026 ×10⁰	0.828±0.013
58.29	2.666±0.019 ×10⁰	0.768±0.011
60.29	2.305±0.016 ×10⁰	0.610±0.010
62.30	1.604±0.012 ×10⁰	0.429±0.010
64.30	9.177±0.095 ×10⁻¹	0.192±0.012
66.31	5.994±0.063 ×10⁻¹	0.174±0.012
68.31	5.771±0.065 ×10⁻¹	0.520±0.013
70.32	7.195±0.070 ×10⁻¹	0.809±0.012

^{182}W 4⁺ (Ex = 0.329 MeV)

Angle (θ_{cm})	Cross section (mb/sr)	Analyzing power (A_y)
24.14	3.226±0.125 ×10⁰	-0.021±0.047
25.14	3.086±0.127 ×10⁰	-0.063±0.051
26.15	2.707±0.045 ×10⁰	-0.022±0.020
27.15	2.594±0.110 ×10⁰	0.007±0.052
30.67	1.461±0.080 ×10⁰	0.194±0.070
31.17	1.431±0.073 ×10⁰	0.181±0.063
32.18	1.032±0.032 ×10⁰	0.156±0.037
33.18	9.880±0.488 ×10⁻¹	0.237±0.062
34.19	8.204±0.221 ×10⁻¹	0.351±0.033
35.19	7.439±0.421 ×10⁻¹	0.415±0.062
36.20	7.069±0.190 ×10⁻¹	0.523±0.028
38.21	7.006±0.125 ×10⁻¹	0.603±0.024
39.21	7.000±0.398 ×10⁻¹	0.709±0.056
40.22	7.607±0.165 ×10⁻¹	0.567±0.025
42.23	7.974±0.045 ×10⁻¹	0.451±0.020
43.23	7.134±0.277 ×10⁻¹	0.443±0.045
44.24	7.592±0.166 ×10⁻¹	0.350±0.025
46.24	6.464±0.128 ×10⁻¹	0.238±0.023
48.25	4.706±0.103 ×10⁻¹	0.216±0.025
49.26	4.080±0.153 ×10⁻¹	0.167±0.045
50.26	3.393±0.067 ×10⁻¹	0.191±0.023
52.27	2.446±0.067 ×10⁻¹	0.428±0.029
54.27	2.172±0.054 ×10⁻¹	0.656±0.024
56.28	2.162±0.053 ×10⁻¹	0.827±0.022
57.28	2.231±0.072 ×10⁻¹	0.846±0.029
58.29	2.336±0.057 ×10⁻¹	0.783±0.022
60.29	2.322±0.053 ×10⁻¹	0.660±0.023
62.30	2.094±0.045 ×10⁻¹	0.535±0.023
64.30	1.526±0.040 ×10⁻¹	0.383±0.028
66.31	1.168±0.028 ×10⁻¹	0.356±0.027
68.31	9.602±0.262 ×10⁻²	0.328±0.031
70.32	8.939±0.244 ×10⁻²	0.564±0.027

^{182}W 6⁺ (Ex = 0.681 MeV)

Angle (θ_{cm})	Cross section (mb/sr)	Analyzing power (A_y)
40.22	8.008±0.929 ×10⁻²	0.490±0.122
44.24	7.682±0.661 ×10⁻²	0.466±0.103
46.24	6.367±0.609 ×10⁻²	0.337±0.090
48.25	5.771±0.298 ×10⁻²	0.135±0.062
50.26	4.620±0.411 ×10⁻²	0.220±0.126
52.27	3.562±0.200 ×10⁻²	0.286±0.068
54.27	2.810±0.156 ×10⁻²	0.634±0.062
58.29	2.805±0.154 ×10⁻²	0.741±0.060
60.29	3.166±0.186 ×10⁻²	0.690±0.073
62.30	2.830±0.148 ×10⁻²	0.716±0.053
64.30	2.454±0.133 ×10⁻²	0.533±0.061
66.31	2.109±0.103 ×10⁻²	0.471±0.055
68.31	1.674±0.104 ×10⁻²	0.302±0.075
70.32	1.492±0.092 ×10⁻²	0.480±0.073

^{182}W 2$^+$ (Ex = 1.221 MeV)

Angle ($\theta_{c.m.}$)	Cross section (mb/sr)	Analyzing power (A_y)
12.13	2.165±0.247 ×10^{0}	0.131±0.129
13.13	2.402±0.245 ×10^{0}	0.070±0.115
14.13	2.172±0.139 ×10^{0}	0.024±0.075
15.13	2.126±0.234 ×10^{0}	-0.129±0.124
16.13	1.767±0.106 ×10^{0}	-0.046±0.071
17.13	1.482±0.105 ×10^{0}	-0.112±0.090
18.13	1.084±0.074 ×10^{0}	-0.098±0.080
19.13	8.979±0.768 ×10^{-1}	-0.072±0.098
20.14	6.037±0.540 ×10^{-1}	-0.121±0.103
21.14	4.769±0.414 ×10^{-1}	0.044±0.101
22.14	3.999±0.359 ×10^{-1}	0.168±0.103
23.15	3.174±0.247 ×10^{-1}	0.206±0.089
24.15	4.077±0.397 ×10^{-1}	0.278±0.108
25.15	4.710±0.302 ×10^{-1}	0.157±0.075
26.16	5.950±0.414 ×10^{-1}	0.231±0.080
27.16	8.166±0.692 ×10^{-1}	0.240±0.100
32.18	6.709±0.352 ×10^{-1}	0.056±0.064
34.19	3.383±0.215 ×10^{-1}	-0.167±0.075
36.20	1.941±0.133 ×10^{-1}	-0.073±0.082
36.21	1.772±0.053 ×10^{-1}	-0.116±0.036
37.20	1.101±0.100 ×10^{-1}	0.083±0.106
38.22	1.010±0.042 ×10^{-1}	0.296±0.048
40.22	1.613±0.052 ×10^{-1}	0.674±0.031
44.24	2.960±0.069 ×10^{-1}	0.445±0.026
46.24	2.689±0.058 ×10^{-1}	0.320±0.025
48.25	1.529±0.049 ×10^{-1}	0.027±0.038
50.25	9.737±0.276 ×10^{-2}	-0.135±0.034
52.26	4.742±0.220 ×10^{-2}	-0.051±0.055
54.27	4.578±0.190 ×10^{-2}	0.453±0.045
56.27	5.969±0.230 ×10^{-2}	0.900±0.031
60.28	7.462±0.256 ×10^{-2}	0.682±0.034
62.29	6.988±0.231 ×10^{-2}	0.570±0.035
64.29	4.512±0.175 ×10^{-2}	0.364±0.044
66.29	2.707±0.118 ×10^{-2}	0.210±0.051
68.30	1.879±0.107 ×10^{-2}	0.301±0.065
70.30	1.971±0.100 ×10^{-2}	0.655±0.050

^{182}W 4$^+$ (Ex = 1.443 MeV)

Angle ($\theta_{c.m.}$)	Cross section (mb/sr)	Analyzing power (A_y)
16.13	8.972±3.334 ×10^{-2}	-0.002±0.358
17.13	1.409±0.345 ×10^{-1}	0.236±0.274
18.13	1.124±0.279 ×10^{-1}	-0.106±0.258
19.13	1.371±0.321 ×10^{-1}	0.049±0.243
20.10	2.445±0.278 ×10^{-1}	-0.044±0.129
20.14	1.071±0.277 ×10^{-1}	0.338±0.259
21.14	1.298±0.220 ×10^{-1}	-0.062±0.188
22.14	1.017±0.174 ×10^{-1}	-0.134±0.188
23.15	1.062±0.165 ×10^{-1}	-0.199±0.170
24.15	1.150±0.220 ×10^{-1}	0.083±0.207
25.15	9.102±1.481 ×10^{-2}	0.131±0.179
37.20	5.895±0.760 ×10^{-2}	0.480±0.140
38.22	5.145±0.301 ×10^{-2}	0.268±0.068
40.22	3.758±0.276 ×10^{-2}	0.265±0.081
42.23	1.961±0.189 ×10^{-2}	0.068±0.110
44.24	1.547±0.182 ×10^{-2}	0.349±0.125
48.25	2.770±0.393 ×10^{-2}	0.473±0.151
50.26	2.952±0.152 ×10^{-2}	0.600±0.052
52.26	2.163±0.148 ×10^{-2}	0.321±0.076
54.27	1.565±0.110 ×10^{-2}	0.185±0.080
56.27	8.793±0.856 ×10^{-3}	0.110±0.111
58.28	7.348±0.757 ×10^{-3}	0.415±0.110
60.28	7.070±0.834 ×10^{-3}	0.553±0.117
62.29	8.310±0.793 ×10^{-3}	0.863±0.079
66.29	1.008±0.072 ×10^{-2}	0.728±0.067
68.30	8.622±0.743 ×10^{-3}	0.577±0.086
70.30	6.639±0.579 ×10^{-3}	0.484±0.091

^{184}W 0$^+$ elastic

Angle ($\theta_{c.m.}$)	Cross section (mb/sr)	Analyzing power (A_y)
11.06	1.935±0.007 ×10^{4}	-0.053±0.005
12.07	1.219±0.002 ×10^{4}	-0.068±0.003
13.08	7.264±0.019 ×10^{3}	-0.114±0.003
14.08	3.821±0.013 ×10^{3}	-0.185±0.005
15.09	2.042±0.007 ×10^{3}	-0.237±0.005
16.09	8.981±0.048 ×10^{2}	-0.205±0.007
17.10	5.666±0.022 ×10^{2}	0.017±0.005
18.10	5.770±0.023 ×10^{2}	0.321±0.006
19.11	6.969±0.024 ×10^{2}	0.354±0.006
20.11	8.671±0.027 ×10^{2}	0.308±0.005
21.12	9.460±0.023 ×10^{2}	0.246±0.004
22.12	9.514±0.019 ×10^{2}	0.170±0.003
23.13	8.758±0.019 ×10^{2}	0.106±0.003
24.14	7.316±0.020 ×10^{2}	0.023±0.003
25.14	5.700±0.017 ×10^{2}	-0.056±0.004
26.15	3.685±0.013 ×10^{2}	-0.162±0.004
27.15	2.561±0.012 ×10^{2}	-0.293±0.006
28.16	1.338±0.007 ×10^{2}	-0.510±0.008
29.16	6.506±0.051 ×10^{1}	-0.751±0.011
31.17	2.025±0.023 ×10^{1}	0.226±0.014
32.18	3.119±0.029 ×10^{1}	0.884±0.014
33.18	5.167±0.038 ×10^{1}	0.837±0.012
34.19	7.406±0.040 ×10^{1}	0.684±0.010
35.19	8.923±0.045 ×10^{1}	0.551±0.008
36.20	9.741±0.024 ×10^{1}	0.443±0.006
38.21	8.434±0.017 ×10^{1}	0.243±0.003
40.21	5.369±0.013 ×10^{1}	0.020±0.003
41.22	3.816±0.023 ×10^{1}	-0.111±0.007
42.22	2.478±0.008 ×10^{1}	-0.266±0.005
43.23	1.534±0.015 ×10^{1}	-0.407±0.013
44.23	9.359±0.052 ×10^{0}	-0.397±0.008
45.24	6.593±0.082 ×10^{0}	0.036±0.015
46.24	6.610±0.042 ×10^{0}	0.652±0.010
48.25	1.033±0.005 ×10^{1}	0.962±0.012
49.25	1.255±0.010 ×10^{1}	0.903±0.013
50.26	1.405±0.006 ×10^{1}	0.793±0.011
51.26	1.445±0.009 ×10^{1}	0.694±0.010
52.26	1.346±0.005 ×10^{1}	0.603±0.008
54.27	9.868±0.035 ×10^{0}	0.381±0.006
56.28	5.742±0.028 ×10^{0}	0.128±0.006
58.28	2.855±0.017 ×10^{0}	-0.087±0.008
60.29	1.898±0.020 ×10^{0}	0.260±0.013
62.29	2.131±0.016 ×10^{0}	0.822±0.012
64.30	2.590±0.019 ×10^{0}	0.971±0.013
66.30	2.604±0.016 ×10^{0}	0.933±0.012
68.31	2.170±0.013 ×10^{0}	0.817±0.011
70.31	1.485±0.011 ×10^{0}	0.649±0.011
72.32	8.962±0.090 ×10^{-1}	0.418±0.012
74.32	5.583±0.069 ×10^{-1}	0.312±0.015
76.32	4.971±0.076 ×10^{-1}	0.486±0.018

^{184}W 2$^+$ (Ex = 0.111 MeV)

Angle ($\theta_{c.m.}$)	Cross section (mb/sr)	Analyzing power (A_y)
14.08	9.714±0.258 ×10^{1}	-0.021±0.033
15.09	8.684±0.190 ×10^{1}	-0.019±0.027
18.10	4.226±0.104 ×10^{1}	-0.181±0.031
19.11	2.914±0.056 ×10^{1}	-0.265±0.024
20.11	1.620±0.044 ×10^{1}	-0.350±0.033
21.12	8.752±0.301 ×10^{0}	-0.409±0.044
22.12	6.722±0.193 ×10^{0}	0.122±0.037
23.13	6.804±0.236 ×10^{0}	0.542±0.039
24.14	1.047±0.032 ×10^{1}	0.630±0.036
25.14	1.600±0.033 ×10^{1}	0.596±0.027
26.15	2.276±0.034 ×10^{1}	0.420±0.019
27.15	2.672±0.039 ×10^{1}	0.374±0.019
28.16	3.064±0.033 ×10^{1}	0.267±0.014
29.16	3.143±0.033 ×10^{1}	0.202±0.013
31.17	2.516±0.026 ×10^{1}	0.038±0.013
32.18	1.938±0.021 ×10^{1}	-0.041±0.014
33.18	1.393±0.019 ×10^{1}	-0.133±0.017
34.19	9.240±0.130 ×10^{0}	-0.247±0.019
35.19	5.386±0.112 ×10^{0}	-0.244±0.027
36.20	3.453±0.042 ×10^{0}	-0.136±0.016
38.21	3.524±0.038 ×10^{0}	0.783±0.014
40.21	6.909±0.057 ×10^{0}	0.794±0.012
41.22	8.412±0.116 ×10^{0}	0.670±0.016
42.22	9.548±0.060 ×10^{0}	0.610±0.010
43.23	1.035±0.013 ×10^{1}	0.513±0.015
44.23	1.015±0.006 ×10^{1}	0.443±0.008
45.24	8.946±0.099 ×10^{0}	0.339±0.013
46.24	7.203±0.041 ×10^{0}	0.205±0.007
48.25	4.217±0.029 ×10^{0}	-0.018±0.008
49.25	2.799±0.044 ×10^{0}	-0.113±0.019
50.26	2.057±0.020 ×10^{0}	-0.097±0.012
51.26	1.558±0.029 ×10^{0}	0.137±0.023
52.26	1.539±0.016 ×10^{0}	0.472±0.012
54.27	2.156±0.018 ×10^{0}	0.884±0.013
56.28	2.880±0.023 ×10^{0}	0.859±0.013
58.28	3.052±0.021 ×10^{0}	0.734±0.011
60.29	2.507±0.024 ×10^{0}	0.588±0.012
62.29	1.716±0.014 ×10^{0}	0.370±0.010
64.30	9.821±0.104 ×10^{-1}	0.176±0.013
66.30	6.271±0.073 ×10^{-1}	0.211±0.014
68.31	6.488±0.070 ×10^{-1}	0.617±0.013
70.31	8.287±0.087 ×10^{-1}	0.828±0.013
72.32	9.530±0.097 ×10^{-1}	0.899±0.014
74.32	9.020±0.093 ×10^{-1}	0.862±0.014
76.32	6.909±0.093 ×10^{-1}	0.795±0.016

^{184}W 4^+ (Ex = 0.364 MeV)

Angle ($\theta_{c.m.}$)	Cross section (mb/sr)	Analyzing power (A_y)
24.64	4.032±0.118 ×10^{0}	−0.032±0.036
25.14	3.844±0.111 ×10^{0}	0.001±0.035
26.15	3.588±0.089 ×10^{0}	−0.014±0.030
27.15	3.017±0.063 ×10^{0}	−0.047±0.026
28.16	2.691±0.048 ×10^{0}	−0.014±0.022
29.16	2.488±0.104 ×10^{0}	−0.107±0.050
32.18	1.406±0.044 ×10^{0}	0.196±0.037
33.18	1.137±0.024 ×10^{0}	0.309±0.026
34.19	9.754±0.324 ×10^{-1}	0.431±0.039
35.19	8.955±0.224 ×10^{-1}	0.532±0.029
36.20	9.747±0.202 ×10^{-1}	0.637±0.023
38.21	9.298±0.179 ×10^{-1}	0.607±0.022
40.21	9.817±0.206 ×10^{-1}	0.480±0.023
41.22	1.009±0.041 ×10^{0}	0.469±0.045
42.22	9.938±0.178 ×10^{-1}	0.422±0.021
43.23	9.667±0.410 ×10^{-1}	0.332±0.049
44.23	9.564±0.184 ×10^{-1}	0.328±0.022
45.24	8.394±0.318 ×10^{-1}	0.231±0.045
46.24	7.052±0.134 ×10^{-1}	0.237±0.022
48.25	5.416±0.107 ×10^{-1}	0.152±0.024
49.25	4.321±0.172 ×10^{-1}	0.253±0.047
50.26	3.818±0.085 ×10^{-1}	0.245±0.025
51.26	3.271±0.134 ×10^{-1}	0.428±0.046
52.26	2.926±0.069 ×10^{-1}	0.522±0.025
54.27	2.757±0.060 ×10^{-1}	0.729±0.022
56.28	2.910±0.071 ×10^{-1}	0.828±0.021
58.28	3.025±0.063 ×10^{-1}	0.741±0.020
60.29	2.763±0.079 ×10^{-1}	0.626±0.030
62.29	2.414±0.052 ×10^{-1}	0.453±0.023
64.30	1.744±0.044 ×10^{-1}	0.350±0.029
66.30	1.301±0.033 ×10^{-1}	0.376±0.029
68.31	1.072±0.028 ×10^{-1}	0.471±0.029
70.31	1.027±0.029 ×10^{-1}	0.659±0.033
72.32	1.079±0.032 ×10^{-1}	0.885±0.027
74.32	1.139±0.032 ×10^{-1}	0.887±0.026
76.32	9.823±0.347 ×10^{-2}	0.846±0.033

^{184}W 6^+ (Ex = 0.748 MeV)

Angle ($\theta_{c.m.}$)	Cross section (mb/sr)	Analyzing power (A_y)
41.22	1.384±0.192 ×10^{-1}	0.299±0.174
42.22	9.385±0.783 ×10^{-2}	0.176±0.100
46.24	7.607±0.630 ×10^{-2}	0.193±0.091
48.25	5.470±0.563 ×10^{-2}	0.229±0.108
49.25	6.549±1.100 ×10^{-2}	0.325±0.211
50.26	4.571±0.220 ×10^{-2}	0.374±0.056
52.26	3.644±0.519 ×10^{-2}	0.570±0.245
54.27	3.409±0.183 ×10^{-2}	0.832±0.059
56.28	4.823±0.241 ×10^{-2}	0.729±0.058
58.28	4.282±0.216 ×10^{-2}	0.756±0.063
60.29	4.556±0.365 ×10^{-2}	0.687±0.104
62.29	3.315±0.178 ×10^{-2}	0.591±0.062
64.30	2.861±0.164 ×10^{-2}	0.402±0.068
66.30	2.339±0.124 ×10^{-2}	0.234±0.064
68.31	1.958±0.107 ×10^{-2}	0.259±0.066
70.31	1.943±0.123 ×10^{-2}	0.557±0.077
72.32	2.002±0.149 ×10^{-2}	0.711±0.093
74.32	2.241±0.154 ×10^{-2}	0.688±0.083
76.32	2.185±0.207 ×10^{-2}	0.742±0.120

^{184}W 2_γ^+ (Ex = 0.903 MeV)

Angle ($\theta_{c.m.}$)	Cross section (mb/sr)	Analyzing power (A_y)
13.12	2.760±0.217 ×10^{0}	0.145±0.090
14.12	2.388±0.180 ×10^{0}	−0.061±0.088
15.12	2.447±0.141 ×10^{0}	−0.020±0.068
16.13	2.309±0.113 ×10^{0}	−0.006±0.059
16.58	2.047±0.156 ×10^{0}	0.019±0.092
17.13	1.939±0.102 ×10^{0}	0.074±0.062
18.13	1.660±0.095 ×10^{0}	0.008±0.069
19.13	1.168±0.071 ×10^{0}	0.001±0.072
20.13	8.217±0.581 ×10^{-1}	−0.017±0.084
21.14	5.260±0.367 ×10^{-1}	−0.096±0.081
22.14	4.527±0.268 ×10^{-1}	−0.190±0.069
30.19	9.411±0.180 ×10^{-1}	0.057±0.023
31.17	8.258±0.400 ×10^{-1}	0.010±0.058
32.19	6.423±0.166 ×10^{-1}	−0.052±0.031
33.20	4.764±0.128 ×10^{-1}	−0.102±0.032
34.20	3.802±0.116 ×10^{-1}	−0.073±0.036
40.22	1.831±0.060 ×10^{-1}	0.715±0.033
42.23	2.713±0.065 ×10^{-1}	0.544±0.027
44.23	2.973±0.069 ×10^{-1}	0.364±0.027
46.24	2.706±0.056 ×10^{-1}	0.190±0.024
48.24	2.088±0.045 ×10^{-1}	0.089±0.026
50.25	1.100±0.036 ×10^{-1}	0.004±0.039
52.26	5.123±0.202 ×10^{-2}	0.051±0.047
54.26	5.310±0.203 ×10^{-2}	0.801±0.035
56.27	7.886±0.274 ×10^{-2}	0.864±0.030
58.27	9.070±0.263 ×10^{-2}	0.749±0.028
60.28	8.966±0.406 ×10^{-2}	0.591±0.046
62.28	7.260±0.235 ×10^{-2}	0.405±0.037
64.29	4.572±0.186 ×10^{-2}	0.177±0.048
66.29	2.770±0.126 ×10^{-2}	0.135±0.054
68.29	2.099±0.103 ×10^{-2}	0.293±0.057
70.30	2.415±0.117 ×10^{-2}	0.752±0.046
72.30	2.721±0.144 ×10^{-2}	0.894±0.043
74.30	3.274±0.158 ×10^{-2}	0.834±0.043
76.30	2.759±0.171 ×10^{-2}	0.898±0.051

^{184}W 4_γ^+ (Ex = 1.134 MeV)

Angle ($\theta_{c.m.}$)	Cross section (mb/sr)	Analyzing power (A_y)
18.13	1.681±0.372 ×10^{-1}	0.048±0.239
19.13	2.013±0.331 ×10^{-1}	0.059±0.180
20.13	1.784±0.308 ×10^{-1}	0.037±0.191
21.14	1.693±0.207 ×10^{-1}	0.005±0.137
22.14	1.718±0.220 ×10^{-1}	−0.053±0.146
23.14	1.507±0.173 ×10^{-1}	−0.156±0.127
24.15	1.420±0.228 ×10^{-1}	0.098±0.176
34.20	6.437±0.587 ×10^{-2}	0.228±0.103
35.20	7.428±0.575 ×10^{-2}	0.327±0.076
36.21	7.767±0.391 ×10^{-2}	0.329±0.058
38.21	7.040±0.461 ×10^{-2}	0.391±0.073
48.24	2.890±0.172 ×10^{-2}	0.446±0.066
50.25	3.381±0.176 ×10^{-2}	0.375±0.058
52.26	3.306±0.163 ×10^{-2}	0.413±0.055
54.26	2.459±0.156 ×10^{-2}	0.246±0.070
58.27	1.168±0.106 ×10^{-2}	0.542±0.096
60.28	1.040±0.162 ×10^{-2}	0.443±0.163
62.28	1.093±0.091 ×10^{-2}	0.612±0.084
64.29	1.349±0.102 ×10^{-2}	0.534±0.079
66.29	1.253±0.084 ×10^{-2}	0.550±0.072
68.29	1.103±0.075 ×10^{-2}	0.545±0.072
70.30	9.282±0.725 ×10^{-3}	0.503±0.083
72.30	6.682±0.714 ×10^{-3}	0.414±0.115
74.30	5.327±0.636 ×10^{-3}	0.351±0.130
76.30	4.434±0.688 ×10^{-3}	0.524±0.157

^{192}Os 0$^+$ elastic

Angle ($\theta_{c.m.}$)	Cross section (mb/sr)	Analyzing power (A_y)
10.13	1.682±0.005 ×10^4	0.018±0.004
11.12	1.095±0.003 ×10^4	-0.019±0.004
12.12	6.648±0.019 ×10^3	-0.065±0.003
13.12	3.986±0.016 ×10^3	-0.102±0.005
14.12	2.086±0.003 ×10^3	-0.171±0.002
15.12	1.073±0.005 ×10^3	-0.216±0.007
16.12	5.262±0.015 ×10^2	-0.183±0.003
17.12	3.280±0.012 ×10^2	0.034±0.004
18.12	3.066±0.012 ×10^2	0.297±0.005
19.13	3.648±0.014 ×10^2	0.357±0.005
20.13	4.482±0.015 ×10^2	0.305±0.005
21.13	4.916±0.016 ×10^2	0.245±0.004
22.13	4.906±0.011 ×10^2	0.173±0.003
23.14	4.599±0.011 ×10^2	0.107±0.003
24.14	3.826±0.007 ×10^2	0.027±0.002
25.14	3.036±0.008 ×10^2	-0.051±0.003
26.15	2.102±0.005 ×10^2	-0.158±0.003
27.15	1.370±0.004 ×10^2	-0.286±0.004
28.15	7.243±0.033 ×10^1	-0.501±0.005
29.16	3.526±0.023 ×10^1	-0.770±0.008
30.16	1.373±0.013 ×10^1	-0.878±0.009
31.16	9.370±0.078 ×10^0	0.178±0.011
32.17	1.629±0.012 ×10^1	0.879±0.008
33.17	2.725±0.016 ×10^1	0.830±0.007
34.18	3.998±0.018 ×10^1	0.677±0.005
35.18	4.883±0.021 ×10^1	0.557±0.005
36.18	5.295±0.019 ×10^1	0.451±0.005
38.20	4.713±0.015 ×10^1	0.251±0.004
40.21	3.044±0.010 ×10^1	0.026±0.004
42.21	1.392±0.007 ×10^1	-0.281±0.006
44.22	4.887±0.034 ×10^0	-0.475±0.008
46.23	3.583±0.026 ×10^0	0.645±0.009
48.23	5.960±0.037 ×10^0	0.965±0.007
50.24	8.226±0.047 ×10^0	0.807±0.007
52.24	8.218±0.039 ×10^0	0.596±0.006
54.25	6.049±0.038 ×10^0	0.375±0.008
56.25	3.443±0.025 ×10^0	0.097±0.010
58.26	1.659±0.017 ×10^0	-0.143±0.013
60.26	1.083±0.012 ×10^0	0.305±0.015
62.27	1.313±0.015 ×10^0	0.873±0.012
64.27	1.661±0.015 ×10^0	0.983±0.009
66.27	1.681±0.017 ×10^0	0.926±0.010
68.28	1.416±0.016 ×10^0	0.808±0.012
70.28	9.660±0.140 ×10^{-1}	0.604±0.018

^{192}Os 2$^+$ (Ex = 0.206 MeV)

Angle ($\theta_{c.m.}$)	Cross section (mb/sr)	Analyzing power (A_y)
16.12	2.263±0.030 ×10^1	-0.028±0.017
17.12	1.990±0.024 ×10^1	-0.075±0.015
18.12	1.426±0.090 ×10^1	-0.021±0.077
19.13	1.612±0.020 ×10^1	-0.097±0.016
20.13	7.356±0.154 ×10^0	-0.187±0.026
21.13	4.354±0.116 ×10^0	-0.171±0.033
23.14	5.115±0.106 ×10^0	0.074±0.026
24.14	4.440±0.071 ×10^0	0.333±0.020
25.14	4.163±0.077 ×10^0	0.508±0.023
26.15	5.851±0.072 ×10^0	0.417±0.015
27.15	7.691±0.111 ×10^0	0.357±0.016
28.15	1.132±0.032 ×10^1	0.341±0.028
29.16	1.511±0.012 ×10^1	0.432±0.009
30.16	1.187±0.022 ×10^1	0.309±0.020
31.16	7.178±0.099 ×10^0	0.142±0.017
32.17	5.245±0.061 ×10^0	0.006±0.015
33.17	3.771±0.046 ×10^0	-0.091±0.015
34.18	2.544±0.031 ×10^0	-0.191±0.016
35.18	1.613±0.025 ×10^0	-0.221±0.019
36.18	9.915±0.170 ×10^{-1}	-0.187±0.022
38.20	7.964±0.129 ×10^{-1}	0.733±0.018
40.21	1.561±0.016 ×10^0	0.783±0.012
42.22	2.259±0.021 ×10^0	0.582±0.011
44.22	2.382±0.022 ×10^0	0.398±0.011
46.23	1.901±0.018 ×10^0	0.209±0.012
48.23	1.167±0.013 ×10^0	0.018±0.015
50.24	5.740±0.087 ×10^{-1}	-0.175±0.019
52.24	3.634±0.062 ×10^{-1}	0.312±0.021
54.25	4.779±0.074 ×10^{-1}	0.896±0.015
56.26	6.878±0.086 ×10^{-1}	0.886±0.012
58.26	7.744±0.103 ×10^{-1}	0.737±0.014
60.26	6.940±0.092 ×10^{-1}	0.589±0.016
62.27	4.720±0.075 ×10^{-1}	0.378±0.021
64.27	2.777±0.050 ×10^{-1}	0.130±0.024
66.27	1.610±0.038 ×10^{-1}	0.055±0.031
68.28	1.527±0.039 ×10^{-1}	0.534±0.032
70.28	2.075±0.050 ×10^{-1}	0.890±0.024

^{192}Os 4$^+$ (Ex = 0.580 MeV)

Angle ($\theta_{c.m.}$)	Cross section (mb/sr)	Analyzing power (A_y)
24.14	1.823±0.039 ×10^0	-0.031±0.027
25.14	1.863±0.044 ×10^0	-0.073±0.030
26.15	1.346±0.029 ×10^0	-0.036±0.028
27.15	1.127±0.028 ×10^0	0.005±0.031
28.15	1.016±0.029 ×10^0	-0.064±0.036
29.16	8.479±0.222 ×10^{-1}	0.048±0.033
30.16	5.883±0.212 ×10^{-1}	0.103±0.045
31.16	6.877±0.173 ×10^{-1}	0.340±0.031
32.17	5.540±0.184 ×10^{-1}	0.485±0.039
33.17	3.832±0.160 ×10^{-1}	0.421±0.052
34.18	4.141±0.123 ×10^{-1}	0.585±0.034
35.18	3.663±0.129 ×10^{-1}	0.598±0.037
36.18	3.808±0.105 ×10^{-1}	0.590±0.033
38.20	4.456±0.139 ×10^{-1}	0.581±0.038
40.21	7.426±0.218 ×10^{-1}	0.419±0.036
42.22	3.193±0.072 ×10^{-1}	0.331±0.028
44.22	2.789±0.067 ×10^{-1}	0.148±0.030
46.23	2.716±0.072 ×10^{-1}	0.199±0.032
48.23	2.301±0.082 ×10^{-1}	0.394±0.040
50.24	6.279±0.111 ×10^{-1}	0.932±0.021
52.24	1.367±0.042 ×10^{-1}	0.729±0.033
54.25	9.997±0.335 ×10^{-2}	0.772±0.035
56.26	9.012±0.284 ×10^{-2}	0.845±0.032
58.26	8.269±0.271 ×10^{-2}	0.687±0.037
60.26	7.776±0.259 ×10^{-2}	0.470±0.042
62.27	5.821±0.225 ×10^{-2}	0.391±0.050
64.27	4.450±0.184 ×10^{-2}	0.233±0.053
66.28	3.039±0.153 ×10^{-2}	0.348±0.064
68.28	2.746±0.161 ×10^{-2}	0.449±0.073
70.28	2.876±0.171 ×10^{-2}	0.815±0.063

^{192}Os 2$_1^+$ (Ex = 0.489 MeV)

Angle ($\theta_{c.m.}$)	Cross section (mb/sr)	Analyzing power (A_y)
22.13	8.633±0.469 ×10^{-1}	0.219±0.069
23.14	9.363±0.496 ×10^{-1}	0.082±0.065
24.14	6.355±0.257 ×10^{-1}	0.217±0.051
25.14	8.297±0.346 ×10^{-1}	0.310±0.055
26.15	1.099±0.028 ×10^0	0.097±0.033
27.15	9.429±0.265 ×10^{-1}	0.181±0.035
28.15	1.095±0.033 ×10^0	0.163±0.038
29.16	1.311±0.028 ×10^0	0.156±0.027
30.16	9.536±0.271 ×10^{-1}	0.072±0.036
31.16	8.239±0.190 ×10^{-1}	0.070±0.029
32.17	7.953±0.192 ×10^{-1}	0.044±0.031
33.17	6.087±0.171 ×10^{-1}	0.010±0.035
34.18	4.225±0.147 ×10^{-1}	-0.078±0.044
36.18	1.356±0.020 ×10^0	0.429±0.018
38.20	1.278±0.057 ×10^{-1}	0.294±0.056
40.21	2.220±0.062 ×10^{-1}	0.600±0.033
42.22	4.159±0.149 ×10^{-1}	0.488±0.048
44.22	5.150±0.129 ×10^{-1}	0.414±0.031
46.23	8.259±0.115 ×10^{-1}	0.589±0.017
48.23	2.402±0.060 ×10^{-1}	0.139±0.032
50.24	1.101±0.037 ×10^{-1}	-0.179±0.042
52.24	6.033±0.250 ×10^{-2}	0.059±0.052
54.25	6.013±0.249 ×10^{-2}	0.722±0.045
56.26	8.150±0.266 ×10^{-2}	0.832±0.033
58.26	1.068±0.031 ×10^{-1}	0.785±0.030
60.26	1.019±0.030 ×10^{-1}	0.629±0.035
62.27	8.012±0.265 ×10^{-2}	0.473±0.042
64.27	4.854±0.193 ×10^{-2}	0.209±0.051
66.28	3.225±0.157 ×10^{-2}	0.141±0.063
68.28	2.210±0.146 ×10^{-2}	0.253±0.084
70.28	2.530±0.162 ×10^{-2}	0.964±0.062

^{192}Os 4^+_1 (Ex = 0.910 MeV)

Angle (θ_{cm})	Cross section (mb/sr)	Analyzing power (A_y)
30.16	6.005±0.929 ×10^{-2}	0.236±0.175
31.17	5.871±0.550 ×10^{-2}	0.544±0.103
32.17	5.937±0.522 ×10^{-2}	0.188±0.109
33.17	6.307±0.524 ×10^{-2}	0.478±0.096
34.18	5.818±0.467 ×10^{-2}	0.659±0.088
35.18	1.020±0.060 ×10^{-1}	0.591±0.068
36.18	8.142±0.525 ×10^{-2}	0.599±0.072
38.20	6.632±0.432 ×10^{-2}	0.223±0.080
40.21	2.385±0.071 ×10^{-1}	0.571±0.035
42.22	3.876±0.287 ×10^{-2}	0.369±0.091
44.22	1.612±0.226 ×10^{-2}	0.063±0.164
46.23	1.897±0.161 ×10^{-2}	0.504±0.097
48.24	1.414±0.187 ×10^{-2}	0.837±0.115
50.24	7.685±0.608 ×10^{-2}	0.856±0.075
52.25	1.742±0.138 ×10^{-2}	0.717±0.085
54.25	1.465±0.128 ×10^{-2}	0.222±0.105
56.26	1.520±0.117 ×10^{-2}	0.367±0.093
58.26	2.499±0.256 ×10^{-2}	0.849±0.074
60.26	5.680±0.233 ×10^{-2}	0.740±0.046
62.27	2.100±0.206 ×10^{-2}	0.780±0.120
64.27	1.103±0.121 ×10^{-2}	0.616±0.127
66.28	7.447±1.088 ×10^{-3}	0.462±0.174
68.28	5.842±0.901 ×10^{-3}	0.684±0.153
70.28	3.754±0.670 ×10^{-3}	0.926±0.189

^{232}Th 0^+ elastic

Angle (θ_{cm})	Cross section (mb/sr)	Analyzing power (A_y)
11.11	2.974±0.071 ×10^{4}	-0.042±0.030
12.11	1.890±0.030 ×10^{4}	-0.050±0.021
13.11	1.235±0.006 ×10^{4}	-0.097±0.007
14.11	6.277±0.038 ×10^{3}	-0.116±0.008
15.11	3.319±0.031 ×10^{3}	-0.089±0.012
16.11	2.063±0.019 ×10^{3}	0.009±0.012
17.11	1.713±0.018 ×10^{3}	0.193±0.014
18.11	1.698±0.011 ×10^{3}	0.247±0.009
19.11	1.808±0.013 ×10^{3}	0.228±0.010
20.11	1.824±0.007 ×10^{3}	0.192±0.005
21.11	1.713±0.008 ×10^{3}	0.127±0.006
22.11	1.523±0.005 ×10^{3}	0.059±0.005
23.12	1.177±0.005 ×10^{3}	-0.018±0.006
24.12	8.171±0.036 ×10^{2}	-0.113±0.006
25.12	5.683±0.031 ×10^{2}	-0.220±0.007
26.12	3.105±0.024 ×10^{2}	-0.388±0.012
27.13	1.656±0.018 ×10^{2}	-0.573±0.015
28.13	7.156±0.102 ×10^{1}	-0.768±0.021
29.13	4.394±0.071 ×10^{1}	-0.225±0.020
30.13	5.482±0.097 ×10^{1}	0.573±0.026
31.14	8.722±0.112 ×10^{1}	0.671±0.019
32.14	1.207±0.011 ×10^{2}	0.574±0.015
33.14	1.542±0.014 ×10^{2}	0.468±0.013
34.14	1.599±0.011 ×10^{2}	0.360±0.011
35.15	1.615±0.013 ×10^{2}	0.259±0.010
36.15	1.363±0.008 ×10^{2}	0.141±0.008
37.15	1.168±0.008 ×10^{2}	0.024±0.009
38.16	7.941±0.054 ×10^{1}	-0.109±0.009
39.16	5.607±0.068 ×10^{1}	-0.285±0.016
40.16	2.973±0.032 ×10^{1}	-0.565±0.015
41.16	1.654±0.025 ×10^{1}	-0.833±0.020
42.18	9.228±0.119 ×10^{0}	-0.716±0.017
44.18	1.045±0.016 ×10^{1}	0.806±0.025
46.19	1.961±0.024 ×10^{1}	0.811±0.020
48.19	2.396±0.025 ×10^{1}	0.602±0.016
50.20	2.109±0.020 ×10^{1}	0.349±0.014
52.20	1.311±0.014 ×10^{1}	0.068±0.015
54.20	5.839±0.096 ×10^{0}	-0.357±0.021
56.21	2.480±0.063 ×10^{0}	-0.414±0.032
58.21	2.347±0.071 ×10^{0}	0.609±0.045
60.21	3.695±0.106 ×10^{0}	0.950±0.046
62.22	4.309±0.096 ×10^{0}	0.835±0.033
64.22	3.816±0.096 ×10^{0}	0.669±0.037
66.22	2.612±0.074 ×10^{0}	0.428±0.038
68.23	1.327±0.048 ×10^{0}	0.064±0.047
70.23	6.583±0.348 ×10^{-1}	-0.300±0.062

^{232}Th 2^+ (Ex = 0.049 MeV)

Angle (θ_{cm})	Cross section (mb/sr)	Analyzing power (A_y)
14.11	2.073±0.401 ×10^{2}	-0.258±0.224
16.11	1.094±0.227 ×10^{2}	0.149±0.230
18.11	5.154±0.596 ×10^{1}	-0.190±0.142
19.11	2.182±0.488 ×10^{1}	-0.549±0.249
20.11	9.337±1.974 ×10^{0}	-0.496±0.247
22.11	8.987±1.639 ×10^{0}	0.718±0.270
23.12	2.271±0.183 ×10^{1}	0.516±0.115
24.12	3.602±0.129 ×10^{1}	0.276±0.050
25.12	4.555±0.124 ×10^{1}	0.255±0.036
26.12	5.056±0.106 ×10^{1}	0.144±0.029
27.13	5.066±0.087 ×10^{1}	0.123±0.022
28.13	4.429±0.066 ×10^{1}	0.046±0.020
29.13	3.895±0.063 ×10^{1}	-0.041±0.020
30.13	2.595±0.050 ×10^{1}	-0.170±0.026
31.14	1.823±0.038 ×10^{1}	-0.254±0.027
32.14	9.903±0.411 ×10^{0}	-0.449±0.063
33.14	5.547±0.384 ×10^{0}	-0.447±0.089
34.14	3.018±0.278 ×10^{0}	0.050±0.118
35.15	4.815±0.390 ×10^{0}	0.686±0.107
36.15	7.961±0.240 ×10^{0}	0.782±0.041
37.15	1.141±0.029 ×10^{1}	0.669±0.034
38.16	1.405±0.024 ×10^{1}	0.523±0.023
39.16	1.631±0.040 ×10^{1}	0.468±0.029
40.16	1.636±0.021 ×10^{1}	0.311±0.018
41.16	1.571±0.021 ×10^{1}	0.262±0.018
42.17	1.300±0.021 ×10^{1}	0.123±0.021
42.18	1.350±0.013 ×10^{1}	0.137±0.012
44.18	7.383±0.096 ×10^{0}	-0.202±0.017
46.19	2.850±0.070 ×10^{0}	-0.393±0.036
48.19	1.967±0.068 ×10^{0}	0.453±0.041
50.20	3.699±0.081 ×10^{0}	0.847±0.026
52.20	5.328±0.091 ×10^{0}	0.713±0.022
54.20	4.960±0.221 ×10^{0}	0.552±0.021
56.21	3.906±0.079 ×10^{0}	0.340±0.026
58.21	2.275±0.056 ×10^{0}	-0.020±0.033
60.21	1.181±0.056 ×10^{0}	-0.059±0.063
62.22	1.132±0.048 ×10^{0}	0.463±0.042
64.22	1.509±0.049 ×10^{0}	0.833±0.033
66.22	1.702±0.053 ×10^{0}	0.927±0.030
68.23	1.591±0.056 ×10^{0}	0.753±0.034
70.23	1.164±0.042 ×10^{0}	0.587±0.038

^{232}Th 4^+ (Ex = 0.162 MeV)

Angle (θ_{cm})	Cross section (mb/sr)	Analyzing power (A_y)
31.14	1.729±0.229 ×10^{0}	0.551±0.175
32.14	2.357±0.159 ×10^{0}	0.390±0.096
33.14	2.927±0.180 ×10^{0}	0.416±0.082
34.14	3.430±0.153 ×10^{0}	0.139±0.061
35.15	3.178±0.143 ×10^{0}	0.196±0.053
36.15	2.967±0.093 ×10^{0}	0.098±0.041
37.15	2.670±0.110 ×10^{0}	0.010±0.053
38.16	1.945±0.077 ×10^{0}	-0.132±0.052
39.16	1.361±0.104 ×10^{0}	-0.267±0.095
40.16	9.434±0.514 ×10^{-1}	-0.403±0.072
41.16	7.382±0.499 ×10^{-1}	0.221±0.085
42.18	5.836±0.300 ×10^{-1}	0.316±0.064
44.18	8.317±0.318 ×10^{-1}	0.743±0.044
46.19	1.124±0.035 ×10^{0}	0.719±0.035
48.19	1.212±0.036 ×10^{0}	0.443±0.036
50.20	1.118±0.034 ×10^{0}	0.234±0.039
52.20	6.692±0.282 ×10^{-1}	0.083±0.055
54.20	3.844±0.229 ×10^{-1}	0.026±0.146
56.21	2.833±0.202 ×10^{-1}	0.350±0.087
58.21	4.779±0.236 ×10^{-1}	0.778±0.053
60.21	5.194±0.260 ×10^{-1}	0.715±0.053
62.22	4.960±0.210 ×10^{-1}	0.554±0.046
64.22	4.085±0.217 ×10^{-1}	0.464±0.062
66.22	2.319±0.164 ×10^{-1}	0.241±0.083
68.23	1.530±0.142 ×10^{-1}	-0.027±0.114
70.23	1.175±0.127 ×10^{-1}	0.464±0.110

^{232}Th 6$^+$ (Ex = 0.333 MeV)

Angle (θ_{cm})	Cross section (mb/sr)	Analyzing power (A_y)
44.18	1.065±0.114 ×10^{-1}	-0.228±0.138
46.19	7.399±0.819 ×10^{-2}	0.028±0.137
48.19	6.114±1.020 ×10^{-2}	0.507±0.181
50.20	1.031±0.109 ×10^{-1}	0.290±0.123
52.20	1.171±0.107 ×10^{-1}	0.552±0.105
54.21	1.423±0.127 ×10^{-1}	0.464±0.102
56.21	1.168±0.110 ×10^{-1}	0.300±0.116
58.21	6.812±0.841 ×10^{-2}	0.065±0.153
60.22	4.983±0.771 ×10^{-2}	-0.000±0.186
62.22	5.132±0.637 ×10^{-2}	0.421±0.139
64.22	5.064±0.801 ×10^{-2}	0.451±0.192
66.23	6.877±0.848 ×10^{-2}	0.669±0.136
68.23	4.740±1.153 ×10^{-2}	0.668±0.336
70.23	5.517±0.773 ×10^{-2}	0.253±0.154

^{238}U 0$^+$ elastic

Angle (θ_{cm})	Cross section (mb/sr)	Analyzing power (A_y)
12.11	2.078±0.007 ×10^{4}	-0.054±0.005
13.11	1.265±0.006 ×10^{4}	-0.096±0.007
14.10	6.857±0.053 ×10^{3}	-0.105±0.010
15.10	3.673±0.038 ×10^{3}	-0.078±0.013
16.10	2.341±0.023 ×10^{3}	0.029±0.013
17.10	1.835±0.021 ×10^{3}	0.161±0.015
18.10	1.795±0.016 ×10^{3}	0.229±0.012
19.11	1.868±0.007 ×10^{3}	0.212±0.005
19.14	1.825±0.006 ×10^{3}	0.220±0.005
20.11	1.844±0.006 ×10^{3}	0.173±0.005
21.11	1.744±0.005 ×10^{3}	0.112±0.004
22.11	1.475±0.005 ×10^{3}	0.046±0.004
23.11	1.186±0.004 ×10^{3}	-0.032±0.004
24.12	8.226±0.035 ×10^{2}	-0.127±0.005
25.12	5.188±0.029 ×10^{2}	-0.255±0.008
26.12	2.991±0.023 ×10^{2}	-0.431±0.011
27.12	1.554±0.013 ×10^{2}	-0.622±0.013
28.13	6.803±0.090 ×10^{1}	-0.690±0.018
29.13	4.730±0.071 ×10^{1}	0.058±0.019
30.13	6.648±0.088 ×10^{1}	0.602±0.016
31.13	9.895±0.112 ×10^{1}	0.623±0.017
32.13	1.349±0.011 ×10^{2}	0.526±0.013
33.14	1.590±0.010 ×10^{2}	0.416±0.010
34.14	1.687±0.010 ×10^{2}	0.323±0.008
35.14	1.563±0.008 ×10^{2}	0.215±0.007
36.15	1.337±0.007 ×10^{2}	0.103±0.007
37.15	1.037±0.006 ×10^{2}	-0.017±0.007
38.15	7.409±0.052 ×10^{1}	-0.178±0.009
39.15	4.410±0.037 ×10^{1}	-0.372±0.011
40.16	2.536±0.029 ×10^{1}	-0.646±0.015
41.16	1.230±0.020 ×10^{1}	-0.913±0.020
42.17	7.593±0.089 ×10^{0}	-0.517±0.016
44.18	1.152±0.012 ×10^{1}	0.850±0.013
46.18	2.039±0.016 ×10^{1}	0.759±0.011
48.19	2.338±0.019 ×10^{1}	0.537±0.012
50.19	1.829±0.013 ×10^{1}	0.278±0.010
52.20	1.045±0.009 ×10^{1}	-0.030±0.011
54.20	4.431±0.060 ×10^{0}	-0.498±0.017
56.20	1.996±0.039 ×10^{0}	-0.288±0.024
58.21	2.476±0.052 ×10^{0}	0.754±0.031
60.21	3.641±0.071 ×10^{0}	0.918±0.030
62.21	3.996±0.086 ×10^{0}	0.801±0.032
64.21	3.293±0.055 ×10^{0}	0.608±0.024
66.22	2.064±0.040 ×10^{0}	0.317±0.025
68.22	1.057±0.027 ×10^{0}	-0.059±0.032
70.22	5.726±0.203 ×10^{-1}	-0.220±0.043

^{238}U 2$^+$ (Ex = 0.045 MeV)

Angle (θ_{cm})	Cross section (mb/sr)	Analyzing power (A_y)
16.10	1.490±0.226 ×10^{2}	0.115±0.179
17.10	1.129±0.099 ×10^{2}	-0.185±0.108
18.10	7.167±0.894 ×10^{1}	-0.099±0.147
19.11	2.281±0.293 ×10^{1}	-0.440±0.181
21.11	6.446±1.671 ×10^{0}	0.609±0.294
22.11	1.428±0.164 ×10^{1}	0.538±0.136
23.11	2.498±0.143 ×10^{1}	0.429±0.074
24.12	3.989±0.122 ×10^{1}	0.365±0.043
25.12	5.299±0.113 ×10^{1}	0.264±0.029
26.12	5.756±0.106 ×10^{1}	0.229±0.024
27.12	6.084±0.080 ×10^{1}	0.125±0.017
28.13	5.280±0.072 ×10^{1}	0.052±0.018
29.13	4.313±0.065 ×10^{1}	-0.081±0.019
30.13	3.000±0.057 ×10^{1}	-0.251±0.025
31.13	1.896±0.044 ×10^{1}	-0.351±0.032
32.13	1.073±0.036 ×10^{1}	-0.499±0.051
33.14	4.614±0.214 ×10^{0}	-0.505±0.065
34.14	3.530±0.226 ×10^{0}	0.359±0.077
35.14	4.503±0.271 ×10^{0}	0.861±0.074
36.15	9.901±0.289 ×10^{0}	0.787±0.037
37.15	1.358±0.027 ×10^{1}	0.688±0.026
38.15	1.730±0.025 ×10^{1}	0.565±0.018
39.15	1.942±0.025 ×10^{1}	0.423±0.017
40.16	2.065±0.024 ×10^{1}	0.318±0.015
41.16	1.828±0.021 ×10^{1}	0.194±0.015
42.17	1.548±0.013 ×10^{1}	0.098±0.011
44.18	8.019±0.084 ×10^{0}	-0.219±0.014
46.18	3.247±0.077 ×10^{0}	-0.345±0.035
48.19	2.775±0.082 ×10^{0}	0.570±0.032
50.19	4.893±0.087 ×10^{0}	0.840±0.021
52.20	6.393±0.085 ×10^{0}	0.686±0.017
54.20	6.235±0.073 ×10^{0}	0.475±0.015
56.20	4.386±0.056 ×10^{0}	0.236±0.016
58.21	2.401±0.045 ×10^{0}	-0.080±0.024
60.21	1.212±0.045 ×10^{0}	-0.155±0.049
62.21	1.170±0.055 ×10^{0}	0.578±0.046
64.21	1.687±0.039 ×10^{0}	0.867±0.021
66.22	2.007±0.039 ×10^{0}	0.861±0.020
68.22	1.864±0.035 ×10^{0}	0.736±0.020
70.22	1.349±0.030 ×10^{0}	0.510±0.025

^{238}U 4$^+$ (Ex = 0.148 MeV)

Angle (θ_{cm})	Cross section (mb/sr)	Analyzing power (A_y)
31.13	2.184±0.164 ×10^{0}	0.579±0.105
32.13	3.050±0.145 ×10^{0}	0.406±0.066
33.14	3.148±0.128 ×10^{0}	0.356±0.054
34.14	3.170±0.108 ×10^{0}	0.252±0.042
35.14	3.091±0.091 ×10^{0}	0.187±0.038
36.15	2.442±0.088 ×10^{0}	0.072±0.045
37.15	1.850±0.075 ×10^{0}	-0.131±0.051
38.15	1.274±0.064 ×10^{0}	-0.187±0.063
39.15	7.720±0.901 ×10^{-1}	-0.321±0.159
40.16	5.441±0.946 ×10^{-1}	-0.436±0.242
41.16	3.670±0.914 ×10^{-1}	0.054±0.258
42.17	5.410±0.261 ×10^{-1}	0.572±0.060
44.18	9.207±0.280 ×10^{-1}	0.760±0.035
46.18	1.270±0.027 ×10^{0}	0.572±0.025
48.19	1.222±0.030 ×10^{0}	0.413±0.030
50.19	8.633±0.250 ×10^{-1}	0.193±0.036
52.20	4.754±0.216 ×10^{-1}	-0.057±0.058
54.20	2.837±0.173 ×10^{-1}	0.148±0.074
56.20	3.100±0.165 ×10^{-1}	0.578±0.063
58.21	4.541±0.177 ×10^{-1}	0.789±0.041
60.21	4.992±0.178 ×10^{-1}	0.725±0.036
62.21	4.798±0.188 ×10^{-1}	0.520±0.054
64.21	3.135±0.126 ×10^{-1}	0.269±0.046
66.22	1.736±0.100 ×10^{-1}	-0.072±0.072
68.22	1.079±0.086 ×10^{-1}	0.196±0.091
70.22	1.354±0.096 ×10^{-1}	0.555±0.074

^{238}U 6^+ (Ex = 0.307 MeV)

Angle ($\theta_{c.m.}$)	Cross section (mb/sr)	Analyzing power (A_y)
41.16	$1.642\pm0.150\times10^{-1}$	-0.003 ± 0.110
42.16	$1.244\pm0.118\times10^{-1}$	0.350 ± 0.110
44.18	$1.053\pm0.064\times10^{-1}$	0.470 ± 0.072
46.18	$9.407\pm0.533\times10^{-2}$	0.703 ± 0.063
48.19	$1.031\pm0.058\times10^{-1}$	0.517 ± 0.066
50.19	$1.551\pm0.071\times10^{-1}$	0.602 ± 0.051
52.20	$1.596\pm0.076\times10^{-1}$	0.375 ± 0.057
54.20	$1.165\pm0.081\times10^{-1}$	0.293 ± 0.084
56.20	$8.401\pm0.608\times10^{-2}$	0.164 ± 0.088
58.21	$6.542\pm0.558\times10^{-2}$	0.164 ± 0.102
60.21	$4.574\pm0.453\times10^{-2}$	0.489 ± 0.118
62.21	$5.777\pm0.611\times10^{-2}$	0.638 ± 0.110
64.22	$7.299\pm0.506\times10^{-2}$	0.750 ± 0.072
66.22	$7.142\pm0.492\times10^{-2}$	0.797 ± 0.068
68.22	$6.446\pm0.487\times10^{-2}$	0.590 ± 0.082
70.22	$4.815\pm0.439\times10^{-2}$	0.477 ± 0.105

Reference

[1] T. Ichihara, H. Sakaguchi, M. Nakamura, T. Noro, F. Ohtani, H. Sakamoto, H. Ogawa, M. Yosoi, M. Ieiri, N. Isshiki, Y. Takeuchi, and S. Kobayashi, Phys. Lett. **149B**, 55 (1984).

[2] I. M. Govil, H. W. Fulbright, D. Cline, E. Wesolowski, B. Kotlinski, A. Backlin, and K. Gridnev, Phys. Rev. **C33**, 793 (1986).

[3] F. Todd Baker, A. Sethi, V. Penumetcha, G. T. Emery, W. P. Jones, M. A. Grimm, and M. L. Whiten, Phys. Rev. **C32**, 2212 (1985).

[4] W. Reuter, E. B. Shera, M. V. Hoehn, F. W. Hersman, T. Milliman, J. M. Finn, C. Hyde-Wright, R. Lourie, B. Pugh, and W. Bertozzi, Phys. Rev. **C30**, 1465 (1984).

[5] T. Ichihara, H. Sakaguchi, M. Nakamura, T. Noro, F. Ohtani, H. Sakamoto, H. Ogawa, M. Yosoi, M. Ieiri, N. Isshiki, and S. Kobayashi, Pys. Rev. **C29**, 1228 (1984).

[6] H. Ogawa, H. Sakaguchi, M. Nakamura, T. Noro, H. Sakamoto, T. Ichihara, M. Yosoi, M. Ieiri, N. Isshiki, Y. Takeuchi, and S. Kobayashi, Phys. Rev. **C33**, 834 (1986).

[7] Y. Takeuchi, H. Sakaguchi, M. Nakamura, T. Ichihara, M. Yosoi, M. Ieiri, and S. Kobayashi, Phys. Rev. **C34**, 493 (1986).

[8] F. Ohtani, H. Sakaguchi, M. Nakamura, T. Noro, H. Sakamoto, H. Ogawa, T. Ichihara, M. Yosoi, and S. Kobayashi, Phys. Rev. **C28**, 120 (1983).

[9] T. Ichihara, H. Sakaguchi, M. Nakamura, M. Yosoi, M. Ieiri, N. Isshiki, Y. Takeuchi, H. Togawa, T. Tsutsumi, and S. Kobayashi, Phys. Lett. **182B**, 301 (1986); Phys. Rev. **C36**, 1754 (1987).

[10] R. M. Ronningen, G. M. Crawley, N. Anantaraman, S. M. Banks, B. M. Spicer, G. G. Shute, V. C. Officer, J. M. R. Wastell, D. W. Devins, and D. L. Friesel, Phys. Rev. **C28**, 123 (1983).

[11] B. G. Lay, S. M. Banks, B. M. Specer, G. G. Shute, V. C. Offecer, R. M. Ronningen, G. M. Crawley, N. Anantaraman, and P. R. DeVito, Phys. Rev. **C32**, 440 (1985).

[12] M. L. Barlett, J. A. McGill, L. Ray, M. M. Barlett, G. W. Hoffmann, N. M. Hintz, G. S. Kyle, M. A. Franey, and G. Blanpied, Phys. Rev. **C22**, 1168 (1980).

[13] L. W. Put and M. N. Harakeh, Phys. Lett. **119B**, 253 (1982).

[14] R. M. Ronningen, R. C. Melin, J. A. Nolen, Jr., G. M. Craley, and C. E. Bemis, Phys. Rev. Lett. **47**, 635 (1981).

[15] C. H. King, J. E. Finck, G. M. Crawley, J. A. Nolen, Jr., and R. M. Ronningen, Phys. Rev. **C20**, 2084 (1979).

[16] P. B. Woollam, R. J. Griffiths, F. G. Kingston, C. B. Fulmer, J. C. Hafele, and A. Scott, Nucl. Phys. **A179**, 657 (1972).

[17] K. Hatanaka, N. Matsuoka, T. Saito, K. Hosono, M. Kondo, S. Kato, T. Higo, S. Matsuki, and K. Ogino, Nucl. Phys. **A403**, 109 (1983).

[18] H. Clement, R. Frick, G. Graw, F. Merz, H. J. Scheerer, P. Schiemenz, N. Seichert, and Sun Tsu Hsun, Phys. Rev. Lett. **48**, 1082 (1982).

[19] T. Ichihara, H. Sakaguchi, M. Nakamura, M. Yosoi, M. Ieiri, Y. Takeuchi, T. Noro, H. Sakamoto,

H. Ogawa, N. Isshiki, and S. Kobayashi, Phys. Rev. **C35**, 931 (1987).

[20] T. Baker, A. Scott, R. C. Styles, T. H. Kruse, K. Jones, and R. Suchannek, Nucl. Phys. **A351**, 63 (1981).

[21] D. L. Hendrie, N. K. Glendenning, B. G. Harvey, O. N. Jarvis, H. H. Duhm, J. Saudinos, and J. Mahoney, Phys. Lett. **26B**, 127 (1968).

[22] T. Cooper, W. Bertozzi, J. Heisenberg, S. Kowalski, W. Turchinetz, C. Williamson, L. Cardman, S. Fivozinski, J. Lightbody, Jr., and S. Penner, Phys. Rev. **C13**, 1083 (1976).

[23] C. W. Creswell, Ph. D. thesis, MIT, 1977 (unpublished).

[24] T. Sasanuma, Ph. D. thesis, MIT, 1979 (unpublished).

[25] P. O. Tjøm and B. Elbek, Nucl. Phys. **A107**, 385 (1968).

[26] R. S. Machkntosh, Phys. Lett. **29B**, 629 (1969).

[27] L. Ray, G. S. Blanpied and W. R. Coker, Phys. Rev. **C20**, 1236 (1979).

[28] K. Van der Borg, M. N. Harakeh, and B. S. Nilsson, Nucl. Phys. **A325**, 31 (1979).

[29] R. V. Jols, J. L. Molina, and V. G. Soloviev, Z. Physik. **A295**, 147 (1980).

[30] V. G. Soloviev and N. Yu. Shirikova, Z. Physik. **A301**, 263 (1981).

[31] V. O. Nesterenko, V. G. Soloviev, A. V. Sushkov, N. Yu. Shirikova, preprint of the Joint Institute for Nuclear Research, Dubna, E4-85-856 (1985).

[32] H. C. Wu and X. Q. Zhou, Nucl. Phys. **A417**, 67 (1984).

[33] X. Q. Zhou and H. C. Wu, Nucl. Phys. **A421**, 159 (1984).

[34] A. Arima, Nucl. Phys. **A421**, 63 (1984).

[35] N. Yoshinaga, Y. Akiyama, and A. Arima, Phys. Rev. Lett. **56**, 1116 (1986).

[36] A. Green, Phys. Lett. **24B**, 384 (1967).

[37] J. P. Jeukenne, A. Lejeune, and C. Mahaux, Phys. Rev. C **16**, 80 (1977).

[38] F. A. Brieva and B. Z. Georgiev, Nucl. Phys. **A308**, 27 (1978).

[39] A. M. Kobos, B. A. Brown, P. E. Hodgson, G. R. Satchler, and A. Budzanowski Nucl. Phys. **A384**, 65 (1982).

[40] D. K. Srivastava, H. Rebel, Zeit. Phys. **A316**, 25 (1984).

[41] J. K. Hamilton and R. S. Mackintosh, J. Phys. **G4**, 557 (1978).

[42] H. Ikegami, S. Morinobu, I. Katayama, M. Fujiwara, and S. Yamabe, Nucl. Instrum. Methods. **175**, 335 (1980).

[43] T. Ichihara, H. Sakaguchi, K. Hatanaka, M. Fujiwara, and K. Hosono, Research Center for Nuclear Physics Anuual Report, 1981, p. 194.

[44] K. Imai, N. Tamura, and K. Nishimura, Research Center for Nuclear Physics Annual Report, 1979, p. 23.

[45] Y. Fujita, K. Nagayama, M. Fujiwara, S. Morinobu, T. Yamazaki, and H. Ikegami, Nucl. Instrum. Methods. **217**, 441 (1983).

[46] K. Katayama and H. Ogata, Nucl. Instrum. Methods. **174**, 295 (1980).

[47] T. Tamura, Rev. Mod. Phys. **37**, 679 (1965).

[48] M. N. Harakeh, *Lecture Note of* 1983 *RCNP-kikuchi summer school* Research Center for Nuclear Physics, 1983, p. 133.

[49] A. Bohr and B. R. Mottelson, *Nuclear Structure*, (Benjamin, New York, 1975), Vol. II.

[50] J. Raynal, code ECIS79 (unpublished), Phys. Rev. **C23**, 2571 (1981).

[51] J. Raynal, International Atomic Energy Agency Report, IAEA-5MR-818, 1972, p. 75.

[52] A. S. Davydov and G. F. Filippov, Nucl. Phys. **8**, 237 (1958).

[53] R. Shau, Phys. Rev. **C29**, 1486 (1984).

[54] A. M. Bernstein, *Advances in Nuclear Physics*, edited by M. Baranger and E. Vogt, (Plenum, New York, 1969), Vol. 3.

[55] G. R. Satchler, *Direct Nuclear Reactions*, (Clarendon Press, Oxford, 1983).

[56] R. S. Mackintosh, Nucl. Phys. **A266**, 379 (1976).

[57] G. R. Satchler, J. Math. Phys. **13**, 1118 (1972).

[58] L. W. Owen and G. R. Satchler, Nucl. Phys. **51**, 155 (1964).

[59] G. F. Bertsch, Phys. Lett. **26B**, 130 (1967).

[60] M. Matsuo, (private communications).
[61] M. Matsuo, Prog. Theor. Phys. **78**, 609 (1987).
[62] B. R. Mottelson and S. G. Nilson, K. Dans. Vidensk. Selsk. Mat.-Fys. Skr. **1**, No. 8 (1959).
[63] Y. R. Shimizu, and K. Matsuyanagi Prog. Theor. Phys. **70**, 144 (1983), *ibid* **71**, 960 (1984).
[64] T. Kishimoto, J. M. Moss, D. H. Youngblood, J. D. Bronson, C. M. Rozsa, D. R. Brown, and A. D. Bacher, Phys. Rev. Lett. **35**, 552 (1975).
[65] A. Bohr and B. R. Mottelson, Phys. Scr. **25**, 28 (1982).
[66] A. Hayashi, K. Hara, and P. Ring, Phys. Rev. Lett. **53**, 337 (1984).
[67] J. W. Negele and G. Rinker, Phys. Rev. **C15**, 1499 (1977).
[68] J. W. Negele and D. Vautherin, Phys. Rev. **C5**, 1472 (1972).
[69] J. W. Negele, Nucl. Phys. **A142**, 225 (1970).
[70] D. Vautherin, Phys. Rev. **C7**, 296 (1973).
[71] A. H. Shaw and J. S. Greenberg, Phys. Rev. **C10**, 263 (1974).
[72] I. Y. Lee, J. X. Saladin, J. Holden, J. O'Brien, C. Baktash, C. Bemis, Jr., P. H. Stelson, F. K. McGowan, W. T. Milner, J. L. C. Ford, Jr., R. L. Robinson, and W. Tuttle, Phys. Rev. **C12**, 1483 (1975).
[73] H. Fisher, D. Kamke, H. J. Kittling, E. Kuhlmann, H. Plicht, and R. Schormann, Phys. Rev. **C15**, 921 (1977).
[74] H. J. Wollersheim, W. Wilcke, Th. W. Elze, and D. Pelte, Phys. Lett. **48B**, 323 (1974).
[75] K. A. Erb, J. E. Holden, I. Y. Lee, J. X. Saladin, and T. K. Saylor, Phys. Rev. Lett. **29**, 1010 (1972).
[76] H. J. Wollersheim, W. Wickle, and T. W. Elze, Phys. Rev. **C11**, 2008 (1975).
[77] J. S. Greenberg and A. H. Shaw, J. Phys. Soc. Jpn. Suppl. **34**, 362 (1973).
[78] R. M. Ronningen, J. H. Hamilton, L. Varnell, J. Lange, A. V. Ramayya, G. Garcia-Bermudez, W. Lourens, L. L. Riedinger, F. K. McGowan, P. H. Stelson, R. L. Robinson, and J. L. C. Ford, Jr., Phys. Rev. **C16**, 2208 (1977).
[79] F. Tood Baker, T. H. Kruse, W. Hartwig, I. Y. Lee, and J. X. Saladin, Nucl. Phys. **A258**, 43 (1976).
[80] R. F. Casten, J. S. Greenberg, G. A. Burginyou, and D. A. Bromley, Phys. Rev. Lett. **18**, 912 (1967).
[81] R. J. Pryor and J. X. Saladin, Phys. Rev. **C1**, 1573 (1970).
[82] C. E. Bemis, Jr., F. K. McGowan, J. L. C. Ford, Jr., W. T. Milner, P. H. Stelson, and R. L. Robinson, Phys. Rev. **C8**, 1466 (1973).
[83] F. K. McGowan, in *Proc Int. Cnf. Radioactivity in Nucl Spectrosc.*, Nashville Tenn, (1969).
[84] H. J. Wollersheim, T. W. Elze, Z. Phys. **A280**, 277 (1977).
[85] E. Veje, B. Elbek, B. Herskind, and M. C. Olesen, Nucl. Phys. **A109**, 489 (1968).
[86] H. J. Wollersheim and Th. W. Elze, Nucl. Phys. **A278**, 87 (1977).
[87] Y. Yoshizawa, B. Elbek, B. Herskind, and M. C. Olsen, Nucl. Phys. **73**, 273 (1965).
[88] F. K. McGowan and W. T. Milner, Phys. Rev. **C23**, 1926 (1981).
[89] R. M. Ronningen, J. H. Hamilton, A. V. Ramayya, L. Varnell, G. Garcia-Bermudez, J. Lange, W. Lourens, L. L. Riedinger, R. L. Robinson, P. H. Stelson, and J. L. C. Ford, Jr., Phys. Rev. **C15**, 1671 (1977).
[90] C. Baktash, J. X. Saladin, J. O'Brien, I. Y. Lee, and J. E. Holden, Phys. Rev. **C10**, 2265 (1974).
[91] F. K. McGowan, W. T. Milner, R. L. Robinson, P. H. Stelson, and Z. W. Grabowski, Nucl. Phys. **A297**, 51 (1978).
[92] L. L. Riedinger, E. G. Funk, J. W. Mihelich, G. S. Schilling, A. E. Rainis, and R. N. Oehlberg, Phys. Rev. **C20**, 2170 (1979).
[93] W. T. Milner, F. K. McGowan, R. L. Robinson, P. H. Stelson, and R. S. Sayer, Nucl. Phys. **A177**, 1 (1971).
[94] R. F. Casten, J. S. Greenberg, S. H. Sie, G. A. Burginyou, and D. A. Bromley, Phys. Rev. **187**, 1532 (1969).
[95] R. Block, B. Elbek, and P. O. Tjom, Nucl. Phys. **A91**, 576 (1967).
[96] We have also show the Numerical values of the measured cross section and analysing poweres for ^{178,180}Hf (Ref. 6) and ^{232}Th and ^{238}U(Ref. 7) for futher refereces.